Summer 7-19-2011

THEORETICAL AND NUMERICAL RESEARCH ON SEDIMENT TRANSPORT IN PRESSURISED FLOW CONDITIONS

Zhaoding Xie
University of Nebraska-Lincoln, zxie@unomaha.edu

Xie, Zhaoding, "THEORETICAL AND NUMERICAL RESEARCH ON SEDIMENT TRANSPORT IN PRESSURISED FLOW CONDITIONS" (2011). *Civil Engineering Theses, Dissertations, and Student Research*. 23.
http://digitalcommons.unl.edu/civilengdiss/23

THEORETICAL AND NUMERICAL RESEARCH ON SEDIMENT TRANSPORT IN PRESSURISED FLOW CONDITIONS

by

Zhaoding Xie

A DISSERTATION

Presented to the Faculty of

The Graduate College at the University of Nebraska

In Partial Fulfillment of Requirements

For the Degree of Doctor of Philosophy

Major: Engineering

Under the Supervision of Professor Junke Guo

Lincoln, Nebraska

July, 2011

THEORETICAL AND NUMERICAL RESEARCH ON SEDIMENT TRANSPORT IN PRESSURISED FLOW CONDITIONS

Zhaoding Xie, Ph.D.

University of Nebraska, 2011

Advisor: Junke Guo

Research of river bed erosion is an important part of designing bridges and transportation networks since the stability and hydrodynamic response of bridges critically depends on river bed scour. The engineering designers traditionally focus on the local scour around hydraulic structures, such as piers and abutments, in open channel flow. The pressurized scour under a submerged bridge deck is seldom researched.

In this study, the commercial CFD codes, FLOW3D and STARCCM+, are adopted to simulate pressure scour under a bridge deck with six girders. Several limitations for FLOW3D are found during its application of sediment transport model: a) the scour model is sensitive to the vertical cell size on the sediment interface, the scour holes impossibly form for the large cell size; b) large sediment diameters fail the drifting model comprised of the scour model; c) the bed load model cannot be available to

simulate the saltation load; d) large computational times are required to obtain the scour results. In STARCCM+, the morphing vertices model on the wall boundary can effectively mock the deformation of river bed dependent on the entrainment rate for sediment transport model that we adopt. Guo’s empirical formulas for pressurized scour profile and time dependent scour depth are incorporated into STARCCM+ as the model of morphing mesh. The recession rate is obtained as the function of the maximum bed shear stress by fitting the numerical results.

A theoretical model for analyzing the sediment bed load with arbitrary bed slopes is developed to calculate the erosion profile on the sediment bed in flow condition. It found that the entrainment rate of sediment particles is also dependent on the changing rate of bed load layer thickness and mixture density from the continuity equation compared to Exner equation. Further, the two dimensional solution shows that the additional shear stress due to the longitudinal slope has an important influence on the bed shear. The modified pressure drop formula based on Ergun equation is developed to compute the gradient of pressure drop for a fluidized bed as well.

The results of this research provide an effective approach to analyze the scour profile with the combination of theoretical and numerical computation.

ACKNOWLEDGEMENTS

I would like to thank the following people who helped me much during my research. First, Dr. Junke Guo, my major advisor, instructed me on my research using his invaluable knowledge, research skills and rich experience in the past two years. He always proposes challenging problems and insightful opinions when instructing me, which makes me keep the thought and encouragement. From his strict requirements of academics, I obtained invaluable inspiration whether for research work or everyday life. Second, Dr. Kornel Kerenyi, Research Manager of FHWA Hydraulics R&D Program, provided the experimental data that were very important for this research. Third, Dr. Steven A.Lottes, Transportation Research and Analysis Computing Center (TRACC) at the Argonne National Lab (ANL), provided this research with significant options and advice. Also, TRACC provided the remote access permission to use the high performance computer, which guarantees the smooth accomplishment of this study. Thanks also go to my classmates, Mr. Haoyin Shan and Ms. Yuan Zhai, for discussing the issues and solutions of my research.

Finally, I would like to thank my parents. Without their support and encouragement, I may never reach where I am today.

TABLE OF CONTENTS

LIST OF TABLES

LIST OF FIGURES

Chapter 1 Introduction

1.0 Overview

The research for river bed erosion is an important part of designing bridges and transportation networks. The stability and hydrodynamic response of bridges critically depends on river bed scour. Engineering designers traditionally focus on local scour around hydraulic structures, such as piers and abutments. However, the hydraulic condition becomes quite different and complicated, once a bridge deck is totally submerged, this called pressure flow. Unlike open channel flows, such pressurized flow conditions create an aggravated scour situation in which the bridge foundation becomes unstable, and even fail. Figure 1.1 shows a partially inundated bridge deck at Salt Creek, NE, which may have developed into the completely submerged flow forming pressure flow underneath the bridge deck.

Figure 1.1 Partially inundated bridge deck at Salt Creek, NE.

The dimensional constriction of the flow domain leads to the occurrence of contraction scour. The alternation of flow domain results from the interference of the bridge abutments and piers as well as the vertical contraction in the pressure flow condition. The decrease of the flow cross-sectional area makes the corresponding magnitude of velocity increase along the opening region. This increase causes additional shear stress on the bed surface, so the corresponding bed scour develop dramatically. The transport of sediment out of the local region induces the increment of the cross section area, the velocity decreasing until the equilibrium status occurs.

The scour occurs in the pressure flow condition when the surface level of water reaches the bridge deck, the continuous increase of water level deepen the degree of scour on the bed and the pressure flow under the bridge deck increases as the ratio of submergence increases. When the approach flow spills over the bridge deck, the flow pattern is altered from exclusively inundated pressure flow to a combination of the crested weir and localized pressure flow. The contraction caused by the bridge deck forces the approach flow downward, which increases the bed scour under the bridge deck. The other part of the approach flow is separated by the bridge deck into the top region. The impact of the approach velocity on the bed scour is uniquely from the water body with the highly downward velocity. Piers and abutments can cause the more complex flow fields, such as the additional turbulence and vortices, thus, for the consideration of simplicity piers and abutments were not included in geometrical structures of the present study, only the bridge deck with six girders was modeled in the pressure condition.

The bridge superstructures are subjected to the catastrophic risks during a flood event. The failure of the bridge may come from the drag, lift and moment acting on the structures, many researchers systematically analyzed hydrodynamic loading, Denson (1982) used dimensionless analysis to find the functional relationship among hydraulic parameters by a series of physical experiments; the research team led by Kerenyi *et al*. (2009) employed CFD methods to obtain force coefficients that compared to physical experiments very well. However, most of the bridge failure events are due to the lost stability of the bridge foundation induced by the local scour except for the defects of bridge structures. Few researchers examine the pressure flow scour underneath a bridge deck instead of conducting the scour prediction in the free-surface flow conditions. The first study of pressure flow was conducted experimentally at Colorado State University by Abed (1991) in which both piers and bridge decks were studied. However, she failed to isolate the pressure flow effect on scour. Richardson *et al*. (1998) provided their investigation on the pressure flow scour beneath a bridge deck without the localized effects of piers, developing a conceptual relationship between pressure flow scour and flow conditions.

Umbrell *et al* (1998) did a series of flume experiments in the FHWA Hydraulics Lab and developed a formula to estimate the scour depth based on mass conservation. However, their formula is still empirical. Guo J. (2009) developed a theoretically analyzed solution for the scour depth of three different flow classifications, which perfectly fits the experimental results from the Federal Highway Administration (FHWA) ---Turner-Fairbank Highway Research Center (TFHRC).

Successful prediction to localized pressure scour required not only traditional laboratory experiments but also the supercomputing technology performing the numerical simulations beyond the reach of the physical modeling. Numerical models in contrast to physical models are very flexible and avoid the limitations of physical scale. One successful numerical model can provide economic benefits and be applied to the physical cases with environmental conditions that cannot be carried out in the laboratory conditions.

The CFD codes become an important tool to analyze and calculate the parameters for the fluid in given fields by solving the Navier-Stokes Equations numerically via the capacity of workstations or computers. Due to the powerful capacity dealing with the floating point numbers for the updated computers, CFD software has been commercialized as different versions, such as FLOW3D, FLUENT and STARCCM+. CFD techniques, as the interdisciplinary research topics, have been comprehensively reported to successfully apply the fields of engineering.

The commercial CFD code provides an economic way to predict potential results. However, most programs cannot handle scour models in hydraulics because of the complex pattern of the scour procedure under pressure flow conditions. FLOW3D, developed by Flow Science Inc., has a powerful capacity to deal with the scour issues. However, its sediment transport model is based on an empirical formula and this model increases the cost of computational time, thus, the simulation for some cases cannot be finished within a reasonable time.

STARCD/STARCCM+ is an advanced commercial code of CFD. Currently, it doesn’t include any model of sediment transport. However, there are potential features of application to develop the pressurized scour model in STARCD/STARCCM+, such as the moving mesh, porous medium material and user-defined subroutines. This research will focus on the development of a theoretical model and investigate the results by incorporating the sediment transport model into numerical scour model into STARCD/STARCCM+ under a pressure flow condition.

The validity of the numerical model will be verified by experimental data from FHWA.

1.1 Research Background

1.1.1 Sediment Transport in a River Channel

The transport of sediment particles by moving water has two forms: bed load and suspended load. The suspended load may include wash load entrained by the upstream sediment load without the composition and properties of the bed material. In the natural conditions there are three modes of particle motion: (a) rolling and sliding; (b) saltation; (c) suspended motion. The sediment particles will begin rolling and sliding or both along the bed when the bed shear stress just exceeds the critical value for the incipient motion of particles. With increasing bed shear stress or shear velocity, the particles acted on turbulent flow will regularly jump or saltate. Furthermore, when the bed shear velocity exceeds the fall velocity of the particles the sediment particles can be lifted by upward turbulent forces or Reynolds stresses which are of higher magnitude than the submerged weight of the particles.

Bagnold (1973) defines the bed load transport as that in which successive contacts of particles with the bed are strictly limited by the effect of gravity, while the suspended load transport is defined as that in which the excess weight of particles is supported wholly by a random succession of upward impulses imparted by turbulent eddies (Leo 1985), wherein the motion of rolling, sliding and saltation for particles occurs in the bed load transport. Einstein (1950) defines a sub-layer thickness of two particle diameters as the motion region of sliding, rolling in which the sediment particles sometimes may jump only to a longitudinal length of several particle diameters. The bed load layer adjacent to the bed is so thin that the turbulent stress cannot influence the sediment particles, and thus the suspension of particles is impossible in this sub-layer. In addition, Einstein assumes that the average jumping length of saltating particles is a constant of 100 particle diameters, and therefore, the saltation of particles is in the suspension mode of transport. In the present study, Bagnold's approach is followed by many researchers because of its relative simplicity.

Van Rijn (1985) employ the approach of Bagnold in their research on the sediment transport, which means the rolling, sliding and saltation are included in the bed load layer in which the turbulence is of minor importance.

The wavy flow condition in some marine environment results in the evolution of the river bed features, such as erosion, ripples, dunes, sorting and grading. The geographic features in nearly all cases result from interaction of a turbulent flow with the sediment particles on the erodible bed. However, when it comes to the turbulent flow structure, the process of scour becomes coupled with small scale eddies approaching the bed wall. In this case, the accurate physical model becomes impossible to explain all phenomena of erosion. Therefore, the lack of accurate physical models of a number of sedimentary structures produced by bed load transport can be explained by the fact that the motion of mixed grain-size sediment, by rolling and saltation along the bed of a turbulent flow, is an inherently complex problem (Schmeeckle 2003). One of the most famous physical models of bed load transport was produced by Bagnold (1956) who proposes that the sediment particles which obtain sufficient momentum from fluid in the bed load layer remain at the critical threshold motion. Ashida and Michiue (1972) applied this boundary condition to develop a semi-theoretical model of bed load sediment flux in which the dynamic friction coefficient and the critical shear stress are empirically required.

Sediment transport models have been developed by many scholars in the past six decades. Depending on their experimental data, the researchers derived a sequence of empirical or semi-empirical bed load models of which the most famous are the models proposed by Einstein (1942), Meyer-Peter and Muller (1948), Bagnold (1966), Fernandez Luque and van Beek (1976), and Yalin (1963).

Einstein (1942) introduced the idea that the sediment particles move in steps or saltating proportional to their size and defined the bed load layer thickness as twice the particle’s diameter. Also, he used the approach of probability analysis to formulate a relationship for sediment discharge on the bed surface as follows,

$$\frac{q_b}{\sqrt{(S-1)gd_s^3}} = 2.15e^{-0.391/\tau_*}, at\ \tau_* < 0.18 \tag{1.1}$$

and

$$\frac{q_b}{\sqrt{(S-1)gd_s^3}} = 40\tau_*^3, at\ 0.18 < \tau_* < 0.52 \tag{1.2}$$

where q_b is the gravel bed load. S is the specific weight of sediment. g is the gravitational acceleration. d_s is the sediment diameter on the bed surface. τ_* is the dimensionless boundary shear stress or Shields parameter on the river bed, defined as $\tau_* = \tau_0/\rho g(S-1)d_s$, in which τ_0 is the bed shear stress.

Bagnold (1966) developed his expression of a suspended load and bed load based on the energy conservation law. They can be written as,

$$q_{sus} = \omega \frac{e_s U_s}{W}(1 - e_b) \text{ for suspended load} \tag{1.3}$$

and

$$q_{bed} = \omega \frac{e_b}{tan\theta} \text{ for bed load} \tag{1.4}$$

where e_s is the suspension efficiency. e_b is the bed load transport efficiency. U_s is the mean transport velocity of suspended grains. W is the fall velocity of suspended grains. ω is the total flow power per unit boundary area. θ is the dynamic friction angle. Bagnold assigned all of the unknown parameters by experiments. Since the energy loss due to bed load transport has been counted twice, Yang (1986) corrected his suspended load formula as,

$$q_{sus} = \omega \frac{e_s U_s}{W} \tag{1.5}$$

For more accurate application, Bagnold's equation is expressed as,

$$q_{bed} = \omega K_b, K_b = \frac{e_b}{tan\theta} \tag{1.6}$$

and

$$q_t = \omega K \; for \; total \; load, K = \frac{e_b}{tan\theta} + \frac{e_s U_s}{W} \tag{1.7}$$

Most researchers agree with K_b depends on the excess shear stress, $\tau - \tau_c$, but the exact form of this relationship is not clear. Therefore, Bagnold's expression for the bed load transport rate is the function of excess shear stress that is similar to other models.

Meyer-Peter and Muller (1948) developed a complex bed load formula for the representative gravel diameter with the median sediment on the bed surface in the following form,

$$\frac{q_b}{\sqrt{(S-1)gd_{50}^3}} = 8(\tau_* - 0.047)^{3/2} \tag{1.9}$$

where d_{50} is the median sediment diameter on the bed surface.

Fernandez Luque and van Beek (1976) performed a series of experiments for different grain materials to measure the rate of bed load transport q_s^*, the average particle velocity V_{*p}, the rate of deposition determined by the entrainment rate E, and the average length L_{*s} of individual steps of saltating bed load particles as a function of the time-mean bed stress τ_*. Note that q_s^*, V_{*p}, E, L_{*s}, and τ_* are dimensionless parameters. Different downward bed slopes up to 22 degree were configured to observe the alteration of parameters. They found that the rate of particle deposition is proportional to the rate of bed load transport, and the average length of individual particle steps is a constant being independent of the solid density and of the mean bed-shear stress. Fernandez Luque and van Beek ‘s (1976) sediment transport model can be expressed as,

$$q_s^* = 5.7(\tau_* - \tau_{*c})^{3/2} \tag{1.10}$$

$$E = 0.0199(\tau_* - \tau_{*c})^{1/2} \tag{1.11}$$

$$V_{*p} = 11.5\left(\sqrt{\tau_*} - \sqrt{\tau_{*c}}\right) \tag{1.12}$$

$$L_{*s} = 16 \tag{1.13}$$

Yalin (1963) derived a significant sediment transport model for the rate of bed load and used Einstein's (1950) data for 0.8 mm and 28.6 mm bed materials to calibrate two constants, 0.635 and 2.45 in his formula as follows,

$$q_s^* = 0.635s(\tau_*)^{1/2}\left[1 - \frac{ln(1+Cs)}{Cs}\right] \qquad (1.14)$$

where

$$C = 2.45(R+1)^{0.4}(\tau_*)^{1/2}, s = \frac{\tau_* - \tau_{*c}}{\tau_{*c}} \qquad (1.15)$$

where R is the hydraulic radius. τ_{*c} is evaluated from the Shields curve. Similarly, Yalin's equation above is also a function of the excess of bed shear stress.

From the bed load models above, they have a similar form as the function of the deficit between the bed shear stress and the critical bed shear stress. None of these formulas has the capability to accurately describe all of the erosion either in the natural condition or in the laboratory environment although fitting their own experimental data very well. For example, Meyer-Peter and Muller found that the relatively simple relationship for the bed load model, $q_s^* = 8(\tau_* - 0.047)^{3/2}$, fit Meyer-Per's (1934) data with $D = 0.52\ cm$ and $D = 2.86\ cm$ and Gilbert's (1914) data with $D = 0.32\ cm$, $D = 0.49\ cm$ and $D = 0.7\ cm$. Fernandez Luque and van Beek (1976) used a similar equation, $q_s^* = 5.7(\tau_* - \tau_{*c})^{3/2}$, to fit their data for low transport rates. Aside from the lower value of the coefficient, Fernandez Luque and van Beek's equation differs from that of Meyer-Peter and Muller in that the dimensionless critical shear stress is explicitly included, namely, the constant 0.047 in the latter equation is essentially an average value for the dimensionless critical shear stress over the range of sizes employed in the experiments. Yalin also developed his bed load equation by setting the transport rate equal to the product of the concentration of material moving over a unit area of the bed surface and the downstream velocity of the material. The sediment concentration was considered to be proportional to the excess shear stress, $(\tau_* - \tau_{*c})$, and the velocity was confirmed from the equation of motion for a saltating particle. Yalin's equation was calibrated by Einstein's data set. Furthermore, Wilson (1966) fitted a Meyer-Peter and Muller type equation and obtained a larger coefficient, $q_s^* = 12(\tau_* - \tau_{*c})^{3/2}$. The variation of the constant for these expressions suggests that the coefficient that related q_s^* to $(\tau_* - \tau_{*c})^{3/2}$ is a function that increases with shear stress, and hence, a modified version can be $q_s^* = S(\tau_* - \tau_{*c})^{3/2}$, S is a function of $(\tau_* - \tau_{*c})$ with a rough arrange between 5 and 15.

The Meyer-Peter and Muller (1948), Einstein (1950) and Yalin (1963) bed load equations all used some subset of the Gilbert's data (1914) and Meyer Peter's (1934) data to determine the coefficients in their equation.

The other feature is that the range of research on the bed load models is very local, which means that the parameters in models are the average value in space and time and therefore, to some extent, limits the accurate application.

1.1.2 Pressure Flow Scour under a Bridge Deck

Bridges that become inundated during floods are subject to pressurized flow conditions, which can create an aggravated scour situation (Edward 1998).The first study of pressure flow was conducted experimentally at Colorado State University by Abed (1991) in which both piers and bridge decks are configured. She experimentally found that the pressurized flow pier scour can reach 2.3 – 10.0 times greater than free-surface pier scour, which shows us that a submerged bridge deck can be subjected to foundation failures due to the pressurized flow conditions. However, she could not separate the pressure flow effect on scour from the total erosion. Edward (1998) provided their investigation on the pressure flow scour beneath a bridge deck without the localized effects of piers, developing a conceptual relationship between pressurized flow scour and the flow conditions. However, the predicted scour depth did not fit the measured value very well due to the limits of Edward’s theoretical approach.

Guo (2009) theoretically analyzed the specific cases of bridge scour in pressurized flow conditions by dividing them into three cases, i.e. downstream unsubmerged, partially submerged, and totally submerged flow. Based on his analysis, the expression of the equilibrium maximum scour depth was proposed, which has been confirmed by physical experiments with two different decks and two sediment sizes.

Most research on the sediment transport traditionally focuses on the average scour in spatial and temporal scale in open channel flow, and thus, the application for this kind of sediment transport models is very limited. For example, they fail to describe the erosion around some bridge structures in the flow field, such as piers and abutments, because the bridge structures have a significant influence on the flow condition. Also, when the bridge deck is submerged, the traditional models are not effective because the pressurized flow condition for a submerged deck is different from an open channel flow. Therefore, it is necessary to develop different sediment transport models for different cases.

Although some numerical methods are adopted to solve the process of erosion in different flow conditions, such as CH3D-SED (Spasojevic and Holly 1994), FAST3D (Landsberg et al. 1998), and DELFT3D (Delft Hydraulics1999), they cannot accurately describe all cases of sediment transport. In this study, FLOW3D and STARCCM+, as the representatives of the successful commercial CFD codes, are employed to simulate the Guo's (2009) physical experiments in the pressurized flow conditions.

1.2 Objectives of Research

In this dissertation, the objective of research is to develop mathematical equations, namely, continuity and momentum equations, to describe the process of scour development. Based on the current model of the sediment transport and assumptions, the parameters relevant to the sediment transport are determined to numerically solve the governing equations. In addition, the commercial CFD codes, FLOW3D and STARCCM+, are employed to simulate the erosion under a bridge deck in the pressurized flow condition to exam their effectiveness for modeling the sediment transport. The specific objectives from three aspects are as follows.

(a) Examination of the commercial CFD codes, FLOW3D and STARCCM+

When it comes to the simulation for physical phenomena with spatial and temporal scale in hydraulics, we tend to depend on the CFD codes to numerically solve the governing equations. Understanding the applicable limitations of CFD codes will have a positive influence on the development of new models. In this dissertation, FLOW3D and STARCCM+ were used to simulate the pressurized scour to compare the physical experiments.

(b) Pressure drop in porous media

The pressure drop or pressure gradient is an important factor effecting the transport of sediment. In this dissertation, we look the packed bed as a porous media while the bed load layer as the fluidized bed. Therefore, the Ergun equation can be applied to the packed sediment layer as a porous media while it is not correct to use for fluidized bed in the bed load layer. Based on the Ergun equation, the modified Ergun equation will be developed and applied to compute the pressure drop in the momentum equation in the bed load layer.

(c) The thickness of a sediment bed load layer

The determination of the thickness of a sediment bed load layer depends on Fernandez's (1976) model sediment transport, and a standard parabolic path-line of particle at a saltating step. Although the path-line of particles in the bed load layer is a complex spline due to a resultant action of drag, lift, immersed weight, and momentum exchange among particles, the assumption of a standard parabolic trajectory for particles based on the current model of sediment transport simplifies the computation of the thickness of a bed load layer at a saltating step.

(d) A two-layer sediment bed load model

Traditionally, the model of sediment transport for describing a bed load of particles is usually confined in the bed load layer with a thickness of several average-diameter of particle in which the exchange of momentum between fluid and sediment particles occurs. However, the influence on the motion of sediment particles from the packed bed layer under the bed load layer is neglected. Therefore, a two-layer bed load model is proposed to derive the continuity and momentum equation. The two-layer model means the derivation of equations is within the bed load layer and packed sediment layer to predict the erosion process. The coupled continuity and momentum equation represent the influence from porous media or packed bed layer on the motion of sediment particles in the bed load layer.

1.3 Scope of Study

The scholars have developed a series of sediment transport equations based on the understanding for the bed load layer where the motion of particles mainly consists of rolling, sliding, and saltation. The pressurized scour under a submerged bridge deck is seldom researched because this condition is seldom satisfied in a flood event.

This study mainly focuses on the development of a theoretical model to describe the process of sedimentary erosion, and the CFD simulation of sediment scour in pressure flow condition using FLOW3D and STARCCM+. During the derivation for the theoretical model with the two-layer sediment bed load model, the parameters in the continuity and momentum equation, such as the pressure gradient, the thickness of the bed load layer, and the areal concentration of particles, are verified by the modified Ergun equation, and Fernandez's model. The physical experiments for pressurized flow scour under a bridge deck are compared by the numerical results to confirm the effectiveness of the theoretical model.

1.4 Dissertation Outline

The research background for sediment transport is introduced in the Chapter 1 in which the significant achievements from scholars in the bed load and pressure flow scour model are concisely described. Chapter 2 includes literature review in developing physical model and computational models in erosion and sedimentation, pressurized flow scour. Chapter 3 demonstrates the limitation of FLOW3D application to the pressurized scour by simulating the case with a six girder deck. Furthermore, the application of STARCCM+'s morphing feature in the deformation of scour shows the reasonable identification with experimental data. In Chapter 4, the sediment mass conservation and momentum equations are employed to develop a two-layer bed load model. The developed two-layer model is iteratively solved and compared with experimental data in Chapter 5. Chapter 6 summarizes the conclusion of this dissertation and describes the future work to improve the two layer model and apply it into STARCCM+.

Chapter 2 Literature Review

2.0 Overview

Erosion and sedimentation is the natural process of the motion of solid particles throughout geological time. They form the present landscape and morphology but can cause severe engineering and environmental problems. For example, erosion may cause on-site damage to agricultural land reduce the productivity of fertile soils, and cause local scour problems along with serious sedimentation downstream. Bridges spanning rivers and streams can be expected to experience scour problems at bridge piers and abutments. The most common causes of bridge failure during floods are attributed to erosion under bridges or around structures.

The mechanism of sediment motion and sedimentary transport has been developed for decades. It involves three fundamental elements of research, experimental observations, physical patterns (chemistry), and mathematical models (numerical computation). The representative models of sediment transport to describe the threshold condition and the load capacity of sediment particles tend to be empirically developed by experimental observations with time-averaged parameters. The numerical computation can deal with the transient parameters to describe the whole process of erosion. A universal formula to describe the mechanism of particle motion is impossible because of local climate, soil, and terrain. Therefore, it is necessary to develop multiple formula based on local data.

Some fundamental concepts and assumptions have to be clarified when conducting a series of physical experiments and computations, such as bed material load, wash load, and suspended load, otherwise, the experimental results will be very different due to different definitions and assumptions. For example, Yanlin's (1977) empirical formula for the entrainment rate of sediment or pick-up rate is about 10 times that of Einstein's (1950) results because they use a different definition for pick-up concept. In addition, Einstein's definition about bed material load is different from Bagnold's, which leads to different results. Their definition and assumption are stated in the following several sections.

A combination of physical and computational models can be used to obtain a better understanding of the processes under investigation (de Vries 1973). In some specific problems, several considerations between physical and computational models should be made, namely, the nature of the problems, the available resources and costs. The computational sediment transport models involve the numerical solution of a series of governing differential equations, continuity, momentum and energy coupled by the interaction of sediment particles and fluid in the computational domain. With the rapid development of high performance computers and computational fluid dynamics, the computational model of sediment transport has become an attractive tool for study of erosion in different environments such as rivers, lakes and coastal areas. An advantage of computational models is that they can be adopted by different physical domains more easily than physical models, which are typically constructed to represent site-specific conditions (Papanicolaou 2008).

2.1 Incipient of Sediment Transport

The fundamental assumption in modeling sediment transport is involved in the mechanism of incipient motion of sediment transport on the bed surface. On the one hand, the stability of granular material in the river bed depends on the angle of repose at which the motion of particles occurs. The angle of repose equals the sweeping angle of the connected line between a particle center of mass and the contact point around which the particle rotates on the bed surface when the particle center of mass is vertically above the contact point, and thus, the angle of repose depends on the shape of the particle, the size of the particle, and the particle orientation on the bed surface. On the other hand, the flowing fluid exerts forces, initiating the motion of particles, on the particles. The threshold conditions are satisfied when the hydrodynamic moments of forces acting on the single particle balance the resisting moments of force. The hydrodynamic forces consist of the weight of the particle, buoyancy force, lift force, drag force, and resisting force. When the ratio of the active horizontal force to the vertically submerged force, called the Shields parameter, exceeds the critical value corresponding to the initial motion of the particle the particle will be in the submerged incipient motion.

Shields (1936) determined the threshold condition by measuring the Shields parameter at least twice as large as the critical value and then plotted Shields curve marking the permanent trend between Shields parameter and the grain Reynolds number for applying other cases. The critical value was determined as 0.047 that has been widely used for a single size particle at high grain Reynolds number.

Actually, the particle size distribution for bed material can vary with time depending on the local bed shear stress in terms of the mixing sediment particles. It is observed that this process can be divided into three stages: (1) the bed material keeps its original distribution of grain size without any motion of the fines at the low bed shear stress; (2) when the bed shear stress increases, the finer particles are entrained with water flow, the bed surface becomes coarse to form an armor layer; (3) finally, all fractions of sediment particles are moved by the sufficiently large shear stress to break the armor layer. It means that an armor layer can only form in well-sorted bed surface on which the finer fractions will be present in the mixture as long as they are shielded by the stable coarser sediment particles as the armor layer. However, all particles will be in the status of motion as long as the bed shear stress exceeds the incipient condition for the coarser sediment particles. Usually, we neglect the influence of the armor layer on the erosion for the uniform size of particles. In this dissertation, only the assumption of uniformity is applied.

The mechanics of bed forms have an important influence on the incipient motion of sediment particles. When sediment particles enter motion, the random patterns of erosion and sedimentation bring very small perturbations of the bed surface elevation. These small perturbations develop with time into the various surface of bed called bed forms. Bed form depends on the main flow characteristics as well as the near-bed flow condition, and thus, it increases the complexity of the threshold condition of particles. The bed forms generally can be classified into eight types identified by Simons and Richardson (1963): a) horizontal bed with clear water flow; b) typical ripple pattern varying from nearly triangular to almost sinusoidal; c) dune pattern much larger than ripple; d) washed-out dunes; e) horizontal bed with wash load of sediment particles; f) Anti-dunes, breaking waves; g) chutes and pools. Types a-d are in the subcritical condition and the sediment transport is relatively low because the particles on the bed move primarily in contact with bed surface. In contrast to the types a-d, types e-h are in the supercritical condition and the bed material transport is high because the contacting particle discharge is continuous, and the suspended sediment concentration is large. Therefore, the total resistance is separated into the grain resistance acting on the individual particle and the form resistance due to bed form configuration.

When it comes to the incipient condition of sediment, it is necessary to provide a mechanistic description of bed load transport. For the uniform equilibrium condition, this mechanism has invariably fallen into two groups. One is the specification of an entrainment rate of particles into bed load transport (pick-up function) as a function of boundary shear stress and other parameters proposed by Einstein. The other one is based on the Bagnold's assumption that a relation for the areal concentration of bed load particles as a function of boundary shear stress derives automatically from the imposition of a dynamic condition at the bed, according to which the fluid shear stress drops to the critical value for the onset of sediment motion. Bagnold's condition of constraint, however, suffers from several limitations as described by Parker (2002): a) the mixing sediment particles on the bed surface have the less mobile than the finer particles which means that the individual size classes have different critical shear stress, therefore, Bagnold's constraint fails to apply in such cases; b) Bagnold's constraint cannot cover the non-equilibrium conditions pertaining to relaxation effects because the bed load transport does not respond immediately to a change in imposed shear stress, but instead has a characteristic time of relaxation.

Seminara (2002) proposed that the straightforward extension of the Bagnold hypothesis to the case of arbitrarily sloping bed is impossible. Preserving the structure of Bagnold's assumption, the equilibrium condition is replaced with that when the entrainment rate of bed particles into the bed load layer equals the deposition rate of bed load particles onto the bed, not when the fluid shear stress at the bed reaches the threshold value. Therefore, the entrainment hypothesis described above, similar to Einstein's structure, is actually a dynamic equilibrium condition, namely, the entrainment equals deposition, rather than a static equilibrium at which no bed particles can be entrained at all (Parker 2002). The entrainment hypothesis avoids two limitations of Bagnold's constraint condition. For example, the differential transport of different sizes in a mixture of sediment can be presented by introducing an implicit function into the entrainment function. The non-equilibrium condition is satisfied when the entrainment rate is not equal to the deposition rate.

The incipient condition of particles and sediment bed load depend significantly on the bed slope. The representative experiment was performed by Fernandez and van beek (1976). Experiments using uniform sediment were conducted with two sand sizes (0.9 mm and 1.8 mm) and one gravel size (3.3 mm). The walnut shell grains (1.5 mm) and magnetite grains (1.8 mm) were also tested during experiments. Tests for all five materials were conducted on stream wise slope with 0^o , 12^o, 18^o, and 22^o in the absence of a transverse slope at low transport rate. Fernandez and van's main empirical results can be expressed in Eq.5.23 – Eq.5.25 in which τ_{*c} is estimated by the following formula,

$$\tau_{*c} = \tau_{*co} cos\alpha \left(1 - \frac{tan\alpha}{\beta_\mu}\right) \tag{2.1}$$

in which τ_{*co} denotes the critical Shields stress on a horizontal slope, α is the bed slope angle, and β_μ is a static coefficient of friction between particles and bed surface.

Seminara, Solari and Parker (2002) developed a general expression for the critical Shields stress and particle velocity with an arbitrarily sloping bed. If neglecting the effect of lift, the critical Shields stress on a transverse slope bed can be expressed as follows,

$$\tau_{*c} = \tau_{*co} cos\varphi \left[1 - \frac{(tan\varphi)^2}{(\beta_\mu)^2} \right]^{0.5} \tag{2.2}$$

in which φ is the transverse slope angle. The expression formula for the particle velocity is a very complex vector equation which is not conveniently applicable, and hence, Francalanci and Solari (2008) numerically employed a power function of the Shields stress ratio between the real bed Shields stress with the bed slope and the critical Shields stress with the horizontal bed to fit Seminara, Solar and Parker's complex vector expression. It is confirmed that the power function is accurate and convenient enough to approximate the vector expression.

How to reasonably express the hydrodynamic equations for describing the process of erosion with time is an important topic in hydraulics. Generally, two categories of sediment transport model equations are used to simulate the motion of sediment in natural river bed. The first one separates sediment into bed load and suspended load according to empirical methods. For instance, the Exner equation is adopted to predict the motion of bed load particles by ignoring the time rate of change of the sediment concentration. An advection-dispersion equation is used to describe the motion of suspended load usually by assuming that the sediment particles transport at the same velocity as the flowing fluid, as the dynamic equations developed by Spasojevic and Holly (1990).

The other category simulates the motion of bed load and suspended load by coupling them into a single equation, as the modeling equation proposed by Wu (2004) and Armanini and Di Silvio (1998).

2.2 Sediment Transport Models and Pressure Flow Scour Model

2.2.1 Sediment Transport Equation

A number of computational sediment transport models have been developed. Generally speaking, these models can be classified in terms of the applicable range (e.g., suspended load and bed load); and the expression in the spatial and temporal continua (e.g., one dimensional models, two dimensional models and three dimensional models). The choice of a certain model tends to depend on the nature of specific problems, the model capabilities, and data availability for calibration. Several important sediment transport models are briefly described as follows.

Kalinske (1947) expressed the rate of bed load transport as a product of the number of particles of motion, the average velocity of the bed load particles, and the particle volume. He assumed that the areal bed load concentration, defined as the total projected area of particles in motion, is a constant value of 0.35. Fernandez (1974) found experimentally, however, that the areal bed load concentration increases linearly with the difference between the average bed shear stress and the critical bed shear stress at the threshold of particles.

Einstein (1950) was the first to use the approach of probability in developing a bed load function for non-uniform sediment. Einstein (1950) proposed the rate of bed load transport as a function of the number of eroded particles per unit area and time, the particle volume and the average distance covered by the bed load particles from the moment at which they are eroded until deposited on the bed. Einstein developed the relation between this distance and the probability of a saltating particle being deposited. He made an assumption that the addition of this probability for a saltating particle being deposited and the probability of a particle eroded on the bed surface at any time is equal to one, and concluded that the total average distance for a saltating particle must increase with increasing bed shear stress. However, Fernandez (1974) found that this total average distance is independent of the time-average bed shear stress based on his experimental analysis, which means that these two probabilities for a particle eroded and deposited are not relevant. Einstein (1950) ‘s approach for applying the theory of probability is still regarded as one of the most thorough in its mathematical treatment and consideration of associated factors (Sun 2000) although its application can be imprecise.

Bagnold (1956) derived a bed load transport model based on the work done by the fluid to entrain the sediment. He assumed that the turbulent bed shear stress equals the critical bed shear stress at the threshold of sediment motion for low bed load concentrations while the turbulent bed shear stress may be neglected for high bed load concentration. However, Fernandez (1974) found that at low bed load concentrations the turbulent bed shear stress equals to the total bed shear stress, not the critical bed shear stress, and at high bed load concentrations, the turbulent bed shear stress must be equal to the critical bed shear stress at the initiation of continuous scour without a bed load. Bagnold (1966) developed a sediment transport equation according to the principle of energy conservation, namely, rate of work done by the flowing fluid on the sediment equals to the product of available power and efficiency. However, as Yang (1986) pointed out in the Bagnold’s suspended load and the total load transport equations, the energy loss due to bed load transport has been counted twice, and thus Yang (1986) gave the correct expression of these equations in his paper.

Yalin (1963) gave a model of the rate of bed load transport based on dimensional analysis and the dynamics of the particles' saltation. He assumes that the particle reaches its maximum height of saltation owing to its initial velocity but the continuous driving force from fluid. However, Fernandez (1974) found that the particles were transported nearly in suspension over most of their trajectory, which means that Yalin's assumption is not reasonable. In addition, Fernandez experimentally found that both the vertical and horizontal accelerations of the particles were very low compared with the acceleration due to a drag force equal to their immersed weight, which implies that the saltating grains experience a lift force from the shear flow over most of their trajectory.

A different sediment transport model tends to naturally depend on some different assumptions and classifications for the sediment load. For example, Einstein defines the saltation of particles belongs to the suspended load. However, Balgnold includes it into the sediment bed load. Gao (2008) studied the transition between two bed load transport regimes by assuming the bed load layer includes the saltation and sheet flow. The saltation regime is characterized as low bed shear stress where sediment grains rolling, sliding, and saltation on the bed surface. The sheet flow regime occurs at high shear stress where the bed particles are entrained by a combined formation of saltation and sheet flow. This sheet flow regime was also verified by Leeder (1979), Hanes and Bowen (1985), Asano (1992), and Bakhtiary (1997). It is a granular fluid flow in which the sediment particles collide with other ones and the bed is completely mobile. If the sheet-flow bed load occurs in the bed load layer, it will have a significant influence on the accuracy of a sediment transport model that does not take it into consideration

2.2.2 Pressure Flow Scour Model

Pressure flow generally exists in a closed system and the driving force for flowing mainly comes from the pressure difference between upstream and downstream like pipe flow. In open channel flow, the region underneath a submerged bridge deck can be considered to be closed, so we call this condition pressure flow.The process of sediment transport is difficult to be successfully described by some analyzed solutions. The scour mechanism tends to be researched in combination with empirical formula. According to the characteristics of flow field, bridge scour can be classified into local and pressure-flow or vertical-contraction scour. Local scour is defined as the dynamic process of erosion to the bed material around piers, spur dikes, abutments and other structures on the river bed. Vertical-contraction scour may occur when the water surface elevation upstream of a bridge rises above the bridge low chord, and the flow experiences a vertical contraction that increases the cross-sectional velocity and possibly sediment transport capacity (Lyn 2008).

The research for pressure scour is still primitive, thus, very little literature was referenced. Arneson and Abt (1998), Umbrell *et al* (1998), Lyn (2008) reported their achievements. Guo (2009) contributed his significant accomplish for the pressure flow from the original views based on the study of Umbrell *et al*. To better understand the pressure flow scour, the following section compares their scour models under the pressure flow condition.

Although the pressure flow condition may not frequently occur because of design practice for 100 years or more, this issue has been proposed to predict scour in extreme flood events. Arneson and Abt (1998) published their experimental results, and analysis for pressure flow scour is expressed as

$$\frac{y_s}{y_1} = a_1 + a_2\left(\frac{y_1}{H_b}\right) + a_3\left(\frac{y_1}{H_b}\right)^{-1} + a_4\left(\frac{V_a}{V_{uc}}\right) \tag{2.3}$$

where y_s = equilibrium depth of scour; y_1 = upstream depth; H_b = bridge opening between the bridge low chord and the bed prior to scour; and V_a = flow mean velocity through the bridge opening. Arneson determined the constants from laboratory data, $a_1 = -5.08$; $a_2 = 1.27$; $a_3 = 4.44$; $a_4 = 0.19$. The critical velocity of incipient sediment, V_{uc}, can be estimated by Neill(1973) equation,

$$V_{uc} = 1.52\sqrt{g(s-1)}\left(\frac{h_u}{d_{50}}\right)^{\frac{1}{6}} \tag{2.4}$$

where g = gravitational acceleration. s = specific gravity of sediment. d_{50} = median diameter of sediment particles.

Eq.2.3 has a spurious correlation, as Lyn (2008) stated, it exhibit unsatisfactory behavior due to an ill-chosen original model equation. Lyn presented a power-law relationship with an asymptotic constant value, as an alternative model, in clear-water conditions. Lyn's model is expressed as

$$\frac{y_s}{h_u} = min\left[0.105\left(\frac{V_a}{V_{uc}}\right)^{2.95}, 0.5\right] \tag{2.5}$$

Umbrell *et al.* (1998) studied the scour caused by pressure flow underneath a bridge deck without piers and abutments. A conceptual relationship based on continuity equation was developed as follows,

$$\frac{y_s + h_b}{h_u} = \frac{V_u}{V_{uc}}\left(1 - \frac{w}{h_u}\right) \tag{2.6}$$

where h_u = water depth before scour. y_s = maximum scour depth. h_b= bridge opening prior to scour V_u = approaching velocity upstream. w = overtopping depth of bridge deck and partially inundated flow condition occurs when $w = 0$. V_{uc} = critical threshold velocity of sediment, estimated by Eq.2.4.

Umbrell *et al* modified Eq.2.6 using their experimental data as

$$\frac{y_s + h_b}{h_u} = 1.102\left[\frac{V_u}{V_{uc}}\left(1 - \frac{w}{h_u}\right)\right]^{0.603} \tag{2.7}$$

The factor in Eq.2.4 is changed from 1.52 to 1.82 for calculating the critical velocity, V_{uc}, in Eq.2.7. As Guo (2009) stated, this model raises two questions, a) the critical velocity under the bridge deck is not necessarily equal to the one upstream; b) The equilibrium time of scour, 3.5 hrs, were employed from their experimental results, however, Lianjun's experimental results from FHWA showed that the equilibrium of scour occurs when it reaches 36 – 48 hrs.

Guo (2009) contributed his research on the pressure flow scour under a bridge deck. He classified this phenomena into three cases based on the flow condition upstream, 1) the bridge deck is slightly submerged upstream or the flow is supercritical downstream; 2) the low chord of deck downstream is partially inundated, which is rapidly varied pressure flow as outlet control orifice; 3) the deck is fully submerged, and divides the flow field into two parts, one can be called weir flow, the other one called orifice flow controls the scour depth.

Based on the experimental data, Guo empirically derived the pressure-flow scour profiles under the six-girder deck as follows,

$$\frac{y}{y_s} = -exp\left(-\left|\frac{x}{W}\right|^{2.5}\right) \text{ for the region upstream} \tag{2.8}$$

and

$$\frac{y}{y_s} = -1.055exp\left(-\frac{1}{2}\left|\frac{x}{W}\right|^{1.8}\right) + 0.055 \text{ for the region downstream} \tag{2.9}$$

The comparison of similar Eq.2.8, Eq.2.9 to experimental results in Fig.2.1 indicates very good agreement for $x \leq 0$, but an overestimation of most scour profiles for $x > 0$.

The horizontal location with maximum scour depth, y_s, is defined as the separation point between the region upstream and downstream. y_s is resolved by the following general solution for case 2 and 3,

$$y_s = (h_b + a)\sqrt{\frac{1 + \frac{\lambda}{F^m}}{1 + \frac{2\beta}{F^2}}} - h_b \tag{2.10}$$

where λ, m, β are constants which can be determined by experimental data.

$$a = min\{h_u - h_b, b\} \tag{2.11}$$

$$F = \frac{V_{ue}}{\sqrt{g(h_u - h_b)}} \tag{2.12}$$

$$V_{ue} = V_{uc} \left(\frac{h_b + a}{h_u} \right)^{0.85} \tag{2.13}$$

Guo (2009) derived the analyzed solution for case 1. As he stated, case 1 is only a short transition to case 2 because of the deposition downstream making the downstream deck submerged shortly. Fig.2.1 and Fig.2.2 shows the comparison between experimental data and theoretical analysis by the non-dimensional method.

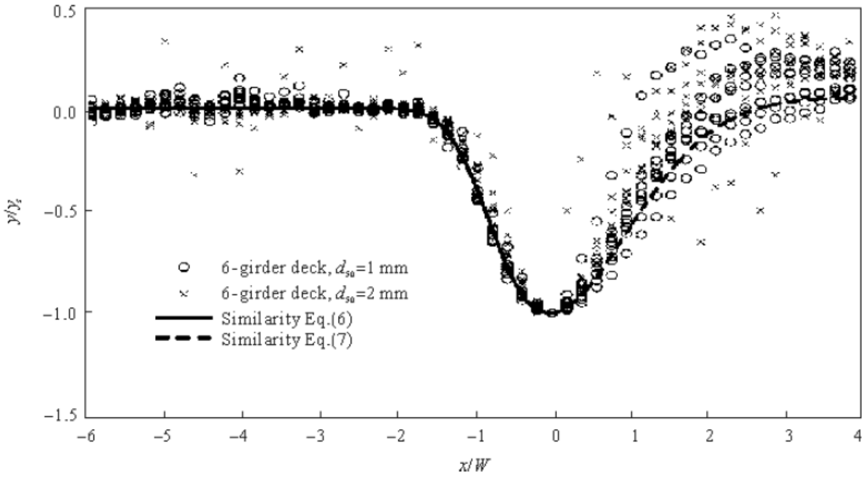

Figure 2.1 Experimental pressure scour data for different girders from Guo (2009).

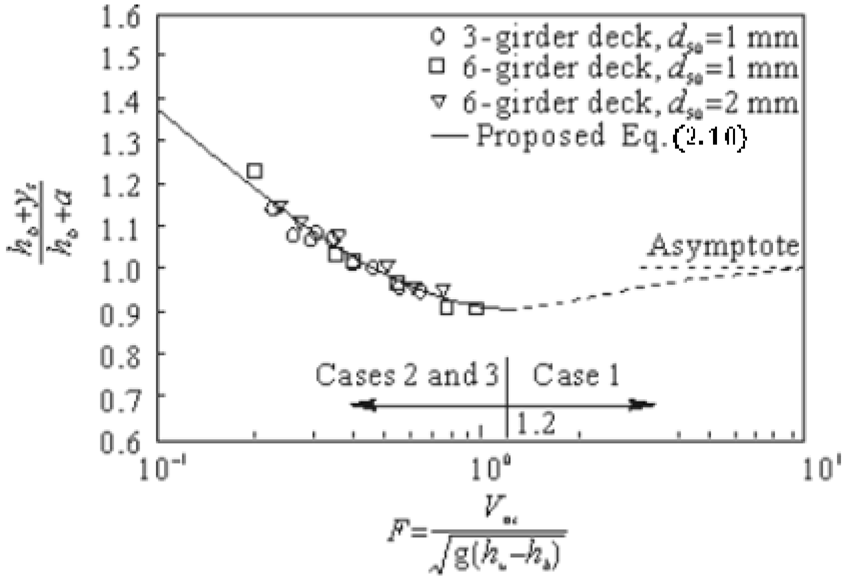

Figure 2.2 Comparison between experiment results and theoretical analysis.

We often demand inspecting the process of erosion with time and space by coupling the sediment transport model into Navier-Stokes equations. Nevertheless, it is often impossible to obtain the analytical solution for this difficult set of equations, and hence, we use numerical methods to compute these coupled equations.

One dimensional models have been successfully adopted in the theoretical research and engineering practice. The representative models of sediment transport are formulated by the conservation equations of mass and momentum of flow along with sediment mass continuity equation as the Exner equation, MOBED by Krishnappan (1981), IALLUVIAL by Karim and Kennedy (1982), DEDICOUP by Holly and Rahuel (1990), 3ST1D by Papanicolaou (2004), and HEC-6 by Thomas and Prashum (1977). Although most of the one dimensional models have capabilities to predict the bulk velocity, water surface stage, bed elevation and sediment transport load in a particular channel, the limitation of capabilities is obvious, for example, 3ST1D cannot separate the total sediment load into bed load and suspended load, HEC-6 are not applicable to unsteady flow conditions. The one dimensional models remain effective tools in rivers and stream applications because of their low requirements for the sources or cost.

The two dimensional models (2D models) have been applied to the hydraulic engineering as guided user interface (GUI) to allow the configuration of pre- and post-process. Most 2D models numerically solve the depth-averaged continuity and Navier-Stokes equations coupled with the continuity equation of sediment mass. For instance, SURENCH-2D developed by van Rijn and Tan (1985) for simulating sediment transport with bed level change by solving Navier-Stokes equations with the general advection-diffusion equations and the settling of sediments. The model has capabilities to deal with the flow conditions of combined quasi-steady currents and wind-induced waves over a sediment bed. MOBED2 developed by Spasojevic and Holly (1990) can simulate water flow, sediment transport, and bed evolution in natural waterways. FAST2D (Minh Duc et al. 1998) is a finite volume hydrodynamic and sediment model to simulate sediment transport and scour problems in alluvial channels. FLUVIAL 12 by Chang (1998) and DELFT-2D (Walstra et al. 1998) is a mobile-bed model and simulates bed load and suspended load transport. CCHE2D developed by Jia and Wang (1999) can simulate the suspended sediment by solving the advection-diffusion equation and the bed load transport by empirical functions (e.g., Yalin 1972; van Rijn 1993).

The three dimensional models (3D models) can be applied to the many problems in which 2D models are not suitable. For example, 2D models do not adequately represent the physical features in the vicinity of piers and near hydraulic structures. The 3D sediment transport models solve the continuity and the Navier-Stokes equations coupled with the equations of sediment mass by the numerical methods of finite difference, finite element, or finite volume. CH3D-SED (Spasojevic and Holly 1994), FAST3D (Landsberg et al. 1998), DELFT3D (Delft Hydraulics 1999) as the 3D models allowed to simulate bed load rate, suspended load rate for steady or unsteady flow conditions by solving a series of differentiate equations with the physical models of sediment transport. With the rapid improvement of computing capacity, more features and models will be incorporated into 3D sediment transport models to attain the accurate simulation of erosion, especially for the scour process in the complex flow condition.

In many applications, however, the essential model limitations reduce accurate simulation. For example, the eddy viscosity models are frequently used to solve the governing equations of turbulent flow including some empirical formulations compounded for empirical sediment transport models. As a consequence, this combination of empirical formulas, at the present stage, cannot accurately and reliably describe the two-phase phenomenon of sediment and flow. In addition, the computational sediment models typically encounter a series of problems affecting the accuracy of simulation as the determination of reference concentration of sediment near the bed, the sediment diffusion term because of turbulent flow and the source term of the advection-diffusion equation.

2.3 Numerical Methods

The rapid development of computational capacity provides a powerful research tool to solve interesting engineering issues. It is cost efficient. Numerical laboratory extends the application of engineering to new level from traditionally physical one. In this research, the major objective is to find an effective and efficient method to predict the process of pressure flow scour, therefore, computational fluid dynamics (CFD) will be as the medium to apply scour issues.

Traditionally, program codes have been written based on the serial computation running on a single computer having a single central process. A problem is broken into a separate series of instructions executed one after another and only one instruction one time. However, the serial computation cannot satisfy the demand to process a huge amount of data, therefore, parallel computing is proposed and applied to the computational field. It is the simultaneous use of multiple compute tasks to solve a practical problem running multiple processors or CPUs. The sub-parts of a problem are solved concurrently and a series of instructions can be applied to each part executed simultaneously on different CPUs. Currently, many commercial CFD programs have this parallel feature to save computational time, such as FlOW3D and STARCCM+, therefore, FLOW3D and STARCCM+ sufficiently take advantage of multi-cores techniques at TRACC to achieve the computational tasks more efficiently.

2.3.1 Model Choice

When it comes to the computational simulation for sediment transport, incorporating a certain degree of simplification into sediment transport models can be acceptable because increasing the model complexity may complicate the problem formulation and require more input parameters, calibration, and computational costs. The trade-off between the model complexity and costs has been illustrated by Overton and Meadows (1976) and Simons (1996).

In general, the rule of choosing a dimension of model (1D versus 2D or 3D) should be in the way that the model components in the chosen dimension retain all relevant terms in a specific problem. Church (2006) provided a guideline for the simulation dependent on the different spatial and temporal scales, as shown in Fig.2.2, a 1D or 2D model may be reasonable to simulate the morphologic scale changes at the basin scale typically occurring over a 1-year period. For the simulation of channel reach and sediment transport with smaller length scales, however, Fig.2.3 indicates that a reference time scale for these problems ranges from seconds to an hour and the function of turbulent flow cannot be neglected. Therefore, 3D models should be adopted to solve the problems related to turbulent microstructure with smaller scales.

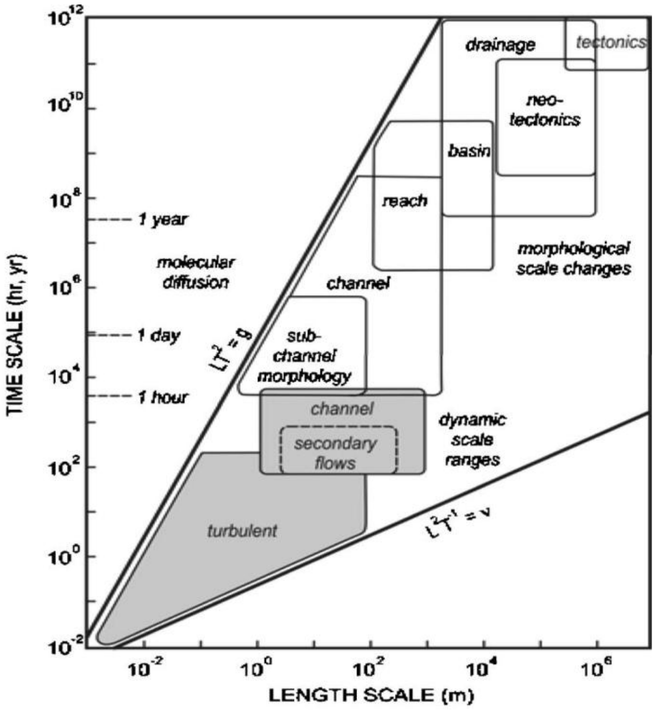

Figure 2.3 Simulation illustration in spatial and temporal Scales (Church 2006).

2.3.2 Model Calibration

Field data as model input and calibration frequently arises some questions: are these data acceptable or collected correctly? For example, the sediment transport as one of the most challenging topics encountered by the hydraulic engineer requires the measurements of bed bathymetry, stages, grain size distributions. The traditional point or cross-sectional measurements in a river channel environment with mobile bed, taken by acoustic Doppler velocimeter (ADV) or acoustic Doppler current profiler (ADCP), are not adequate for capturing the flow distribution at a certain cross section because of bed form propagation, which means that the traditional approaches are adaptable to static conditions. With the development of electronic sensor technology, however, the techniques of sediment measurements may alleviate the limitations of sampling data to calibrate and verify the models.

The other issue mentions the grid refinement and grid sensitivity of computational domain. For example, are grid-independent tests necessary and practical? Can a coarse grid lead to misleading results? What is the optimum grid size for capturing turbulence-resolving scales (Athanasios 2008)? Fortunately, improved computing facilities allow better grid refinement and 3D simulation.

2.3.3 Model Limitations

A mismatch frequently exists in the theoretically computational results and sediment transport models, which is attributed to the fact that turbulent modeling appropriately cannot represent the flow features in the hydrodynamic equations. For example, all turbulent fluctuations in turbulent models (e.g., RANS) are locally averaged in temporal and spacious scales, which lead to the loss of important information. The other two turbulent models, DNS and LES, are better applicable for simulating complex turbulent flows. DNS requires enormous computing costs and is limited to low Reynolds numbers as a valuable research resource for studying the transition from laminar to turbulent flow. LES can be used at low and high Reynolds numbers by capturing the larger scale turbulent structures by solving 3D unsteady Navier-Stokes equations. The smaller scale turbulent structures are modeled by special near-wall treatment. Despite the limitations that LES may have especially for high Reynolds numbers, LES is the most advanced modeling tool currently available for modeling 3D complex flows (Mahesh et al. 2004). Actually, both DNS and LES allow the realistic prediction of complex eddies around structures, such as piers, fish ladders and dams.

The simulation of the sediment transport processes is controlled by not only randomness in flow but also by irregularities in land form and bed surface geometry.

Therefore, the sediment transport models developed so far are not universal. Currently, the models of sediment transport are based on some assumption of limitations. One of them is that sediment incipient is not dominated by the turbulent flow near the bed but by the excess shear stress term, $(\tau - \tau_c)$ in which the shear stress τ is determined by assuming uniform flow conditions. However, recent findings have shown that turbulent sweeps, outward interactions, and ejections are the primary triggering mechanisms of sediment entrainment (Papanicolaou et al. 2001). The excess shear stress models and settling velocity models as the representative traditional approach in developing sediment transport model have been to apply to the transport rate. These approaches use the median size of sediment as the characteristic parameter, and thus under-predict or over-predict the transport rate of individual fractions. Furthermore, some models adopt uncoupled or semi-coupled approach to separate flow and sediment so that bed form and material have an approximate influence on the flow field. The spatially averaged inner and outer variables for the traditional treatment of the dispersion and diffusion coefficients, such as the shear velocity, depth-averaged velocity, channel width and mean flow depth, may not be good approximations in channel contraction or expansion and external flow condition (e.g., flow around hydraulic structures). Most of sediment transport models do not account for the source term caused by the bed slopes. Minimizing error in the prediction of sediment transport model requires the connection of the bed slopes with in-stream hydrodynamics by the new technologies, such as GPS, biogeochemical tracers, and remote sensing.

Another important limitation of model for sediment-flow (two-phase flow) interaction processes is that certain terms in the governing equations that are typically neglected in other fields may require a different treatment. For example, the stress between fluid and sediment particles is usually neglected when it is much smaller than the turbulent stress between fluid particles. Similarly, the stress between sediment particles is neglected when sediment particles do not touch one another. The two neglects above are doubtable in the case of high sediment concentration (Papanicolaou et al. 2001). In addition, the two-phase flow governing equations requires the additional modeling based on knowledge of turbulence and experimental data to achieve system closure.

Chapter 3 Analysis for Limitation of FLOW3D and STARCCM+ in Application of Sediment Transport

3.0 Overview

The commercial CFD code, FLOW3D was employed to simulate the procedure of scour beneath the bridge deck. FLOW3D has a powerful capacity to investigate the behavior of liquids and gases specializing in the solution of transient, free-surface problems and sediment transport. It uses a non-hydrostatic finite difference model to solve the 3D Navier-Stokes equations.

In this dissertation, the capacity of FLOW3D to simulate the bed scour was examined to determine the affectivity and efficiency of the model. The two dimensional model was created so as to reduce the computational cost of time instead of three dimensions. FLOW3D software was installed and remotely accessible on the ANL-TRACC clusters which makes the parallel tasks of computation possible. All the configurations of numerical model were based on the data and conditions of the physical experiments. Cell sensitivity analysis was performed to obtain reasonable velocity gradient associated with the distribution of the bed shear stress.

Although there is no sediment transport model in STARCCM+, the moving mesh theme as the potential approach is capable of achieving the simulation of ‘river bed’ erosion or distortion by applying the user-defined field function. The field function as a user-define parameter is computed by a sediment transport model developed by user. Furthermore, the time step size related to the entrainment rate is variable with the computation to satisfy the convergence of solution. Therefore, STARCCM+

potentially can be employed to visualize the erosion profile and analyze the effectiveness of a pick-up function.

3.1 Sediment Transport Model in FLOW3D

The sediment scour model in FLOW3D can predict the movement of the packed and suspended sediment, which applies to the erosion around bridge piers and other interested structures. The model has two important modules, drifting and lifting, as described by Brethour J.(2003). Drifting models produces the driving force on the sediment particle to be suspended in the flow, which is called the drift-flux model. Lifting model functions as the lift force produced by the local bed shear stress to separate the particle from the sediment bed. The sediment behavior is controlled by the drag model. When the sediment concentration exceeds a cohesive solid fraction defined by users, it behaves as the solid and the drag model is activated.

In FLOW3D, the distribution of sediment in flow field consists of the suspended and packed sediment. Suspended sediment particles are advectional and drifting; packed sediment particles without the advection can move only if they become suspended when lifting and drag models initialed particles. The fluid viscosity increases as the concentration of the suspended sediment increases. When the solid or sediment concentration reaches or exceeds the cohesive solid fraction, it will not have any influence on the alteration of the fluid viscosity. At that point, the solid-like behavior of sediment occurs, which is reflected by the interaction among particles. An additional linear drag term to the momentum equation, $-K\boldsymbol{u}$, predicts the solid-like behavior as follows (Flow3D User Manual) ,

$$\frac{\partial \boldsymbol{u}}{\partial t} + \boldsymbol{u} \cdot \nabla \boldsymbol{u} = -\nabla P/\bar{\rho} + \nabla \cdot \boldsymbol{\tau}/\bar{\rho} + \boldsymbol{g} - K\boldsymbol{u} \tag{3.1}$$

where the average density $\bar{\rho}$ on the packed sediment bed is calculated from,

$$\bar{\rho} = \rho_l + f_s(\rho_s - \rho_l) \tag{3.2}$$

In which ρ_l and ρ_s is the local density of liquid and sediment particles, respectively. $\boldsymbol{\tau}$ is the shear stress due to the fluid viscosity. K is the drag coefficient among particles, which can be calculated by the following formula based on the assumptions of the solid-like behavior,

$$K = \begin{cases} 0 & for\ f_s < f_{s,co} \\ \left(\frac{f_{s,cr} - f_{s,co}}{f_{s,cr} - f_s}\right)\left(\frac{f_{s,cr} - f_{s,co}}{f_{s,cr} - f_s} - 1\right) & for\ f_{s,co} < f_s < f_{s,cr} \\ \propto & for\ f_s > f_{s,cr} \end{cases} \tag{3.3}$$

In which f_s is the solid fraction of the sediment. $f_{s,co}$ is the cohesive solid fraction over which the interaction among particles occurs and fluid viscosity does not increase with the sediment concentration. $f_{s,cr}$ is the critical solid fraction over which the fluid flow ceases and behaves as the solid mass.

The local velocity vectors of particles have two components, u_{drift} and u_{lift} , modeled by the following equations (Flow3D User Manual),

$$u_{drift} = \frac{f_l d^2}{18\mu} \frac{\nabla \mathrm{P}}{\bar{\rho}} (\rho_s - \rho_l) \tag{3.4}$$

$$u_{lift} = \alpha n_s \sqrt{\frac{\tau - \tau_{crit}}{\bar{\rho}}} \tag{3.5}$$

where d is the mean sediment diameter, μ is the liquid viscosity (increased by the turbulent viscosity in the turbulent model), which can be obtained from,

$$\mu = \mu_l \left(1 - \frac{min\left(f_s, f_{s,co}\right)}{f_{s,cr}}\right)^{-1.55} \tag{3.6}$$

μ_l is the molecular viscosity of the liquid. The formula above illustrates that the average viscosity of fluid will increase as the solid fraction or sediment concentration increases until the solid fraction is equal to the cohesive solid fraction where the solid-like model activate and the fluid viscosity cannot increase; when the solid fraction is equal to the critical solid fraction, the fluid viscosity become infinite meaning that the complete status of solid forms, which is identical to the model of the drag coefficient.

f_l is the liquid fraction, u_{drift} become zero in the regions of $f_l = 0$. α $(0 < \alpha < 1)$ is a factor of probability of a particle's lifting from the packed sediment surface. n_s is the normal vector to the bed surface. τ_{crit} is the critical shear stress required to friction the particle away from the packed sediment interface, which is modeled by the critical Shields number,

$$\theta_{crit} = \frac{\tau_{crit}}{g(\rho_s - \rho_l)d} \tag{3.7}$$

The drifting model as the suspended bed model assumes that the suspension and advection dominate the transport of most sediment particles away from the packed bed interface. The scour depends on the shear stress of fluid, the critical shear stress starting the erosion and the difference of density between the fluid and solid particles. In FLOW3D, the sediment concentration closed to the sediment interface is a function of $(\tau - \tau_{crit})^{1.5}$. The lifting model simulates the bed-load movement and predicts the local flux of sediment eroded on the packed bed interface. Generally speaking, the sediment flux occurs when the normalized bed shear stress is higher than the critical value.

An important parameter is called the angle of repose producing the influence of the bed slope on the threshold movement of the packed sediment particles in a static flow region. A low angle of repose provides the easier condition to slide along slopes while a high angle of repose has the particles more difficultly start. In the sediment erosion model of FLOW3D, the angle of repose as a constant can be defined by user. The critical shear stress in the slope interface of sediment is dependent on the ratio of the actual slope to the angle of repose as follows,

$$\tau_{crit} = \tau_{crit}^{0}\sqrt{1 - \frac{sin^2\varphi}{sin^2\omega}} \tag{3.8}$$

where τ_{crit} is the critical shear stress on the packed sediment bed with a slope, τ_{crit}^{0} is the critical shear stress with a horizontal bed. φ is the actual angle between the normal vector of the bed interface and the gravity vector. ω is the angle of repose. When $\varphi = \omega$, the locally critical shear stress, τ_{crit} , is equal to zero, which means that any disturbance from the flow region can drive the sediment particles to slide along the slope; when $\varphi = 0$, the locally critical shear stress is restored to the critical value with the horizontal slope.

In FLOW3D, the advection-diffusion equation is employed to model the motion of the suspended sediment in the flow domain as follows,

$$\left(\frac{\partial C_s}{\partial t}\right)_x + \boldsymbol{u}\cdot\nabla C_s = D\nabla^2 C_s - \boldsymbol{u_{lift}}\cdot\nabla C_s - \boldsymbol{u_{drift}}\cdot\nabla C_s \tag{3.9}$$

in which $\boldsymbol{u}$ is the local velocity of advection. C_s is the local concentration of the suspended sediment. D is the diffusion coefficient. In the advection-diffusion equation, two additional items originate from the influence of the drifting and lifting of the sediment. $\boldsymbol{u_{lift}}$ is zero in the region where the local shear stress cannot exceed the critical value, τ_{crit}, so there is no influence of lifting on the motion of the suspended sediment in the most flow domain except in the vicinity of the packed sediment interfaces.

There are several limitations in the sediment scour model in FLOW3D although it can be adopted to simulate the phenomena of scour. (a) Too large sediment diameter fails the drifting model, successful prediction become impossible (b) No bed load model available to simulate the saltation load. (c) Non-uniform sediment particles are not included in the range of the simulation.

3.1.1 Case Analysis and Limitation

FLOW3D mesh generator uses the FAVOR$^{\text{TM}}$ method to handle the complicated geometries in an orthogonal mesh defined in Cartesian or cylindrical coordinates. Only the orthogonal mesh is allowed to simplify the process of meshing domain in FLOW3D. The obstacles and baffles are embedded in the orthogonal mesh, which allows separate definition of the mesh and geometry, so the modification of geometry has not any influence on the mesh.

The bridge deck with the six girders, as shown in Fig.3.1, is simulated. The center of the bridge deck is located at $x = 13\ cm$ in the flow domain. In Fig.3.2 the red region reflects the packed sediment bed with the thickness of 20 cm and the blue region is clear water with the depth of 25 cm. The mean approach velocity is *42 cm/s*, the pressure flow scour will occur beneath the submerged bridge deck. The deck opening, the distance from the bed to the girders, is 13 *cm*. The grid interval of mesh in the flow field is 0.4 *cm* except in the packed sediment interface refined to the cell size of 0.1 *cm* because the interaction among particles reflecting the process of scour is strongly dependant on the cell size, the analysis of cell sensitivity is illustrated for this dependence in the following section. The cell distribution in the vicinity of the bridge deck and the interface of sediment bed is shown in Fig. 3.3

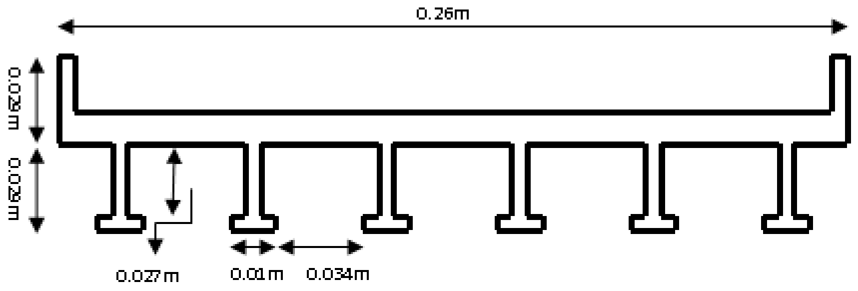

Figure 3.1 The bridge deck geometry.

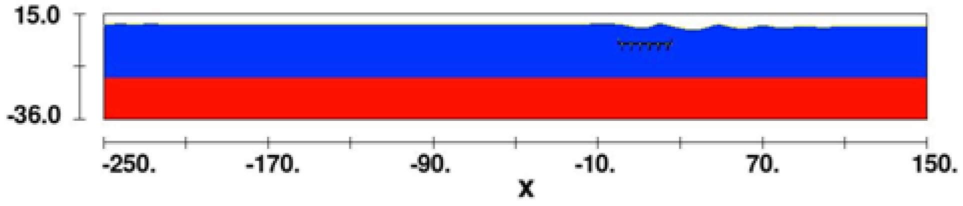

Figure 3.2 2-D numerical model configuration (unit: centimeter).

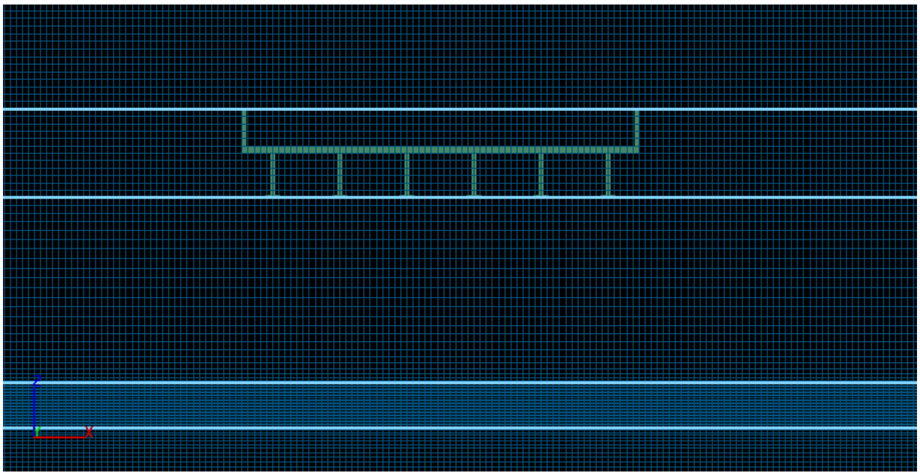

Figure 3.3 The cell distribution.

The procedure of the simulation includes two sub-simulations. The first sub-simulation was utilized as the initial condition of the second sub-simulation by the ‘restart’ techniques in FLOW3D. In the first sub-simulation, the erosion of the sediment bed is prevented by configuring the large Shields Number of 100 such that the local velocity in the vicinity of the bed interface becomes the log-law distribution in some time; otherwise, the non-fully developed flow in the interface of bed will destroy the threshold process of scour because of high velocity gradient. The first sub-simulation ended up in 60 sec and the flow domain reached the steady status.

Fig.3.4 (a) and (b) shows the distribution of velocity vector in the initial and stable status, respectively. The velocity distribution closed to the interface of sediment in Figure 3.4 (b) is acceptable as the fully-developed flow condition, thus, this steady status will be used as the initial condition in the ‘restart’ simulation. Table 3.1 shows the configuration of parameters.

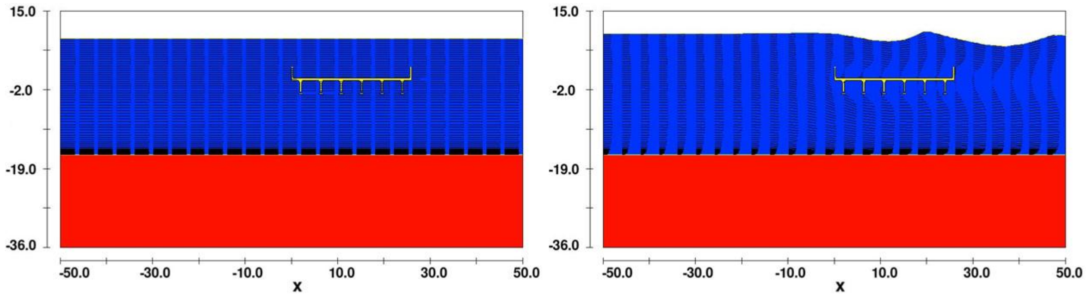

(a) (b)

Figure 3.4 (a) The initial status for sub.(1) (b) The steady status for sub.(1).

Table 3.1 The configuration of parameters for sub-simulation (1) and (2).

Parameters	**Sub-Simulation (1)**	**Sub-Simulation (2) or Restart**
Sediment Diameter	2 mm	2 mm
Sediment Density	2650 kg/m^3	2650 kg/m^3
Shields Number	100	0.048
Coehesive Solid Fraction	0.3	0.3
Critical Solid Fraction	0.65	0.65
Scour Adjustment Factor	1	1

During scour simulations, the packed bed erodes through mesh cells and the bed interface will in general be in the interior of a cell. Tests were run to check the effect of having the bed interface run through the interior of cells with ¼, ½, and ¾ of the cells filled with the stationary bed under flat bed conditions. These cases were run in a simulated flume 0.25 m deep with the entry velocity of 0.41 m/s and no obstructions in the flow. The velocity profiles halfway across the sand bed are compared in Fig 3.5. The location of the bed is at ZCOR = 0. The slope of the velocity profile at the bed (the velocity gradient) clearly varies as a consequence of where the bed is located with respect to cell boundaries. The effects of this variation extend well up into the main flow away from the bed. This variation may be a consequence of the coarseness of the mesh in the vicinity of the bed. These results indicate that a grid sensitivity study needs to be done to determine if mesh refinement can yield grid independent results when a scouring bed profile is moving through cells in the mesh.

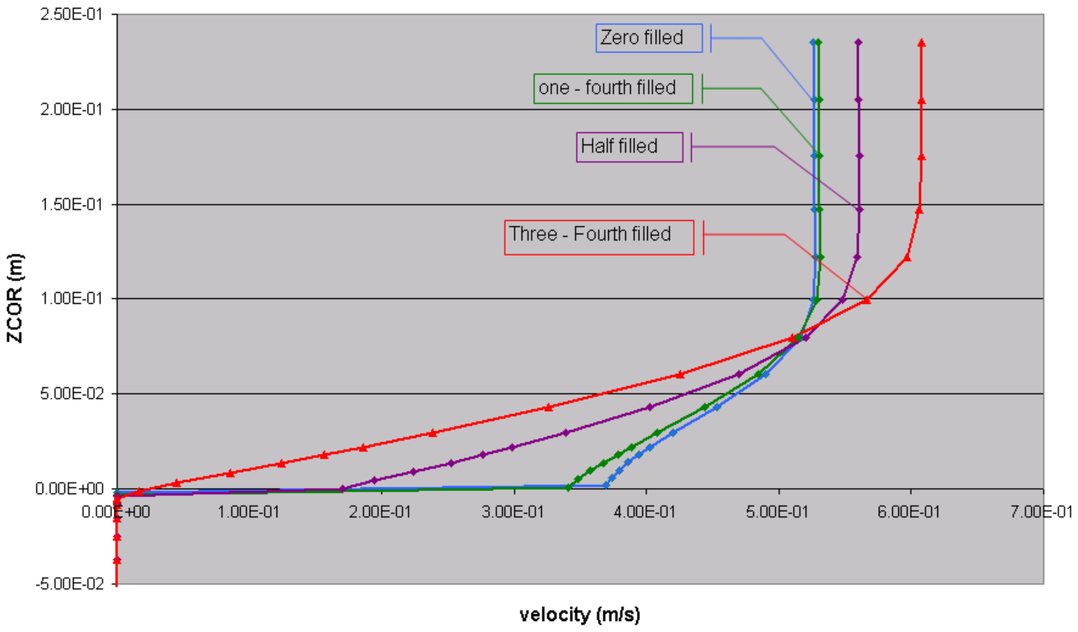

Figure 3.5 The velocity comparison with different filled value.

The FLOW3D scour model has a sediment transport scalar equation without momentum equations for sediment movement. The difference between local bed shear stress and critical bed shear stress in an empirical formula is used to determine erosion rate. In this formulation, the fluid-fixed bed interface is in the interior of the computational domain. There is not any form of wall function used to compute shear stress at the bed interface. The shear stress may be highly sensitive to the resolution of the grid in the vicinity of the interface. This same sensitivity would occur in any high gradient zone in the interior of a domain, and would require a highly refined mesh in that zone if the gradients there could impact either the flow or the results of interest. Therefore, a primary activity in evaluating FLOW3D for scour computations is carrying out grid sensitivity studies.

FLOW3D uses the finite difference to solve partial differential equations, so the selection of the vertical cell size closed to the sediment surface affects the distribution of velocity gradient related to the shear stress, thus to some extent impacting the scour profile. In the tests of sensitivity, Shields number for scour bed was set up to 100 as the approximate solid boundary to compare with the wall boundary of smooth wall boundary. Fig.3.6 shows the computational domain for the scour bed case. There is a corresponding block in back and front of the scour bed. Fig.3.7 indicates that the scour bed is replaced by the block with the smooth surface to compare the velocity gradient closed to the surface.

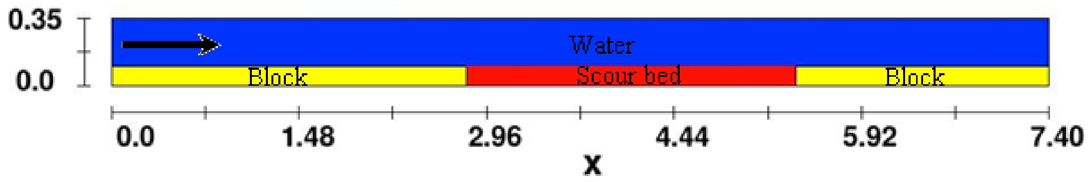

Figure 3.6 Scour bed case

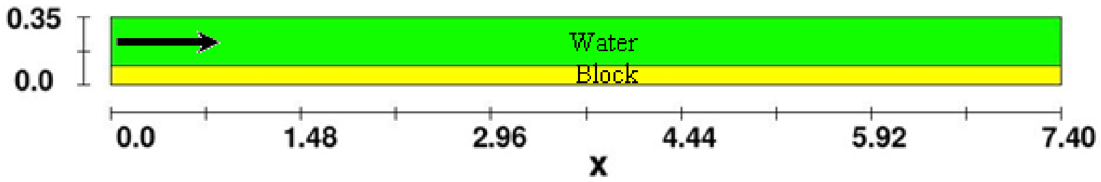

Figure 3.7 Smooth wall block instead of scour bed.

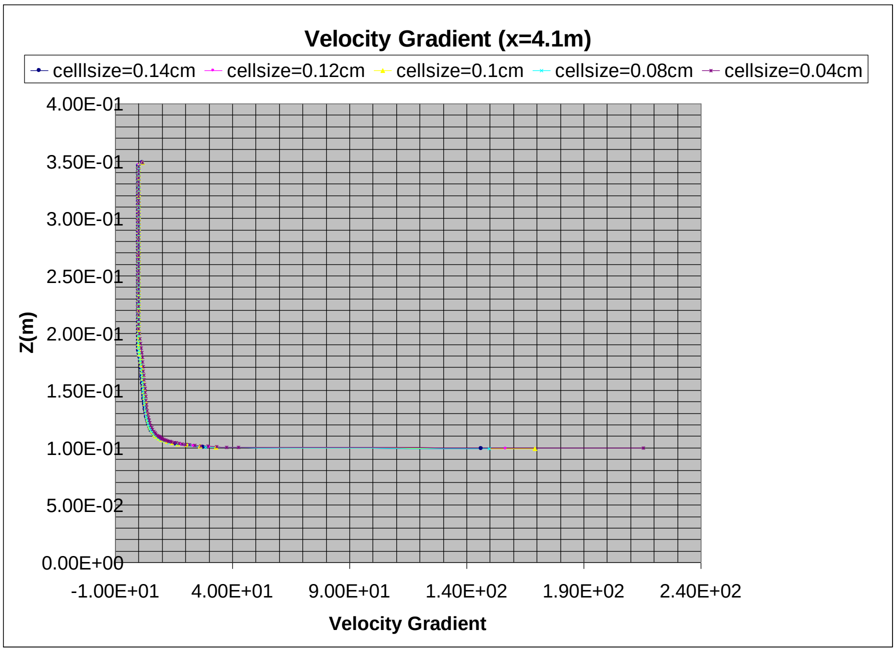

Figure 3.8 Velocity gradient distributions with different cell sizes.

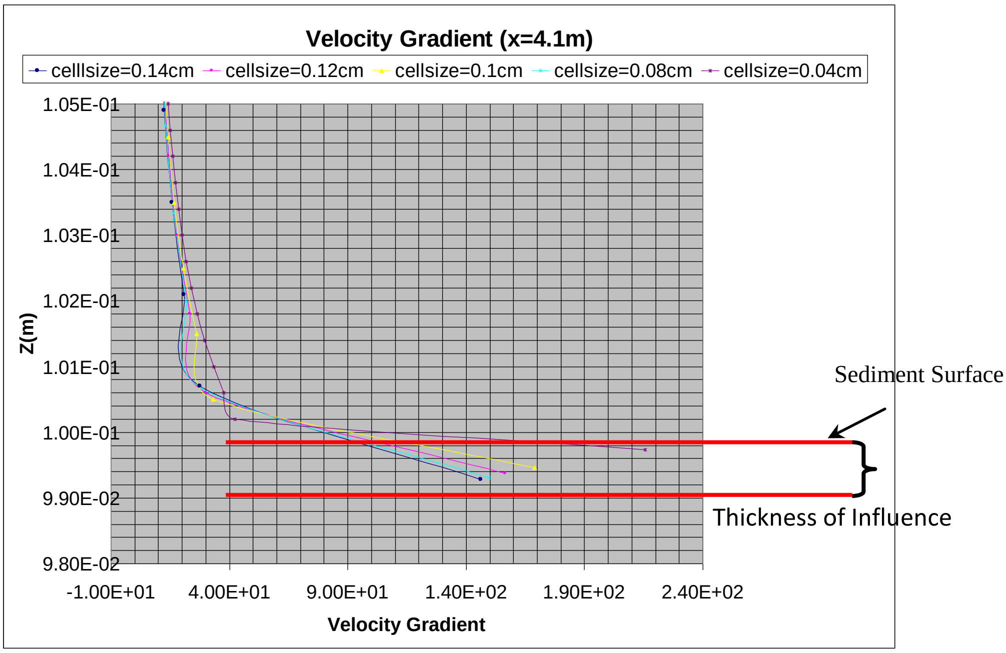

Figure 3.9 The region closed to sediment bed zooming in.

Fig.3.8 shows that the difference of velocity gradient with different cell grids closed to sediment surface occurs at the region adjacent to bed, which is zoomed in as shown in Fig.3.9. The thickness of influence from velocity gradient is about 1mm. Therefore, the incipient motion of sediment locates at the level of 1mm below the sediment surface, not really on it, or the scour may occur layer by layer at initial time step because of this penetration. On the other hand, the maximum gradient of velocity for the cell size of 0.04 cm is larger than the responding values of other sizes, which may lead to the discrepancy of scour rate with cell sizes. However, for this range of cell size from 0.04 cm to 0.14 cm, the difference of scour equilibrium profile and scour rate may be limited within the thickness of 1mm. Generally speaking, there exists little influence of cell size on scour results.

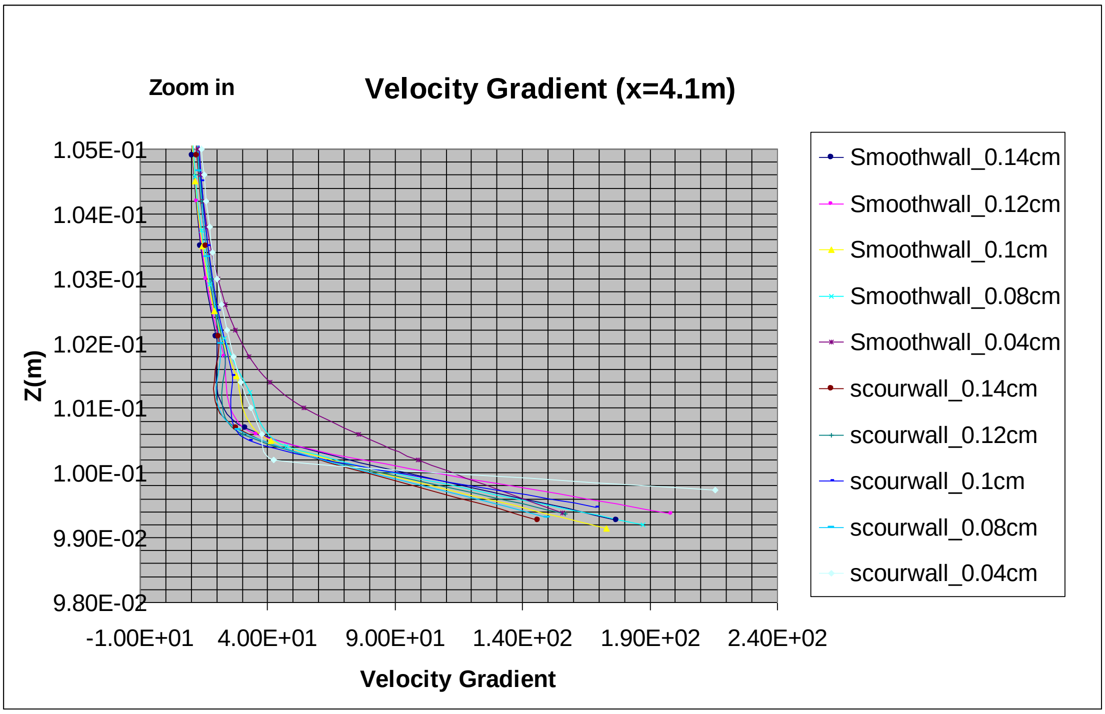

Figure 3.10 Velocity gradient comparisons between smooth and scour wall condition.

Fig.3.10 illustrates that there are good comparisons of velocity gradient between smooth and scour wall except for the cell size of 0.04 cm. That means that sediment bed can be as solid surface for certain cell element, namely smooth wall, when no scour occurs because they have very closed velocity gradient.

Based on the above analysis, we may select the cell size of 0.1 cm closed to sediment bed as far as the accuracy and efficiency are concerned in FLOW3D. The scour behavior could be layer by layer or block by block with the maximum thickness of 0.1 cm as far as the incipient of sediment is concerned.

Actually, the shear stress on the sediment surface can be estimated by the product of dynamic viscosity and velocity gradient in the elements including or adjacent to the sediment surface. Due to the disappearing of turbulence flow closed to the sediment bed dynamic viscosity approximately equals molecular viscosity. Therefore, the shear stress has the same error as velocity gradient to theoretical values. However, this influence of cell size on the procedure of scour is insignificant as far as the velocity distribution, which is described in the following section mentioning the practical case.

The first step of simulation is to use Shields Number of 100 instead of a real value of 0.048 so that the bed may be viewed as wall boundary at which the log-law velocity distribution is developed; the second step is to use the ‘restart’ configuration of Shields Number of 0.048 based on the ultimate data of the first step. The velocity distribution is adjusted to the more reasonable status of log-law after the computation of 4 seconds in the second sub-simulation, namely, the velocity magnitude is closed to zero on the sand surface, the flow can’t penetrate sand layer; it means that the influence of the cell of 1 mm to initial scour or the penetration of flow into the sand layer is only lasting 4 seconds from the initial status of ‘restart’ simulation. Fig.3.11 (a) and (b) show the contour of velocity distribution between the initial and 4 seconds afterward status.

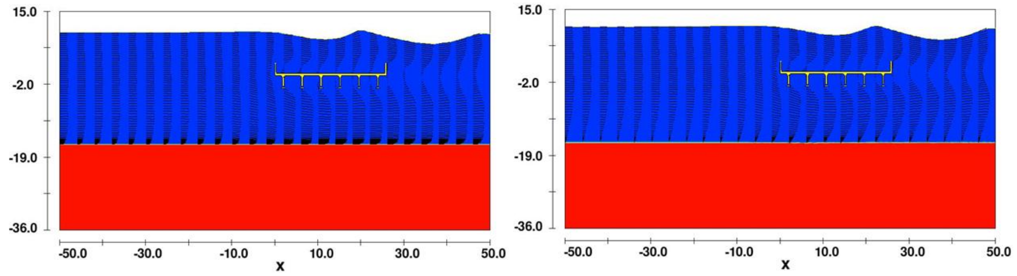

(a) (b)

Figure 3.11 (a) The initial status of ‘restart’ simulation, (b) 4 s afterward status.

The sediment scour is generally dependent on the initial scour profile to some degree. Fig.3.11 (a) and (b) indicate that the transition from the status (a) to (b) has little influence on the initial scour profile based on the assumption of initial condition replaced by the stable status with Shields Number of 100, this influence on the thickness of scour is limited to be less than 1 mm as analyzed before. If the vertical cell size on the interface of sediment is too large, the velocity gradient closed to the sand bed will not be reasonable and results in the incorrect shear stress distribution. Also, the flow body can penetrate the several cells in the vicinity of sediment interface and induce the dramatically impractical scour at the beginning stage. Fig.3.12 and Fig. 13 shows the comparison for the vertical cell size of 2 mm and 3 mm, respectively. Fig.3.12 (b) and Fig.3.13 (b) obviously have more scouring than Fig.3.11 (b) beneath the bridge deck and this difference will further increase with computational time as shown in Fig.3.14. From Fig. 14 (c) we can see there is no scour hole forming for the 3 mm cell case underneath the bridge deck, therefore, the scour profile is very dependable on the vertical cell size.

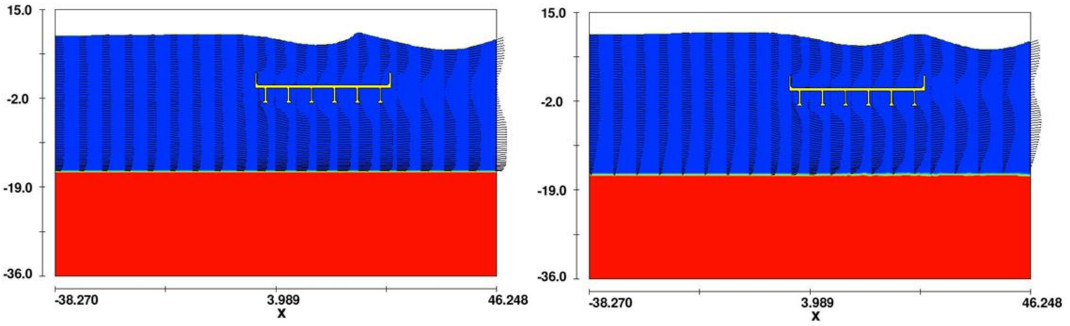

(a) (b)

Figure 3.12 (a) The initial status for 2 mm cell, (b) 4 s afterward status for 2 mm cell.

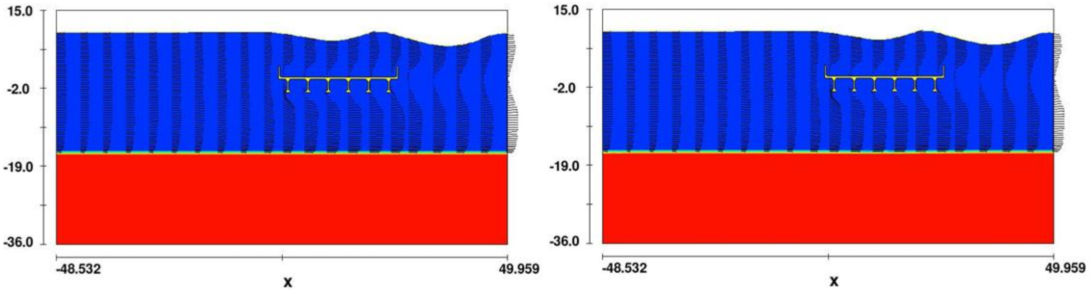

(a) (b)

Figure 3.13 (a) The initial status for 3 mm cell, (b) 4 s afterward status for 3 mm cell.

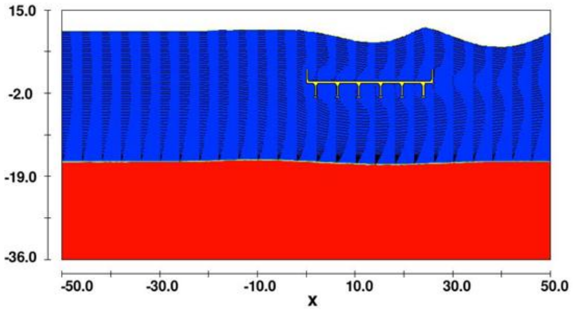

(a)

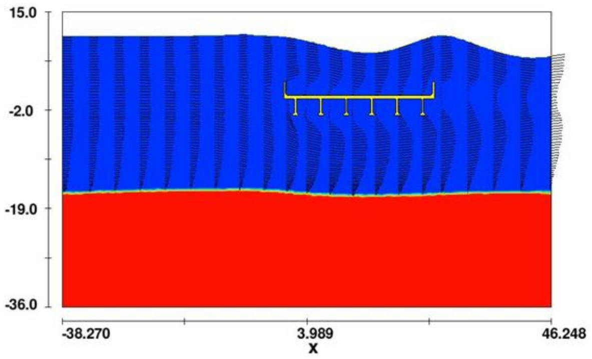

(b)

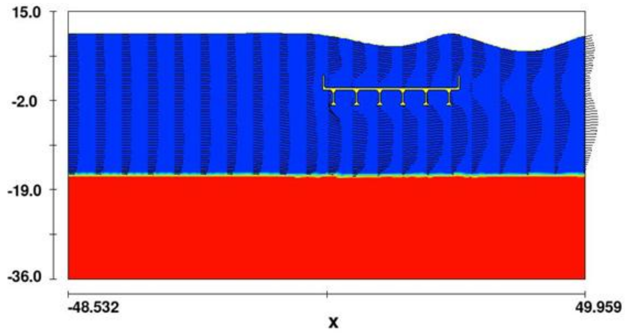

(c)

Figure 3.14 (a) Scour profile with 1 mm cell at time = 120 s (b) Scour profile with 2 mm cell at time = 120 s (c) Scour profile with 3 mm cell at time = 120 s.

The scour profile on the interface of sediment was simulated in the pressure flow condition. The vertical cell size of 1 mm in the vicinity of sediment interface was used. The qualitative analysis to this simulation is necessary to compare the physical experiments. The vortex distribution, velocity distribution, and turbulent energy were analyzed qualitatively. The distribution of vortices were mainly located in the space among girders and the region of wake, not in the scour hole under the bridge deck. The maximum of turbulent energy occurs in the scour hole. The incipient movement of the sediment particles was centralized on the sediment surface underneath the middle of the bridge deck because of the pressure flow condition.

In the natural erosion of sediment, a number of vortices around the structures are the main factor leading to the local transport of sediment. However, that is not the case for the pressure flow scour. Fig.3.15 is a contour of velocity with vortex feature. From Fig.3.15 we can see that the vortices do not exist in the scour hole. They come up in the interval among girders, the top of deck and the wake region. Thus, the vortex flow is not the reason resulting in the further development of the scour hole because no rotating flow is formed there as shown in Fig.3.15.

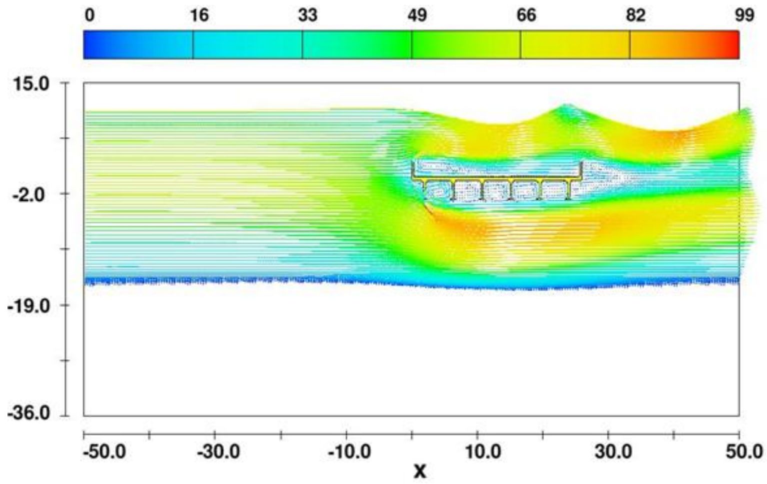

Figure 3.15 Vortices in a velocity contour.

Fig.3.16 shows the distribution of turbulent energy in the pressure flow condition. The high energy of turbulence is located at the region of sediment interface under the bridge deck, which illustrates that the intensified turbulent energy underneath the deck results from the pressure flow. Also, the maximum turbulent energy at different times is distributed in the mid region beneath the deck, therefore, the measure of protection should be taken in the mid region of sediment interface under the deck to avoiding the damage to other structures, such as piers.

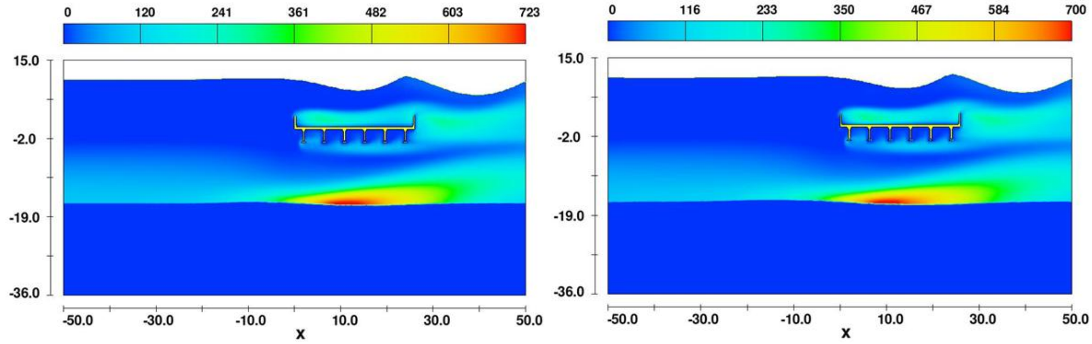

(a) time = 1 min (b) time = 5 min

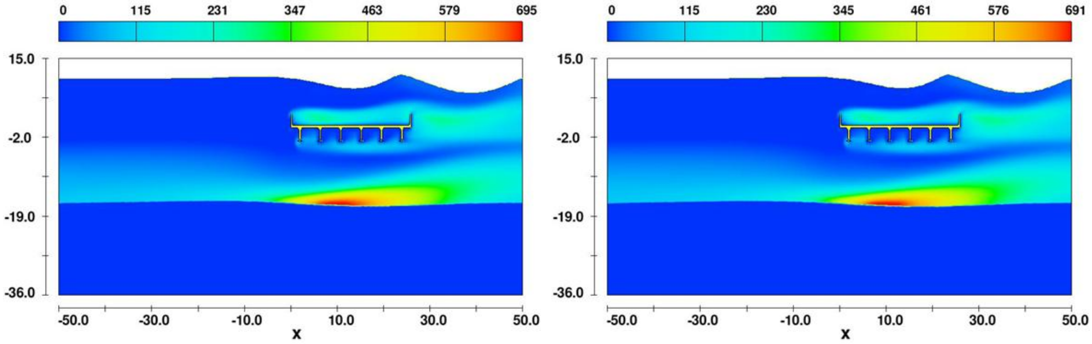

(c) time = 8 min (d) time = 12 min

Figure 3.16 Turbulent energy contour at different stages.

Fig.3.17 displays the x velocity distribution along the interface of sediment. Obviously, the velocity gradient under the bridge deck is larger than in the region upstream and downstream. Therefore, the scour begins under the bridge deck.

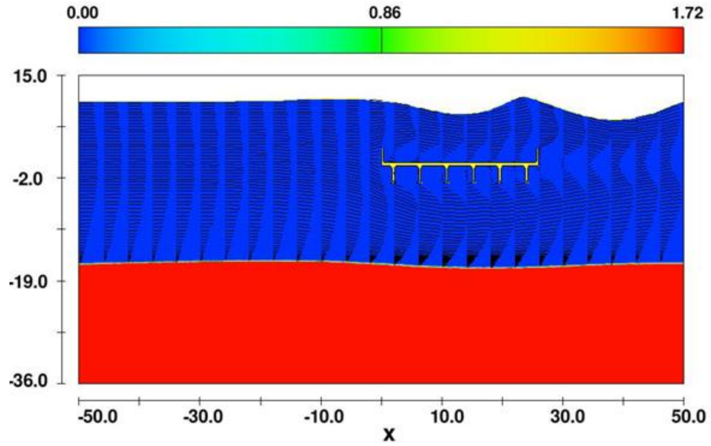

Figure 3.17 Packed solid fraction with x-velocity distribution.

Fig.3.18 shows the contour related to the scour process with time. The initial scour from 1 min to 5 min has more erosion rate of sediment than the stage from 5 min to 12 min as shown in Fig.3.18, which is reasonable qualitatively because the degree of vertical area contraction becomes weak with the development of time. However, the deposition of sediment downstream does not obviously form the sand dune we expected because of the limitation of the scour model in FLOW3D.

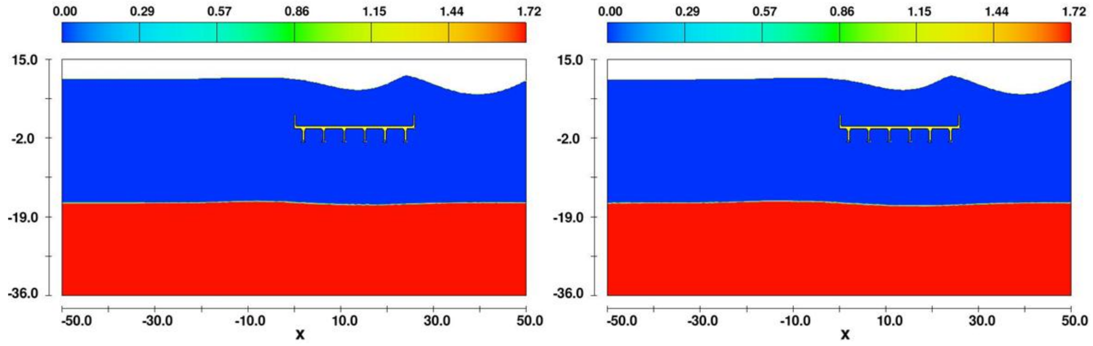

(a) time = 1 min

(b) time = 3 min

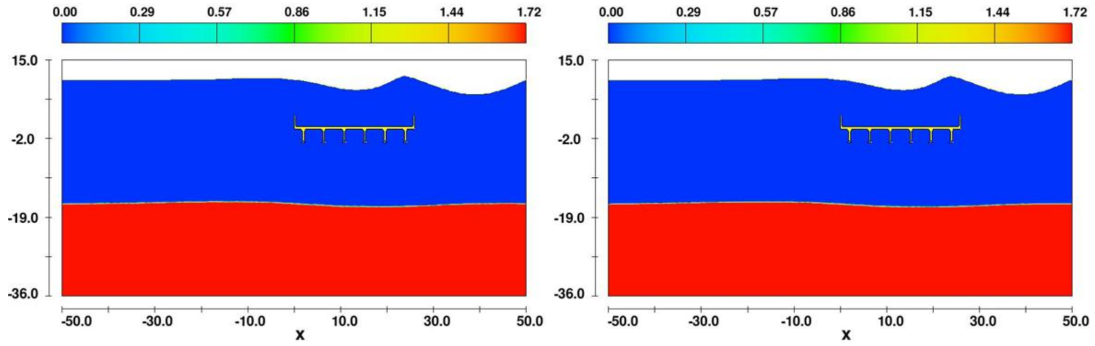

(c) time = 5 min (b) time = 7 min

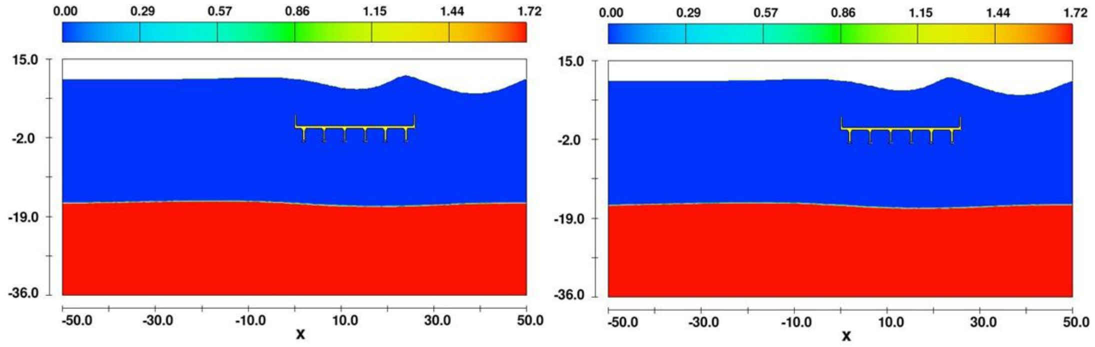

(e) time = 9 min (f) time = 12 min

Figure 3.18 The scour profiles with time.

In this analysis, the cell sensitivity within the range less than 1.4 cm was analyzed and the cases for the cell size of 1 mm, 2 mm and 3 mm were simulated respectively. All this analysis is based on the same configuration of parameters for 2 mm sediment diameter. Three conclusions can be summarized as follows,

(a) In FLOW3D, the effective scour model is sensitive to the vertical cell size on the sediment interface. The vertical cell size should not exceed the dimension of sediment diameter of 2 mm in our case. Within the vertical cell size of 1.4 mm the sediment scour is not obviously dependent on the cell size. The alteration of cell size within that range only affects the thickness of the sediment layer of 1 mm below the interface of sediment as shown in Fig.3.9.

(b) The sediment interface with Shields Number of 100 in the sub-simulation (1) can be approximated as the solid boundary. The steady flow field in the sub-simulation (1) can be effective as the initial status of sediment transport in the ‘restart’ or sub-simulation (2) with the normal Shields Number of 0.048.

(c) When the vertical cell size on the sediment interface is too large, for example, if it is 3 mm, the sediment transport underneath the bridge deck will not reflect the influence of pressure flow condition and no scour hole forms there.

(d) The qualitative analysis to the vortex distribution, x velocity profile, the contour of scour profile, and the scour model of sediment is reasonable; however, the results of 12 min simulation takes the computational time of 40 days, which results in that we cannot get the equilibrium status to compare with physical experiments within reasonable schedule because the equilibrium status physically requires more than 40 hours.

3.2 Morphing Mesh in STARCCM+

The moving mesh feature activated in STARCCM+ functions by altering vertex coordinates as a function of time. In the most general case, the grid meshed can be characteristic of transformation, rotation and distortion in any prescribed way when specifying time-dependence function for some interested cell vertices. Actually, the requirements for accuracy and stability limit the degree of distortion that can be tolerated, which makes the mesh arbitrary motion impossible. STARCCM+ will solve an additional equation, relating the alteration in cell volume to the cell-face velocity, called ‘space conservation law’ to adapt the situation of moving mesh or distorted domain.

In STARCCM+/STARCD, three factors control the mesh distortion; they are aspect ratio, internal angle and warp angle, as sketched in Fig.3.19.

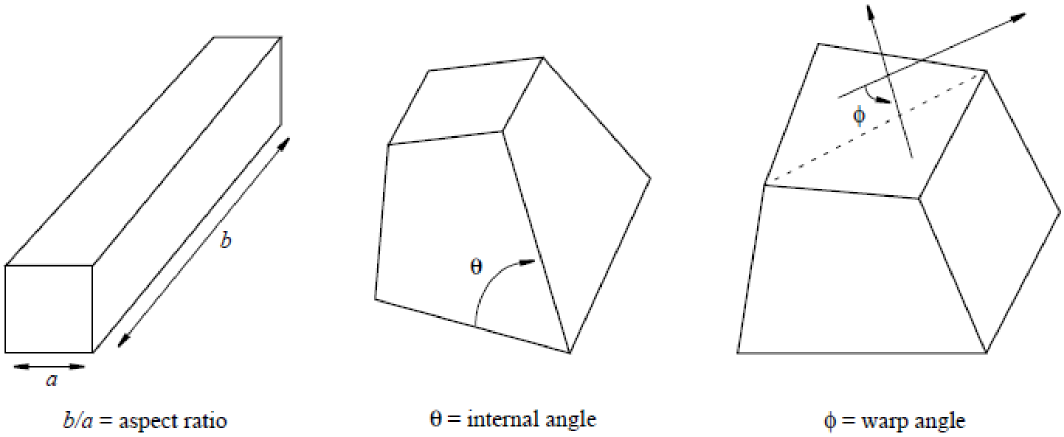

Figure 3.19 Classification of mesh distortion in STARCCM+.

The values of the aspect ratio can be allowed to be over unity but unity is preferable, it isn’t suggested to exceed 10; the internal angle should be kept a minimum when departing from 90 degree intersections between cell faces and 45 degree is the upper limitation of departure; and the optimum of the warp angle is zero for co-planar cell vertices; it isn’t good consideration to exceed 45 degree. If the combined effect from these three factors is simultaneously present in a single cell, the suggested limits might not be enough. STARCCM+ automatically employs the internal morphing interpolation function to solve the position of mesh vertices, and thus avoid the incorrect configuration.

The morphing motion redistributes grid vertices with the slave correlation to the movement of control points. Control points and their constrained conditions are used by the relative morphing algorism to generate an interpolation field throughout the domain. This interpolated field is used to displace the old vertices of the mesh. The constrain conditions for a series of control points can be a displacement or grid velocity. The displacement constraint will be independent on the time step whatever the time step is; however, the grid velocity constrain is proportional to the time step. Usually, the control points are configured by the mesh vertices on a boundary.

The process of morphing can be summarized as, a) the morpher collects control points and their known displacements or velocity on the boundary regions; b) the interpolation field is generated by those control points and displacements; c) the interpolation field function is employed to all mesh vertices in the computational domain; d) some adjustments for the updated vertices are performed on boundaries. The morphing accuracy is controlled by the parameter, Morpher Tolerance, which is non-dimensional parameter used to specify acceptable accuracy when morphing. The minimum value of allowable morphing is the product of Morpher Tolerance and the longest edge length of the bounding box enclosing the morphing region.

For the 2D case of scour issue under the pressure flow condition, only considering the vertical distortion of cell is a reasonable assumption to simulate the bed distortion acted by bed shear stress. For the convenient application, STARCCM+ uses a damping factor to control the computation of morphing transitioned from the zero morphing region to the morphing on the boundaries. Accurately applying this morphing to the case of pressurized scour requires the calibration of parameters related to the shear stress in STARCCM+. This calibration is described in the following section 3.2.1

The morphing vertices on the wall boundary will mock the deformation of river bed. The morphing velocity or the recession rate is dependent on the entrainment rate for the sediment transport model we adopt. The deformation of bed inversely affects the shear stress on the wall boundary, and then the recession rate based on the computation of the sediment transport model. The periodic process above ultimately stops at the equilibrium state according to the pickup function.

3.2.1 Case Configuration

The purpose of this case is to calibrate the entrainment rate with Lianjun’s experimental data. Lianjun’s experiment for measuring the entrainment rate under the critical condition is based on the open channel flow with the horizontal bed but without any bridge in the flume. We assume that the entrainment rate is not obviously dependent on the bed slope when the bed slope is approximated to be horizontal. Usually, the bed slope under a bridge or block in the pressure scour is just several degrees. Therefore, the entrainment rate for horizontal bed can be employed to calibrate the cases with a several degree slope.

The numerical experiment has the same geometries and boundary condition as physical experiments except for that the free surface of water is not included in the numerical configuration. The sketch is displayed in Fig.3.20. The length of domain is 6.5m, the water depth is 0.25 m; the distance from the front of the rectangular block to the inlet of flow is also a constant as the value of 4.0 m. The block size is 0.26 m by 0.058 m.

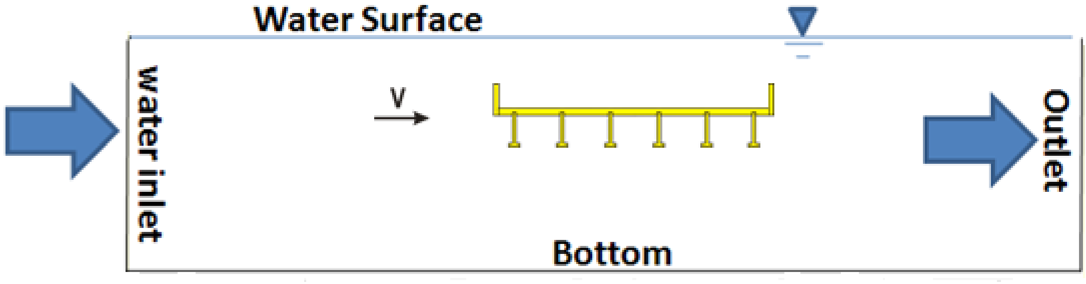

Figure 3.20 The sketch for computational domain in STARCCM+.

The mean upstream velocity $V = 0.48\ m/s$, which is the critically threshold velocity of sediment. The entrance on the left side is configured as Velocity Inlet boundary, the exit as Pressure Outlet boundary, the top as Symmetry boundary, and the bottom and surface of the block as Wall boundary. The wall surface on the bottom is morphing by a constraint from grid velocity.

The following parameters are calculated as,

The hydraulic diameter, $d_h = 0.565\ m$, the effective roughness $k_s = 0.004\ m$ for 2 mm sediment diameter. The Reynolds number $Re = 3.55 \times 10^5$, the relative effective roughness $k_s/d_h = 7.07 \times 10^{-3}$.

From the parameters, we can obtain the friction factor to calculate the critical bed shear stress based on the Colebrook-White equation or Moody diagram, namely $f = 0.0346$ and $\tau_c = 1.41pa$.

The morphing velocity on each vertice attached to the bottom boundary is a function of the bed shear stress or the sediment transport model, thus, an appropriate field function used to compute the recession rate need to be defined to keep a reasonable grid velocity of morphing. Furthermore, the convergence of solution requires that the time step size must be within certain range, here, the constant time step of 0.02s is used.

The roughness function parameters in STARCCM+ are as follows,

$$B = 0, C = 0.253, R^{+}_{smooth} = 2.25, R^{+}_{rough} = 90$$

Note that the roughness function in STARCCM+ is employed to modify the log-law coefficient, which is a segmented-function of the dimensionless parameters R^{+}. R^{+}_{smooth} and R^{+}_{rough} in which R^{+} is defined as $\rho r u^{*}/\mu$ where r is an effective roughness number and u^{*} is a local reference velocity. When $R^{+} \leq R^{+}_{smooth}$, the wall boundary is considered to be smooth; when $R^{+} > R^{+}_{smooth}$, the wall boundary is fully rough.

We employ Guo’s two empirical formulas which are based on scouring experiments as field function to morph bed and compute the recession rate. One of them is the scour profile formula consists of two parts as follows,

$$\frac{y}{y_s} = -exp\left(-\left|\frac{x}{W}\right|^{2.5}\right) \text{ for the region upstream}$$

and

$$\frac{y}{y_s} = -1.055exp\left(-\frac{1}{2}\left|\frac{x}{W}\right|^{1.8}\right) + 0.055 \text{ for the region downstream}$$

where y is depth at different location on the bed for the equilibrium status. y_s is maximum depth of scour. W is bridge width (reference Fig.2.1).

The other formula is a time-dependent relationship for maximum scour depth on the bed as follows,

$$Y = \left(1 - e^{-T/T_c}\right)^{0.239}$$

$$or \quad \frac{dY}{dT} = \frac{0.239}{T_c}\left(\frac{1}{Y^{\frac{1}{0.239}-1}} - Y\right) \tag{3.10}$$

where Y is dimensionless time-dependent scour depth, defined as defined as η/y_s in which η is the maximum depth of scour at certain time. T is dimensionless time, defined as tV_u/H_b in which V_u is upstream velocity and H_b is bridge opening. T_c is characteristic dimensionless time, and $T_c = 1.56 \times 10^5$.

We assume that Eq.3.10 can be applied to the different locations on the bed profile at certain time, not only limited to the max. scour depth, namely, it can be as the scale factor for the whole scour profile so that it scales the bed profile with different scour times. Fig.3.21- Fig.3.26 show the comparison between experimental and scaled scour profiles.

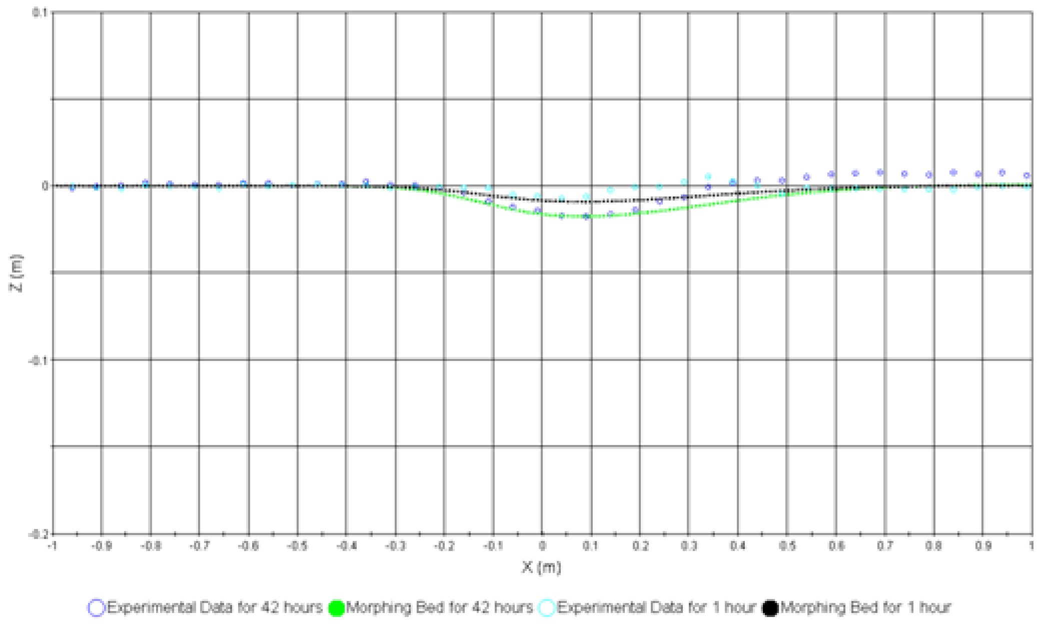

(a)

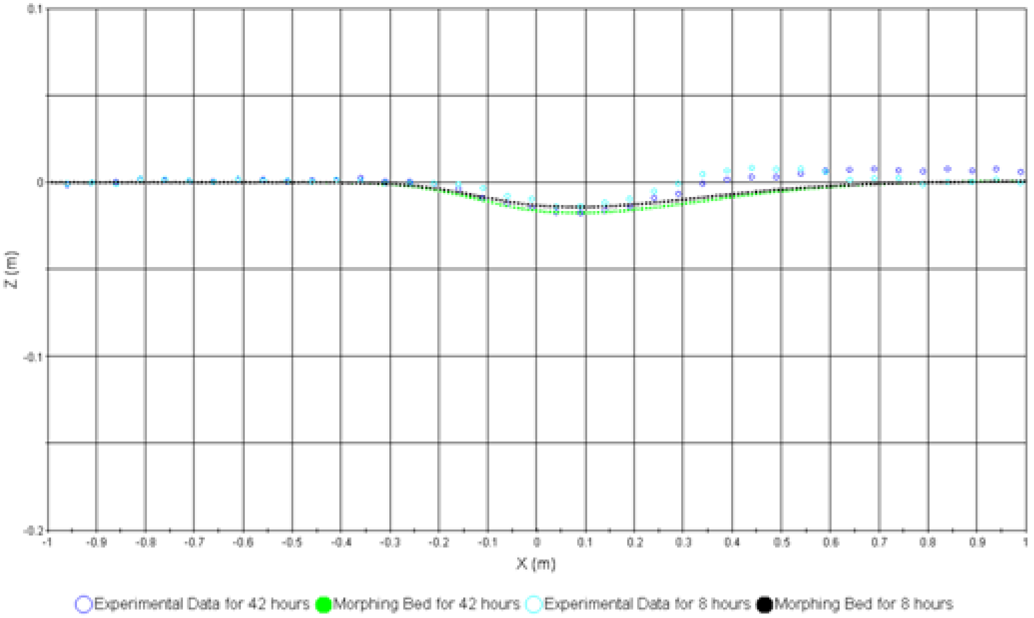

(b)

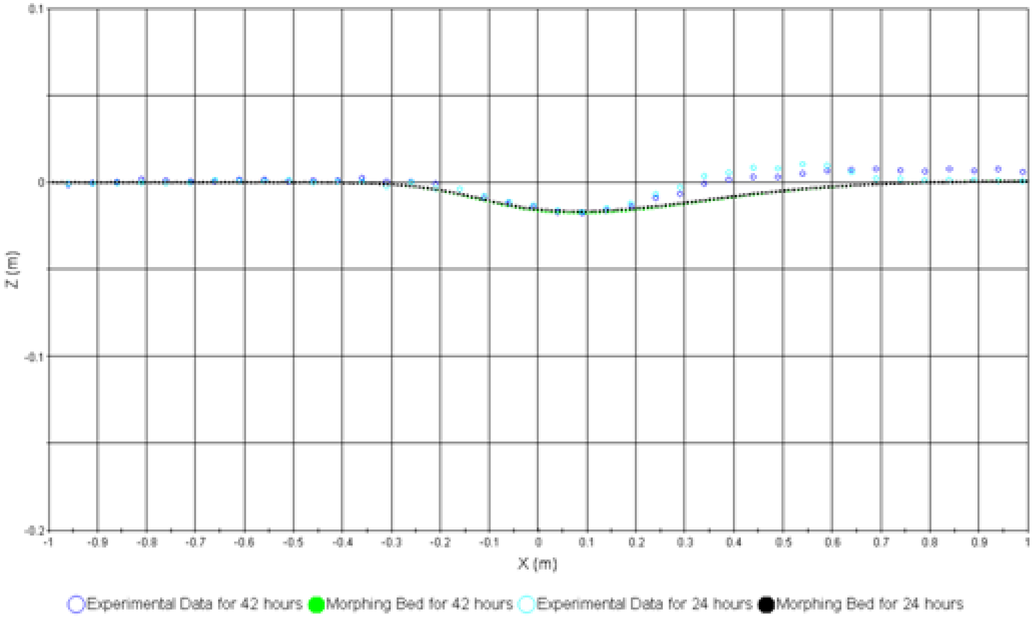

(c)

Figure 3.21 Scaled scour profile verse experimental results $h_b = 0.19\ m$ (a) 42 h and 1 h (b) 42 h and 8 h (c) 42 h and 24 h. Note that the case for 42 h is the equilibrium status based on experimental analysis.

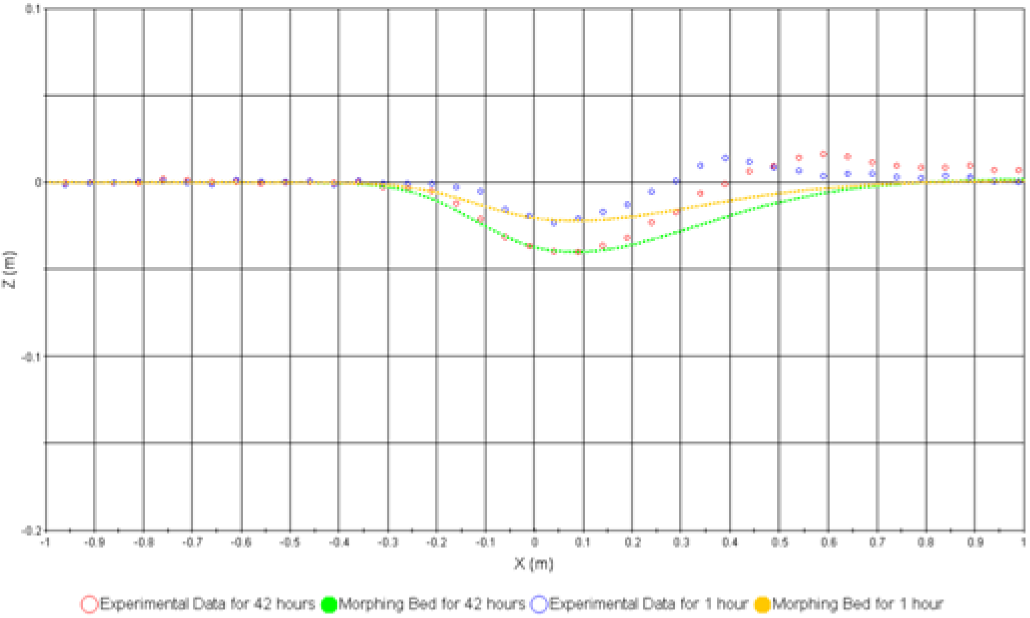
0.1
0
-0.1
-0.2
Z (m)
-1
-0.9
-0.8
-0.7
-0.6
-0.5
-0.4
-0.3
-0.2
-0.1
0
0.1
0.2
0.3
0.4
0.5
0.6
0.7
0.8
0.9
1
X (m)
○ Experimental Data for 42 hours
● Morphing Bed for 42 hours
○ Experimental Data for 1 hour
● Morphing Bed for 1 hour

(a)

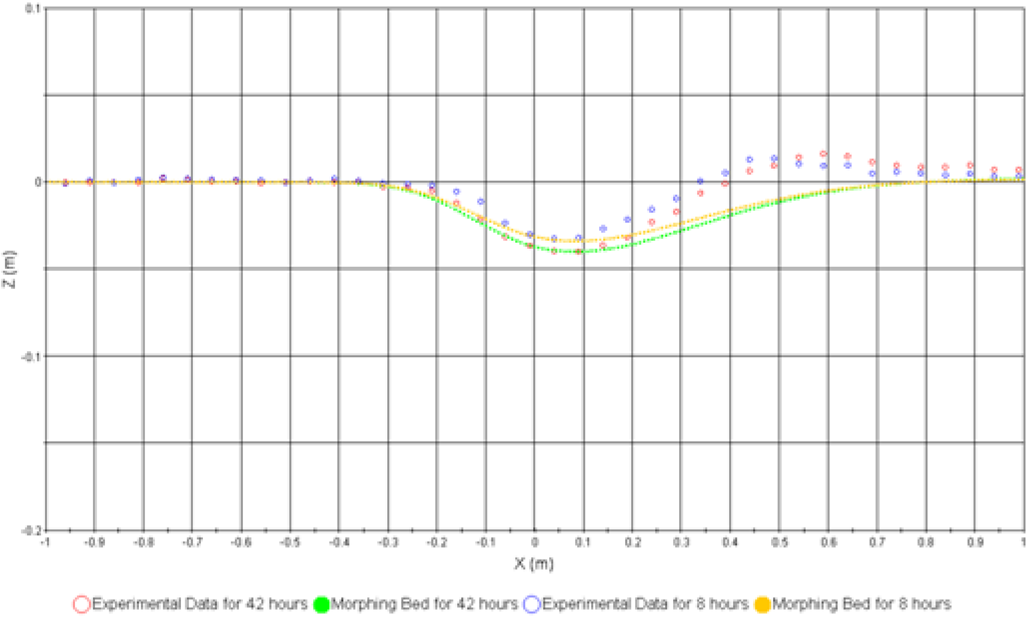
0.1
0
-0.1
-0.2
Z (m)
-1
-0.9
-0.8
-0.7
-0.6
-0.5
-0.4
-0.3
-0.2
-0.1
0
0.1
0.2
0.3
0.4
0.5
0.6
0.7
0.8
0.9
1
X (m)
○ Experimental Data for 42 hours
● Morphing Bed for 42 hours
○ Experimental Data for 8 hours
● Morphing Bed for 8 hours

(b)

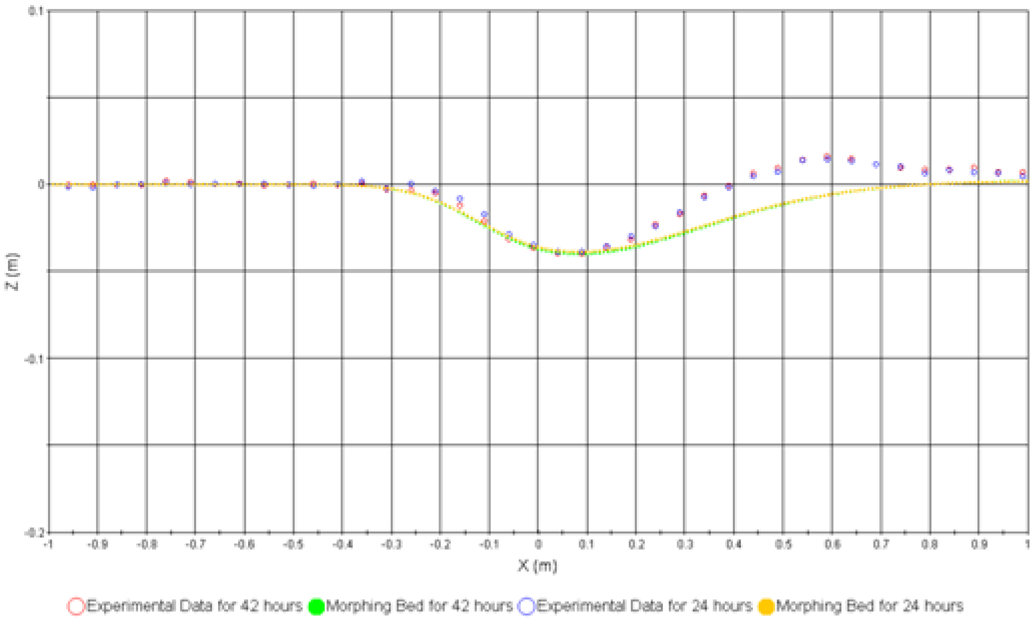

(c)

Figure 3.22 Scaled scour profile verse experimental results $h_b = 0.135\ m$ (a) 42 h and 1 h (b) 42 h and 8 h (c) 42 h and 24 h. Note that the case for 42 h is the equilibrium status based on experimental analysis.

From Fig.3.21 and Fig.3.22, we found that Guo's formula is not capable of explaining the deposition of particles downstream underneath a bridge deck based on the comparison of morphing bed to the experimental data, therefore, the scour profile downstream cannot fit experimental data very well but it is closed to the experimental data upstream. On the other hand, the scaled profiles, such as 1 h, 8 h and 24 h, are accurate enough to match experimental data upstream, which means that Eq.3.10 may be as scale function to deform the bed.

The mesh of grid around the bridge deck for equilibrium status is shown in Fig.3.23 – Fig.3.25. Fig.3.23 is the original mesh before morphing. We can see that the mesh in domain is self-adjusted and blended to better fit the morphing bottom as the bottom is morphing as shown in Fig.3.24 and Fig.3.25.

The shear stress distribution for different scaled scour profiles is plotted in Fig.3.26 and Fig.3.27. Through the numerical results of shear stress distribution can we develop a functional relationship between the entrainment rate calculated by Eq.3.10 and the maximum bed shear stress as the field function so that the boundary of domain is morphed as the law of this function although the results of the shear stress distributions are not accurate because of the difference between the morphing bed and experimental data downstream. The computational shear stress distribution on the bed in STARCCM+ overestimates critical shear stress for the equilibrium status, which is limited by: a) the wall function adopted by STARCCM+, and b) the approximately empirical scour profile.

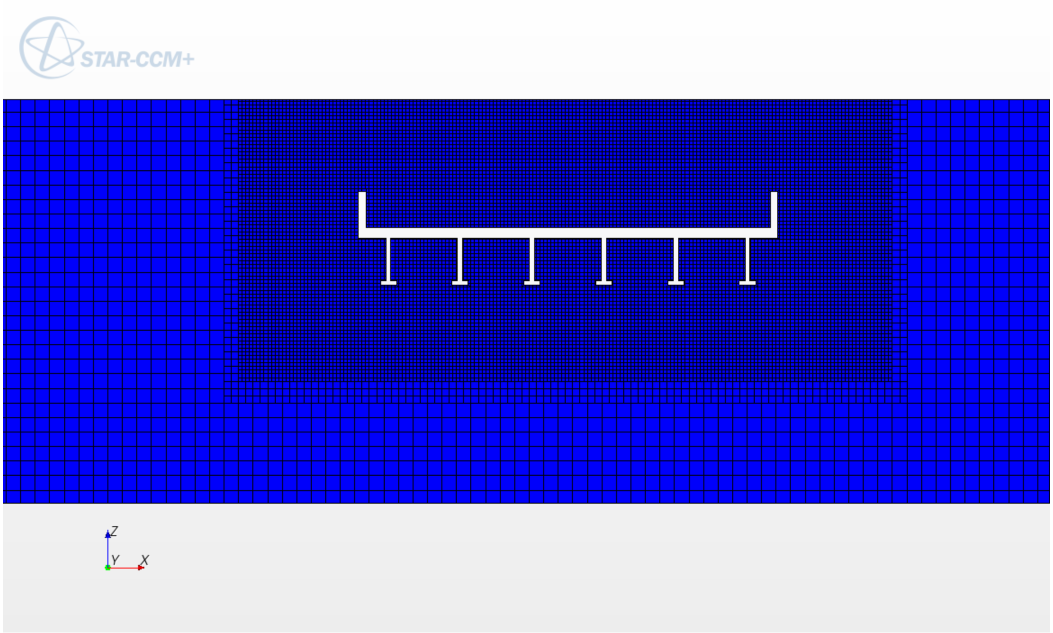

(a)

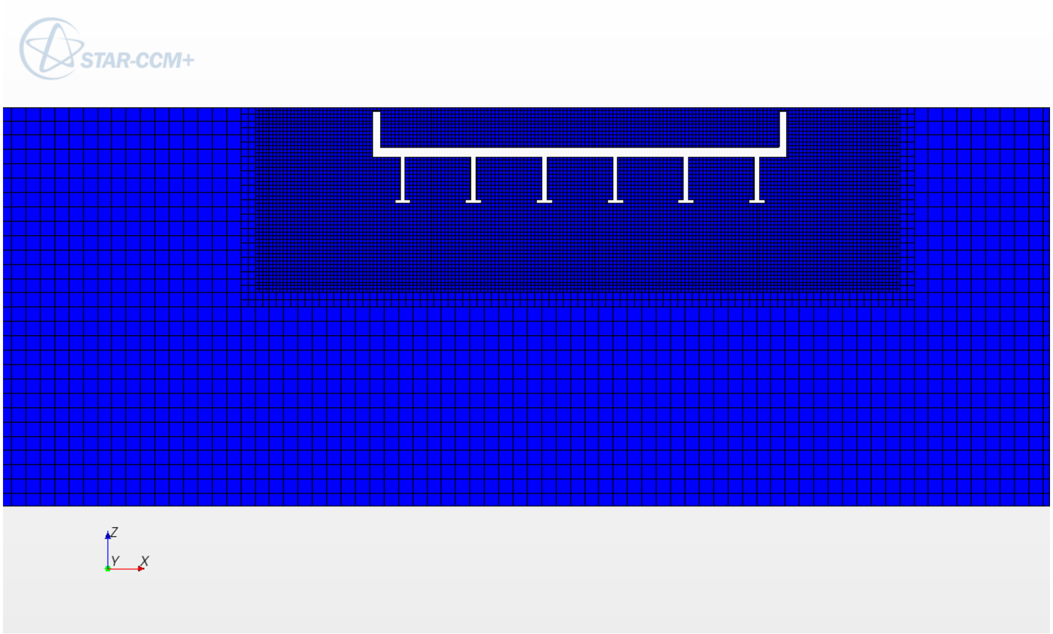

(b)

Figure 3.23 Original domain mesh with 42 h for (a) $h_b = 0.135\ m$ (b) $h_b = 0.19\ m$.

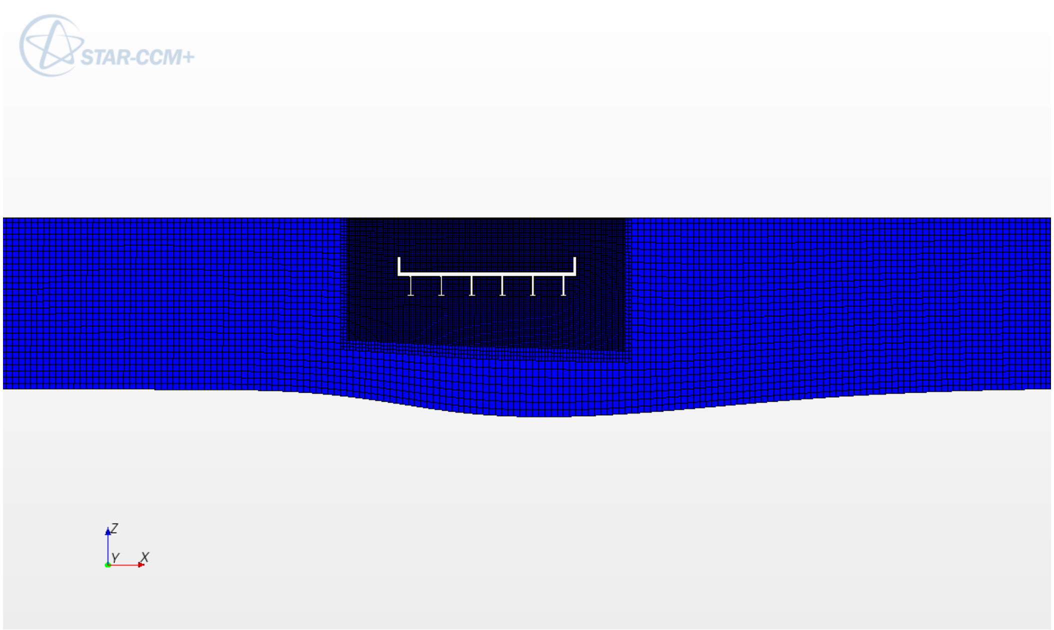

(a)

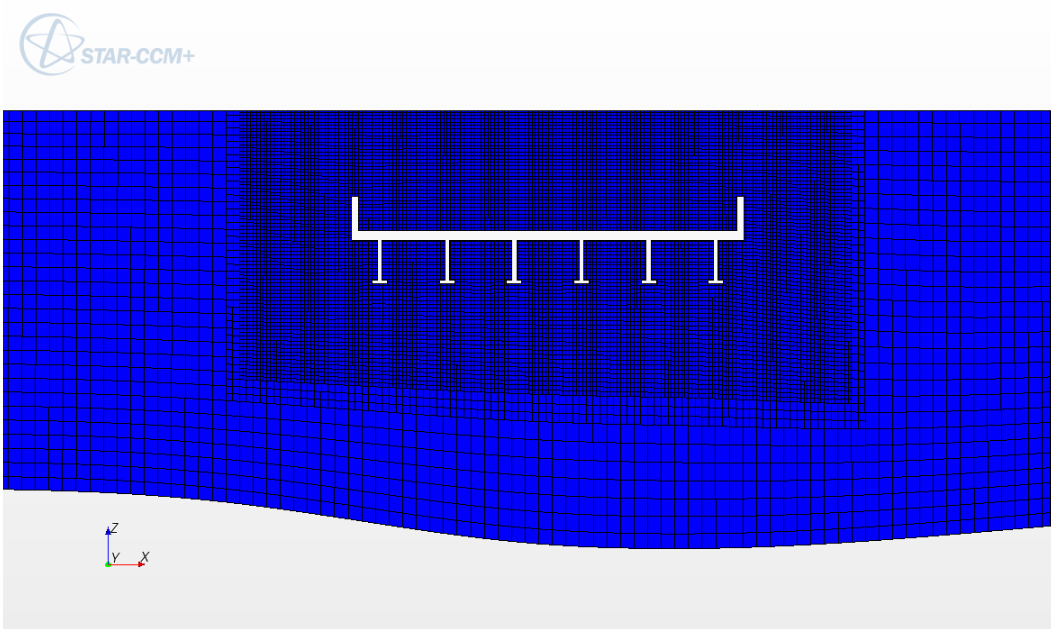

(b)

Figure 3.24 Domain mesh with 42 h for $h_b = 0.135\ m$. Note: (b) is zoom-in of (a) .

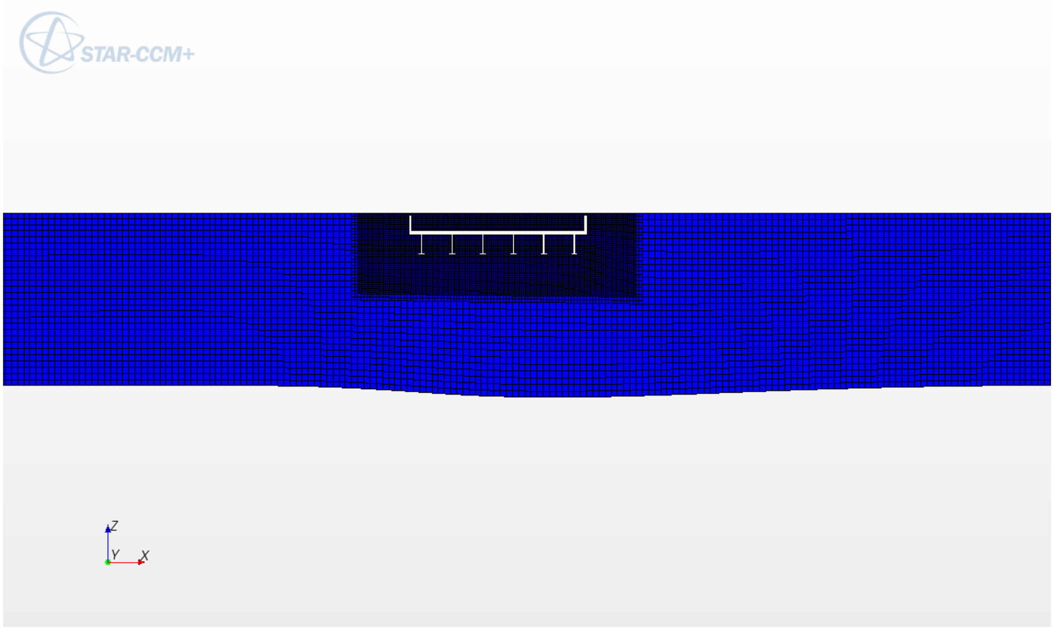

(a)

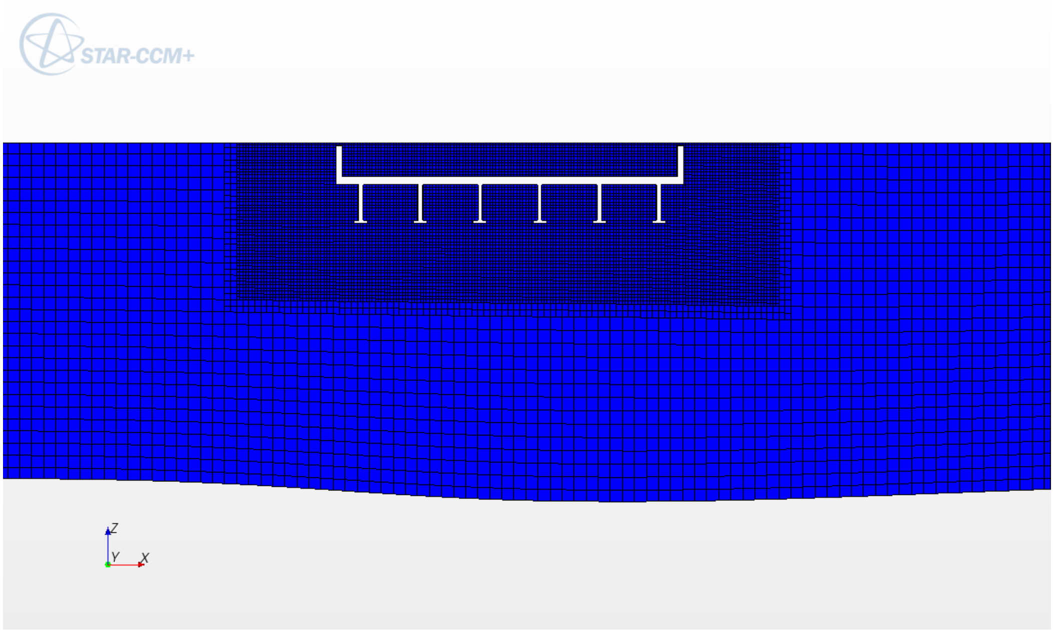

(b)

Figure 3.25 Domain mesh with 42 h for $h_b = 0.19\ m$. Note: (b) is zoom-in of (a).

The functional relationship between the recession rate and the maximum bed shear stress for $h_b = 0.135\ m$ and $h_b = 0.19\ m$ is fitted by Matlab as shown in Fig.3.28 and Fig.3.29 with the fitting formula as follows,

$$f(x) = ae^{bx} + ce^{dx} \tag{3.11}$$

in which x denotes the maximum bed shear stress. $f(x)$ denotes the recession rate. $a = 2.933\text{e} - 011$, $b = 4.034$, $c = -0.001206$, $d = -4.645$ for $h_b = 0.135\ m$, and $a = 5.565e - 016$, $b = 7$, $c = -0.000609$, $d = -4.175$ for $h_b = 0.19\ m$.

The Eq.3.11 as the similar formula of expression illustrates that the recession rate for the cases with different h_b is a linear combination of two expontential forms with individual constant coefficients.

Based on Guo's formula, the location of maximum scouring depth is where the distance is 0.04 m away from the rear edge of bridge deck, namely, $x = 0.09\ m$ in the coordinate system of simulation. The Fig.3.30 plots the maximum bed shear stress for different time and the corresponding values at $x = 0.09\ m$. The Fig.3.30 illustrate that the maximum bed shear stress is closed to one at $x = 0.09\ m$ with the process of scour except for the initial stage of scour with $h_b = 0.135\ m$, and the good identity for $h_b = 0.19\ m$ except that the maximum values of bed shear stress are a little higher than ones at $x = 0.09\ m$. Table 3.2 and Table 3.3 list the horizontal location for the maximum of the bed shear stress with different time along the bottom. Table 3.2 shows that this location for $h_b = 0.135\ m$ is gradually moved to the rear edge of bridge deck with time. In Table 3.3, the location for $h_b = 0.19\ m$ is approximately at $x = 0.045\ m$.

The velocity contours are plotted in Fig.3.31 and Fig.3.32 in which the velocity magnitude under the bridge deck become larger than the one upstream. The flow with larger velocity closed to bottom initializes the motion of particles. In the early stages of scour, there is a different location of maximum of bed shear stress for each opening space because of different condition of continuity. This location is gradually moved to downstream with process of scour and around the maximum of scour depth in equilibrium status. From Table 3.2 and Table 3.3, the location, when scour initializes, is at $x = 1.7\ cm - 5.3cm$ away from the centroid of the bridge deck according to different h_b.

The scaled morphing bed with process of scour is shown in Fig.3.33 and Fig.3.34. The disadvantage for this assumption about scale factor is that the maximum of scour depth is always located at $x = 0.09\ m$, independent on time, which is not reasonable in experimental observation. This location should be up to upstream in early stages.

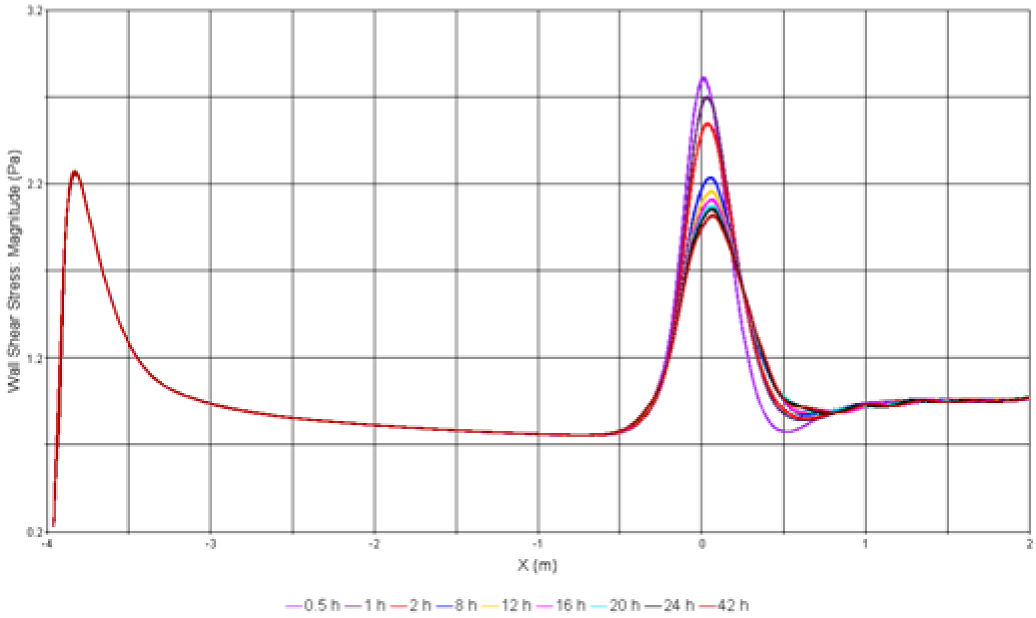

Figure 3.26 Bed shear stress distributions along the bed for different scaled scour profiles with $h_b = 0.135\ m$.

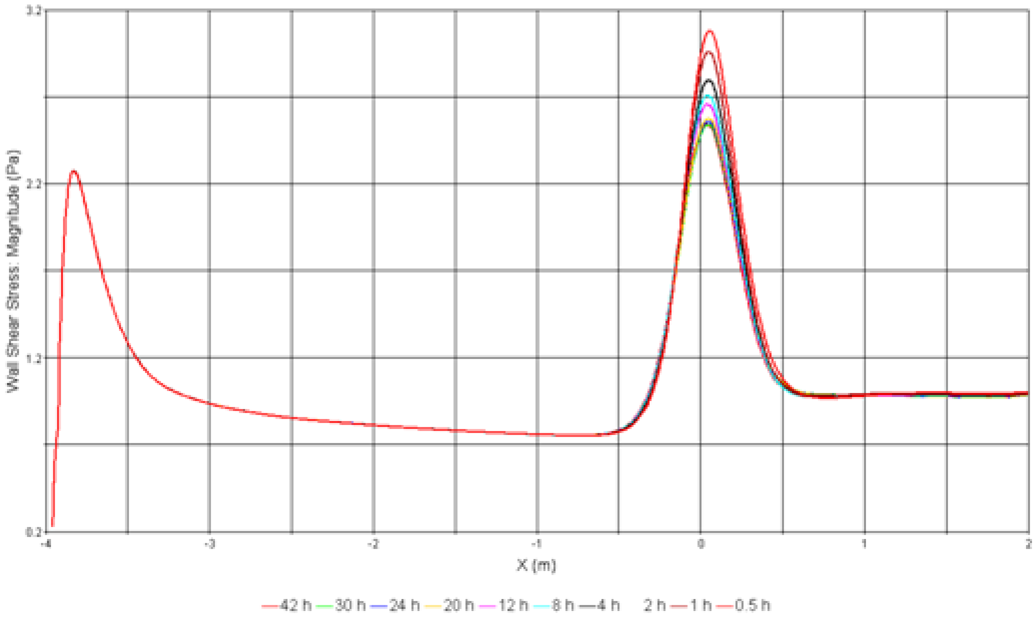

Figure 3.27 Bed shear stress distributions along the bed for different scaled scour profiles with $h_b = 0.19\ m$.

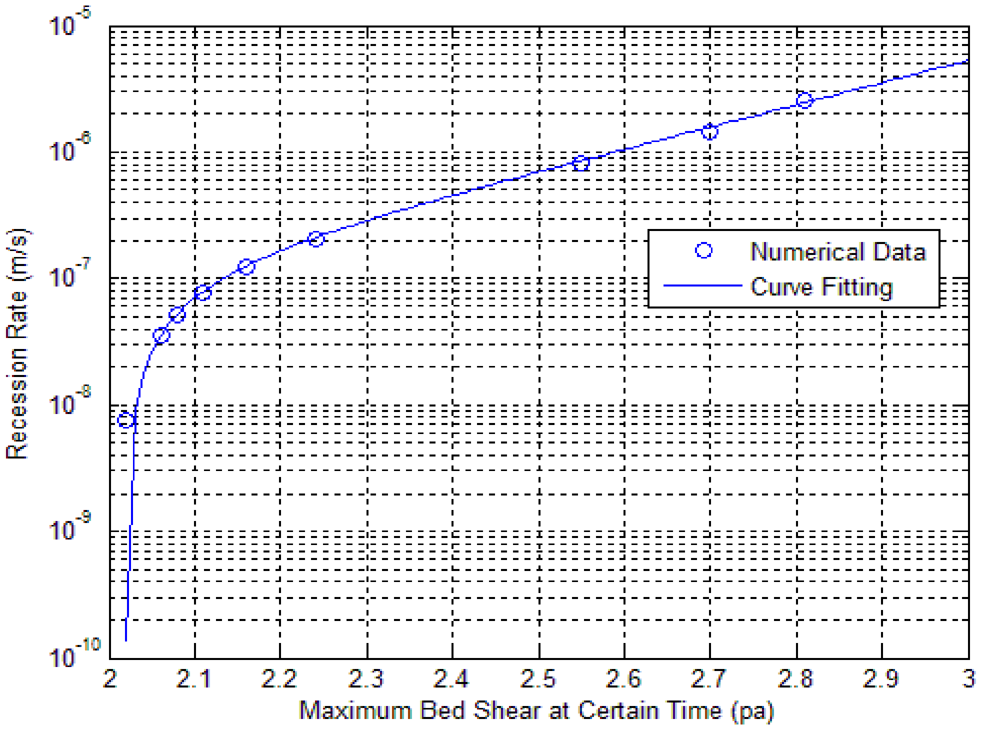

Figure 3.28 Recession rate verse maximum bed shear with $h_b = 0.135\ m$.

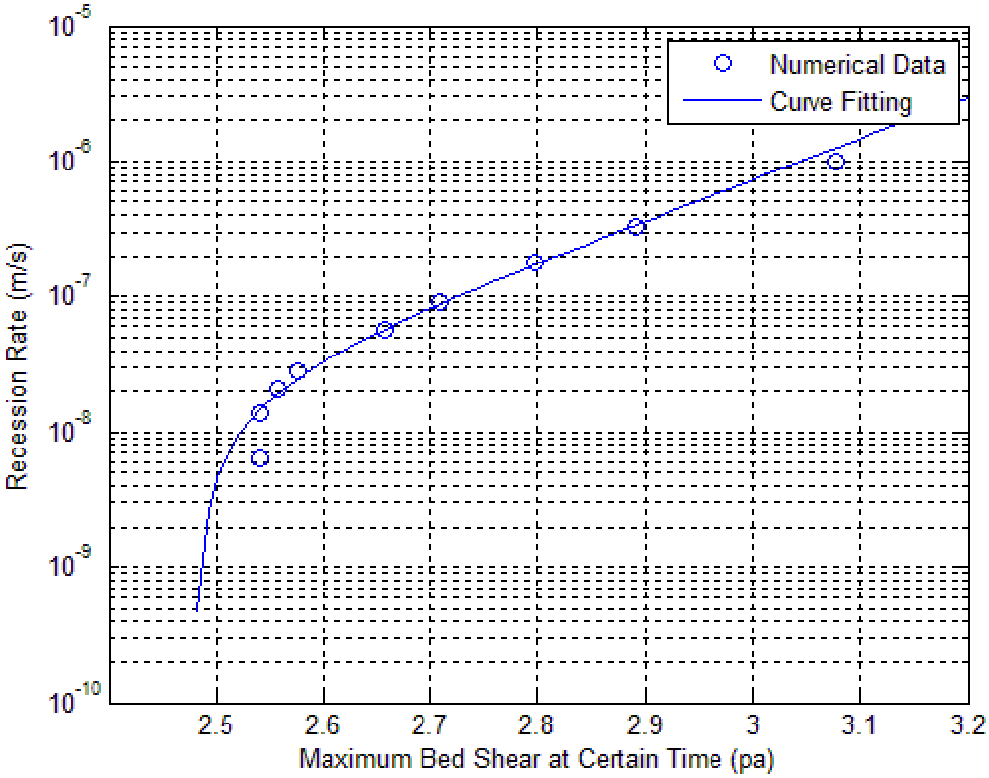

Figure 3.29 Recession rate verse maximum bed shear with $h_b = 0.19\ m$.

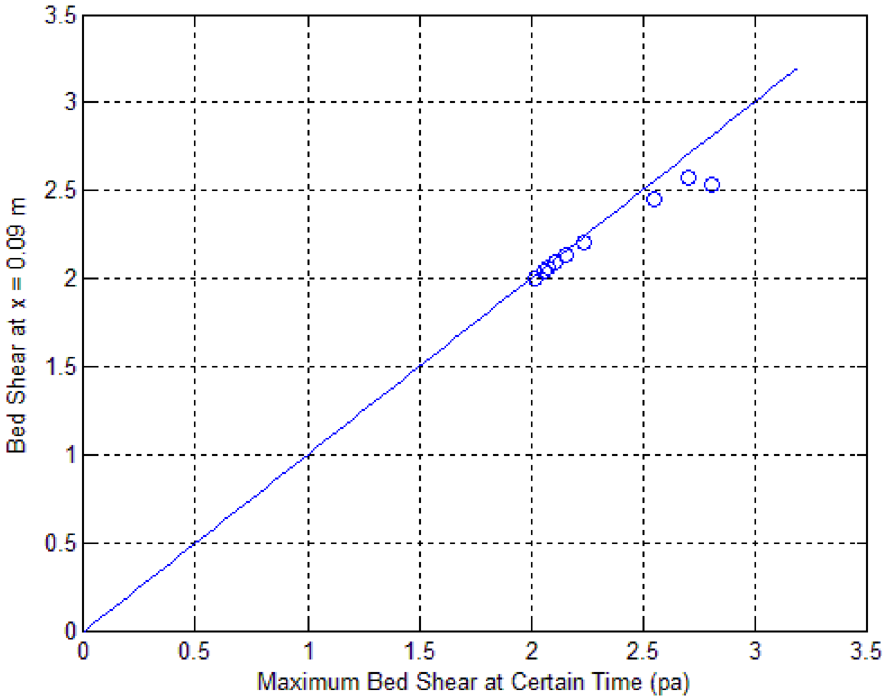

(a) $h_b = 0.135\ m$

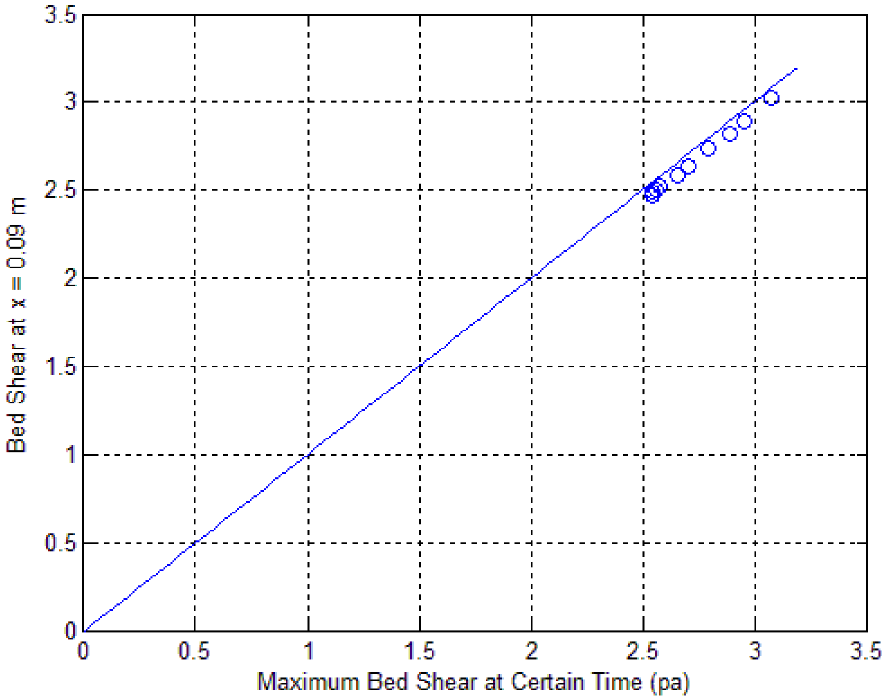

(b) $h_b = 0.19\ m$

Figure 3.30 The bed shear stress compared to the maximum bed shear stress.

Table 3.2 horizontal location for maximum bed shear for $h_b = 0.135\ m$.

Time (hour)	Max. Bed Shear $h_b = 0.135\ m$	X Location for Max. Bed Shear (m)
0.5	2.814453	0.0165
1	2.703914	0.0345
2	2.54911	0.0345
8	2.23672	0.0525
12	2.158636	0.0615
16	2.110519	0.0615
20	2.075319	0.0615
24	2.058272	0.0705
42	2.021364	0.0705

Table 3.3 the horizontal location for maximum bed shear for $h_b = 0.19\ m$.

Time (hours)	Max. Bed Shear $h_b = 0.19\ m$	X Location for Max. Bed Shear (m)
0.5	3.077727	0.0525
1	2.95946	0.0525
2	2.796992	0.0525
8	2.709234	0.0435
12	2.656686	0.0435
16	2.575644	0.0525
20	2.557513	0.0435
24	2.540434	0.0525
42	2.54119	0.0435

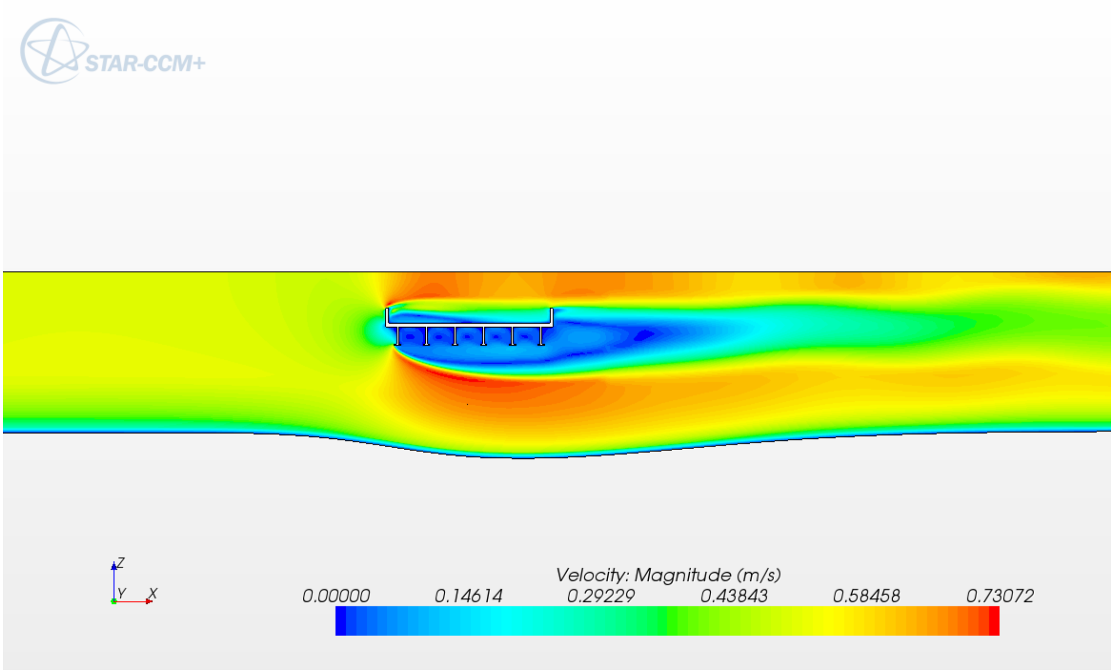

Figure 3.31 Velocity contour for $h_b = 0.135\ m$.

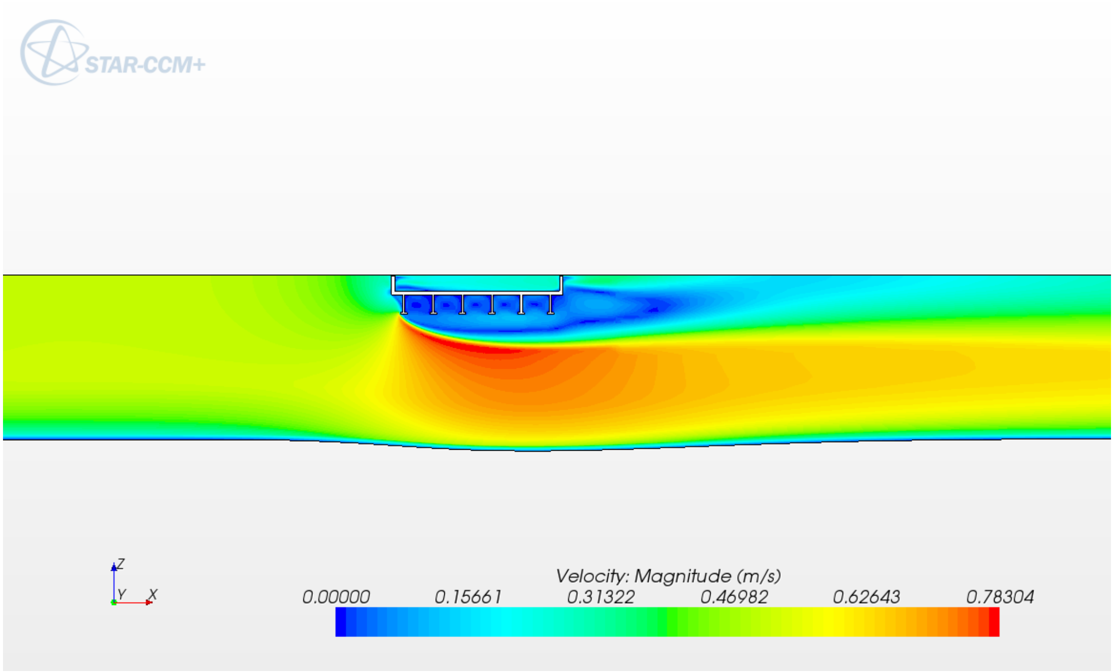

Figure 3.32 Velocity contour for $h_b = 0.19\ m$.

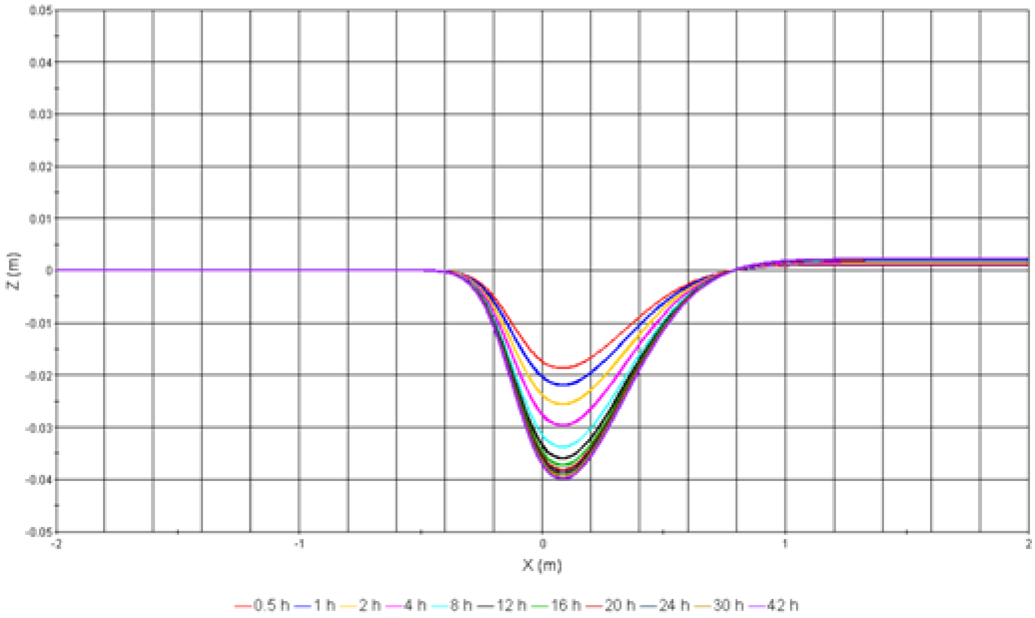

Figure 3.33 Scaled morphing bed for $h_b = 0.135\ m$.

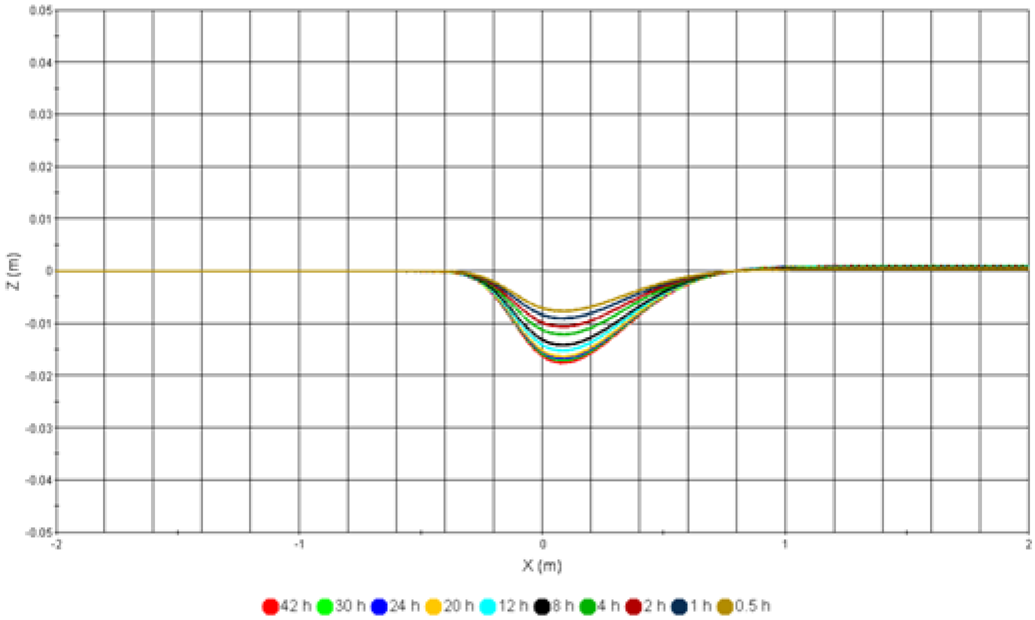

Figure 3.34 Scaled morphing bed for $h_b = 0.19\ m$.

Chapter 4 Theoretical Approaches and Analysis for Sediment Bed Load

4.0 Overview

The analysis of sediment mass conservation and momentum equations is fundamental to solve a series of erosion problems in sedimentation and hydraulics. Exner (1925) developed his equation for sediment mass balance as part of a pair of remarkably sophisticated studies of river morphology through a number of simplifying assumptions. Despite the relative simplicity of this model, the modeling results are in good agreement with what is observed. The original Exner equation can be written as,

$$\frac{\partial h}{\partial t} = -C\frac{\partial U}{\partial x} \tag{4.1}$$

where h is bed elevation relative to a given datum, t is evolving time, C is a coefficient, U is average flow velocity, and x is downward distance along the sedimentary bed. From this equation, we can see that Exner intended the flow velocity of U as medium for the sediment flux. Based on the Exner equation, a variety of forms have mostly been done for adapting it to a particular problem. For example, Parker (2005) summarized some forms appropriate for channelized systems and sediment mixtures descended from Exner equation. According to the specific problems, these forms of mass balance equations include some terms and leaves out others. Paola and Voller (2005) developed a generalized Exner equation for sediment mass balance which is useful for geologic problems for which processes such as tectonic uplift and subsidence, soil formation and creep, and dissolution and precipitation become important.

Developing governing equations of sediment transport tends to depend on the assumption of the ensemble average that is an average over a number of realizations of a flow to filter other minor fluctuations of variables especially in advection-diffusion equation. The ensemble average may be time-average, volume-average, concentration-average, or other average depending on the understanding for problems. In addition, time-averaging is equivalent to the situation in which the flow is statistically stationary while volume averaging is equivalent to the spatially uniform flow condition. Therefore, different assumptions for averaging variables need to be made in developing mass balance and momentum equations for given problems. In this dissertation, some variables, such as the components of velocity in the bed and packed sub-layer, are based on the local volume averaging to neglect the influence of fluctuations of variables.

The determination of pressure drop in a porous media or packed bed is important in the field of chemical processes. Ergun (1952) conducted a series of experiments to verify the gradient of pressure drop for fluid flow through a column of packed particles. The pressure gradient is a complex function as fluid superficial velocity, fluid viscosity, porosity of packed bed, and the particles' property at low Reynolds number which is not enough to lift the stationary particles. For the case of high Reynolds number, the particles on the bed are unsteady and fluidized, Ergun equation cannot represent the correct pressure drop, and thus it is necessary to modify it to satisfy the fluidized status. The theoretical approach for studying pressure drop through packed beds is also successfully applied to the field of hydraulics. We will analyze the Ergun equation on detail and modify it in the fluidized bed load layer.

4.1 Model Statement and Assumption

Sediment transport on the river bed is a complicated research topic in hydraulics. Depending on the size of sediment particles and flow characteristics, the status of their motion is in the bed load and suspended load. The particles' motions are classified as three different processes verified by the bed shear velocity. The sediment particles roll and slide when the bed shear velocity just exceeds the incipient velocity of particles. With the increase in the bed shear velocity, a successful jump of the particles is coming along the bed, which is called saltation. When the bed shear velocity exceeds the fall velocity of particles, the particles will be lifted in the status of suspension and move in the streamwise direction. We define the maximum saltation height, computed by the equations of motion, for a specific flow condition as the thickness of bed load layer. We can neglect the suspended load in a clear water condition in which the rolling, sliding and saltation of particles are predominant in the bed load layer. In this dissertation, the two-layer model means the derivation of equations is within the bed load layer and packed sediment layer to predict the erosion process wherein we need to derive continuous and momentum equations coupled from the two layers. Fig.4.1 provide a general information that is necessary to solve the two surface equation $\varphi_1(x,y,t)$ and $\varphi_2(x,y,t)$ to obtain the scour profile.

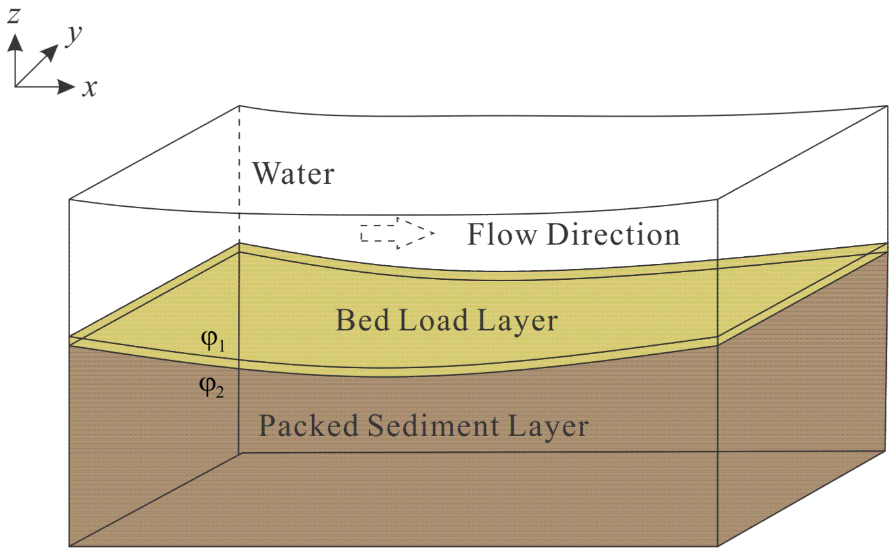

Figure 4.1 Two layer model sketch

$\varphi_1(x, y, t)$ and $\varphi_2(x, y, t)$ in Fig.4.1 represent the surface function for the top surface and the bottom interface of bed load layer, respectfully, as the scour profile functions required to be solved. We can name the model shown in Fig.4.1 two-layer sediment transport model. The transport of sediment particles is limited within the bed load layer with the maximum height of saltation. When the sediment particles are in motion, the bed load layer will be characterized, presumly, as the fluidized bed. The packed sediment layer is assumed to be a porous medium with a certain void porosity.

The bed load layer is comprised of the fluidized sediment particles and fluid. One of the important parameter in a fluidized bed is the pressure drop or pressure gradient between the cross sections within the fluidized bed. The pressure drop in the transport equations of sediment consists of a part of source term to influence the motion of particles. This parameter demands being modeled. We employ the modified Ergun equation, developed in the section 4.3, to calculate the pressure drop flowing through the fluidized bed in the momentum equation. The extending height for the fluidized bed on the bed surface is assumed to be equal to the thickness of the bed load layer in our case. On the other hand, the pressure drop in the packed sediment layer can be approximated by the Ergun equation due to the characteristics of porous media.

The model statement for the Ergun equation and modified Ergun equation is interpreted in the section 4.3. The derivation for the continuity equation, momentum equation based on the Fig.4.1 is specifically described in the section 4.5.

4.2 Parameters Definition and Conception Description

The dimensionless characteristic parameters are widely used to develop a variety of functional relationship in the sedimentation. These parameters for the most frequent usage are particle diameter, particle mobility parameter, excess bed shear stress, suspension parameter, and transport rate, which can be defined as follows,

(1) Particle parameter, D_*

This parameter represents the combined influence of immersed gravity of particle, density of particle, and fluid viscosity, written as,

$$D_* = \left[\frac{(s-1)g}{\nu^2}\right]^{1/3} d_{50} \tag{4.2}$$

in which d_{50} is the median particle diameter of the bed material, s is specific gravity, ν is kinematic viscosity coefficient, g is acceleration of gravity.

(2) Particle mobility parameter

This parameter for a plane bed reflects the ratio of the hydrodynamic force proportional to $\rho d_{50}^2 u_*^2$ and the submerged particle weight proportional to$(\rho_* - \rho) g d_{50}^3$. It yields a ratio as,

$$\theta_s = \frac{\rho d_{50}^2 u_*^2}{(\rho_* - \rho) g d_{50}^3} = \frac{u_*^2}{(s-1) g d_{50}} = \frac{\tau_b}{(\rho_* - \rho) g d_{50}} \tag{4.3}$$

in which τ_b is an overall time-averaged bed shear stress, u_* is an overall bed shear velocity equal to $\sqrt{\tau_b/\rho}$.

If the effect of bed form exists in the flow condition, the effective bed shear stress instead of the overall bed shear stress should be adopted to calculate the parameter θ_s because the form drag is not effective to entrain the sediment particles from the bed material into the fluid field.

(3) Excess bed shear stress parameter E_b

The excess bed shear stress parameter is experimentally verified to be a main factor to affect the sediment bed load, defined as,

$$E_b = \frac{\tau_b - \tau_{b,cr}}{\tau_{b,cr}} \tag{4.4}$$

in which $\tau_{b,cr}$ is critical time averaged bed shear stress. This parameter controls the process of sediment transport in many hydraulic models, such as pickup function, velocity of particle saltation, deposition rate, etc.

(4) Suspension parameter, S_z

The parameter S_z reflects the ratio of the downward submerged gravity and the upward dynamic forces acting on a suspended particle of sediment as follows,

$$S_z = \frac{w_s}{C_z \kappa u_*} \tag{4.5}$$

in which w_s is particle fall velocity in clear water, C_z is ratio of sediment and fluid mixing coefficient, κ is Von Karman constant.

(5) Sediment transport rate, q_*

The dimensionless formation of sediment transport can be represented as,

$$q_* = \frac{q_t}{\sqrt{(s-1)gd_{50}^3}} \tag{4.6}$$

where q_t is volumetric total sediment transport rate. If considering the transport rate of bed load, q_t is replaced with the volumetric sediment transport rate in the bed load layer q_s.

An important concept is how to define the pick-up rate of bed material particles. Researchers have studied the pick-up of the bed material particles. Einstein (1950) proposed that a particle can be picked up only after a period of rest, which means that the total travel distance between two successive periods of rest may cover several saltations. Yalin (1977) assumes that a particle can be in the pick-up status whenever it leaves the bed surface due to saltation, which means that each jump of particle begins with a pick-up and ends in deposition. The pick-up rate of Yalin's definition may be about 10 times as large as the corresponding rate defined by Einstein. Yalin's definition for the pick-up rate is used by many researchers. The original definition of the pick-up rate of bed material particles can be described in terms of the number of particles picked up from the bed material per unit area and time written as,

$$N_p = \chi n_p P_s \tag{4.7}$$

in which χ is fraction of susceptible particles to move exposed to flow per unit area, n_p is number of particles at rest on the bed surface per unit area, equals $1/(\alpha_1 d^2)$, d is particle diameter, α_1 is shape constant of particles ($1/4\pi$ for a sphere particle), P_s is number of pick-ups for each particle per unit time.

Based on the statistical analysis, Einstein derived the pick-up rate of sediment as,

$$E = \alpha_e \rho_s [(s-1)gd_{50}]^{0.5} P_e \tag{4.8}$$

where E is pick-up rate of particles in mass per unit area and time, P_e is probability of the lift force acting on the particle with exceeding the immersed weight of particle, α_e is a coefficient verified by experiments.

Fernandez (1974) proposed his pick-up function based on experiment data based on Einstein's definition about pick-up of particle as follows,

$$E = \alpha_f \rho_s [(s-1)gd_{50}]^{0.5} \left(\theta_s - \theta_{s,cr}\right)^{1.5} \tag{4.9}$$

where α_f is a coefficient as 0.0199, θ_s is particle mobility parameter or Shields number, $\theta_{s,cr}$ is critical value of particle mobility parameter or Shields parameter.

Yalin's pick-up function can be written as,

$$E = \alpha_y \rho_s u_* P_y \tag{4.10}$$

in which α_y is a coefficient, P_y is pick-up probability based on Yalin's definition about pick-up.

In this dissertation, the bed load transport is defined as the mode of rolling and saltating along the bed surface. The transport rate of the bed load is defined as the product of the particle velocity, the saltation height and the volume concentration of bed load. The bed load's meaning is still very confusing as a basic concept in sediment transport. The concept of 'bed load' used in sediment transport equations does not necessarily have the same meaning as the one used in bed form migration, and thus, it is necessary to verify the identical definition before comparing the calculated bed load and measured bed load from bed form migration data.

The first definition (type A) of 'bed load' in terms of bed form migration is the sediment passing the crest of a migrating bed form which is trapped in the lee side. For this definition generally used in marine environments, bed form migration data are only an indirect measurement of the sediment transport but the direct observation of the process of sediment transport. The second definition (type B) of 'bed load' in terms of the mode of grain motion, or the mechanism of momentum transfer from the theoretical viewpoint is a dynamic one, as described in the beginning of this section, that includes rolling, sliding, and saltating. These grains transfer momentum to the stationary bed surface by solid/solid contacts (collisions) (Bagnold 1966). The solid-to-solid contacts produce the momentum exchange balancing the immersed weight of the bed load particles. The flow turbulence, however, leads to the momentum of fluid to solid suspended as suspended load. Since the most field of measurements of bed load transport used the first definition, whereas the calculated transport rate of bed load is based on the bed load transport equation adopting the second definition, they are obviously different when compared. The table 4.1 gives the comparison of bed load definitions (Yang 1986).

Table 4.1 Comparison of bed load definitions (Yang 1986).

Bed form migration measurements	Sand grain size distribution	Mode of grain movement	Mechanism of momentum transfer	Sediment transport function	
Bed load definition A bed material discharge	Traction population	Sliding	Bed load with definition B Momentum transfer by solid/solid contacts (collisions)	Bed load transport function	Total sediment transport function
		Rolling			
	Intermittent suspension population	Saltation			
		Intermittent suspension	Suspended load momentum transfer by fluid turbulence	Suspended load transport function	
	Suspension population	Suspension (wash load)		Wash load transport does not depend on local flow hydrodynamics	

The pick-up function of sediment, defined as the pick-up rate in mass per unit area and time, is equal to the product of the bed load transport and the saltation length of particle. Usually, the pick-up function or called entrainment rate is empirically determined by measuring the deposition rate of particle.

4.3 Pressure Drop through Porous Media

When fluid flow through the packed particles the pressure drop will occur between inlet and outlet. The pressure gradient is dependent on the superficial velocity of fluid, fluid viscosity, porosity of packed particle and particles' diameter. The Ergun equation described the correlation of pressure gradient to those factors as follows,

$$-\frac{dp}{L} = aV^2 + bV \tag{4.11}$$

The first term on the left side is the influence of an inertial resistance, the second one results from the viscous resistance. a, b are the variable coefficients related to the physical parameters in a porous media, confirmed as,

$$a = \frac{1.75\rho(1-\emptyset)}{\emptyset^3 D}, b = \frac{150\mu(1-\emptyset)^2}{\emptyset^3 D^2} \tag{4.12}$$

where ρ is the fluid density, $\emptyset$ is the porosity, D is the mean diameter of particles, μ is the coefficient of dynamic viscosity.

Therefore, for our case, the pressure gradient is obtained as,

$$-\frac{\partial p}{\partial z} = aw^2 + bw \tag{4.13}$$

However, the Ergun equation is only appropriate for the non-fluidized bed, namely, in our packed layer. For the fluidized bed load layer, we require to modify it for satisfying its feature.

In our two-layer mathematical model described before, the packed bed layer can be analogous to porous media. For flow through porous media, it is desirable to predict the pressure drop as an important term in the momentum equation. The most famous equation modeling porous media is the Ergun equation (1952). Therefore, Ergun equation can be employed to model the pressure drop in the packed bed layer. However, it cannot describe the pressure drop in the bed load layer because the bed load layer consists of a fluidized bed distinguished from the static porous media, which requires a modified Ergun equation to model the situation in the bed load layer.

A fluidized bed plotted in Fig.4.2 is defined as a packed bed through which fluid flows at such a high velocity of fluid through the gas distributor plate that the bed material is loosened and the particle-fluid mixture behavior as fluid. In the fluidized status is the particle force balanced by drag and gravity. Both gas and liquid flows can be adopted to fluidize the bed particles. In the chemical fields, the most common reason for fluidizing a bed is to obtain vigorous agitation of the solid particles in contact with the fluid, which results in the uniform temperature in the process of chemical reaction. The analysis for fluidized bed is usually applied in catalyst regeneration, solid-gas reactors, coal combustion, roasting of ores, drying, and gas adsorption operations.

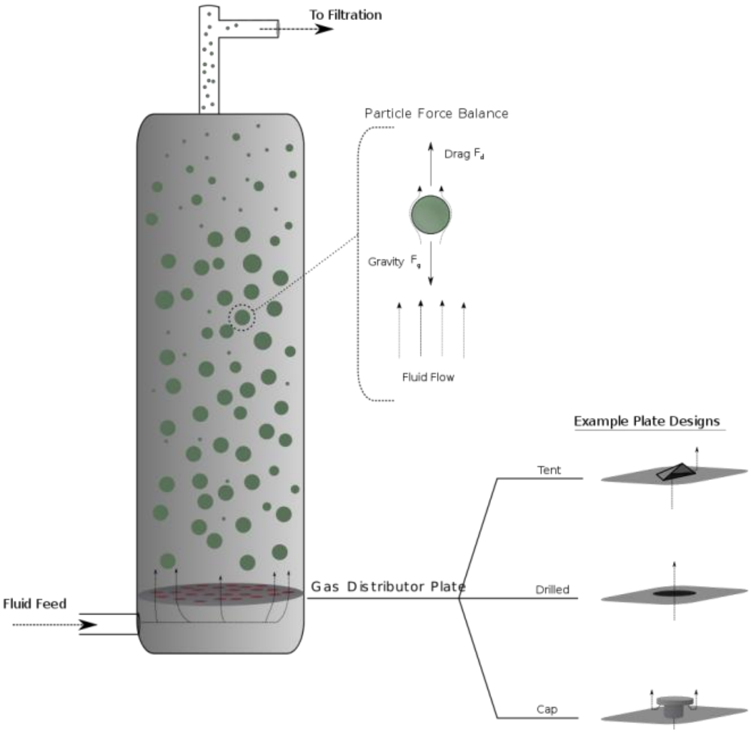

Figure 4.2 Fluidized bed (http://en.wikipedia.org/wiki/File:FluidisedBed.svg).

The sketch is drawn in Fig.4.3 for illustrating the course of bed fluidized, where V_f is the superficial velocity from fluid flow. H_b is the bed height

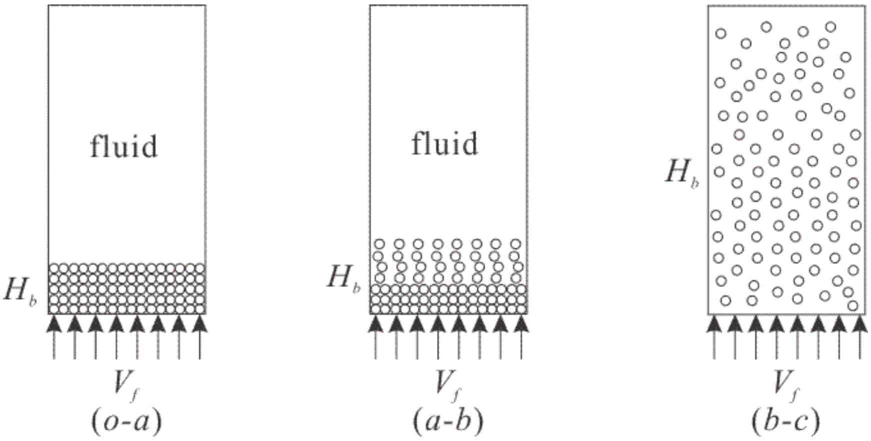

Figure 4.3 Fluidization of packed bed

Corresponding to the process of fluidization in Fig.4.3, the typically functional curves for pressure drop verse vertically superficial velocity and bed height verse vertically superficial velocity are qualitatively shown in Fig.4.4.

As shown Fig.4.4, the pressure drop, at first, is zero because of zero upward flow velocity, and the bed height has an original packed thickness. The pressure drop gradually increases with the increment of vertically superficial velocity along the path *o-a*, while the bed height remains the original value because the upward superficial velocity is not enough to lift sediment particles. The curve path *o-a* can be approximately modeled by Ergun equation for a packed bed layer. As the superficial velocity further increases, the sediment particles on the bed are lifted up to balance their submerged weight at the critical point *b* with the minimum fluidization velocity while the bed height will increase after that point. The path of curve *a-b* is the transition region from the static bed to the fully fluidized bed. The pressure drop along the path *b-c* increases no longer as the superficial velocity increases because all particles are fluidized over the minimum fluidization velocity, in the meanwhile, the bed height continues to increase with the increment of the superficial velocity along the path of curve *b-c*.

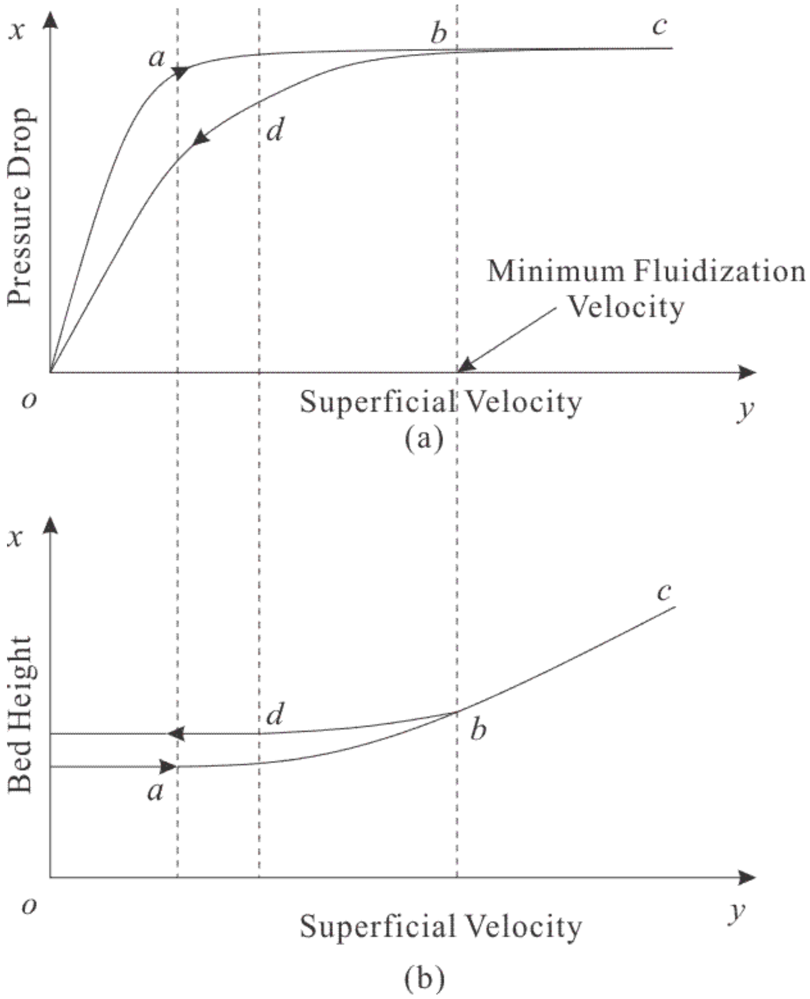

Figure 4.4 Flow through a porous media (a) Superficial velocity verse pressure drop (b) Superficial velocity verse bed height.

If we keep track of the reverse path, we find that the pressure drop stays constant until reaching the point *b* as the upward velocity decreases. In the meanwhile, the bed height descends until the superficial velocity becomes critical. For the reverse path *c*-*o*, the transition path goes along *b*-*d* from the fully fluidized status to the fully settling-down. The bed height keeps the fixed value in spite of the decrease of the superficial velocity from the point *d*. The reason why the fixed bed height on the reverse path is larger than the bed height in the initial path is that the bed height after fluidization is more loosen or porous than the original height, which also results in that the pressure drop on the reverse path *b-o* is smaller than the original path.

Although we can approximate the pressure drop for the path of *o-a* by using the Ergun equation, we cannot calculate the pressure drop along the path of *a-b* as the transition curve. The following will introduce how to derive the transition stage.

At first, we need to derive the formula for the ultimate situation with the path of *b-c*. For this case, we employ the approach of control volume for the energy equation to derive the formula of pressure drop. According to the first law of thermodynamics for a system, the time rate of increase of the total stored energy of the system equals the addition of the net time rate of energy by heat transfer into the system and the net time rate of energy by work transfer into the system, which can be expressed as,

$$\frac{D}{Dt}\left[\iiint e\rho\, dV_{vol}\right]_{sys} = \left(Q'_{net} + W'_{net}\right)_{sys} \tag{4.14}$$

where e is the total stored energy per unit mass fluid, which is related to the internal energy per unit mass, I_e , the kinetic energy per unit mass, $V^2/2$, and the potential energy per unit mass, gz by the following equation,

$$e = I_e + V^2/2 + gz \tag{4.15}$$

For the control volume, the right side of Eq.4.14 is coincident at an instant of time. Furthermore, the time rate of increase of the total stored energy of the system equals the addition of the time rate of increase of the total stored energy of the contents of the control volume and the net rate of flow of the total stored energy out of the control volume through the control volume, and hence, Eq.4.14 is also expressed as,

$$\frac{\partial}{\partial t}\left[\iiint e\bar{\rho}\, dV_{vol}\right]_{cv} + \iint e\bar{\rho}\, V \cdot ndA = \left(Q_{net}^{'} + W_{net}^{'}\right)_{cv} \tag{4.16}$$

Reference the graph in Fig.4.2 for the situation with the approximately constant pressure drop, we consider the flow status to be steady, and thus, the time rate of increase of the total stored energy in the control volume equals zero. Also, the adiabatic process is assumed during the fluidizing course of bed. The equation above is simplified as,

$$\iint e\bar{\rho}\, V \cdot ndA = \left(W_{net}^{'}\right)_{cv} \tag{4.17}$$

For convenient writing, we use $W_{net}^{'}$ instead of $\left(W_{net}^{'}\right)_{cv}$. The average density of the mixture of particles and fluid, assuming a constant, can be written as,

$$\bar{\rho} = \alpha(\rho_s - \rho) + \rho \tag{4.18}$$

The work power from the pressure flow $W_{net}^{'}$ is the product of the distributed pressure force on the control surface and the fluid velocity by the equation,

$$W_{net}^{'} = -\iint p\, V \cdot ndA \tag{4.19}$$

The negative sign means that the pressure force always normally directs the control surface. Substituting Eq.4.15 and Eq.4.19 into Eq.4.16, we have the following formation of expression,

$$\iint \left(e + \frac{p}{\bar{\rho}}\right)\bar{\rho}\, V \cdot ndA = 0 \tag{4.20}$$

Then, we have,

$$\left(I_e + V^2/2 + gz + \frac{p}{\bar{\rho}}\right)_{out} \bar{\rho} V_{out} A_{out} = \left(I_e + V^2/2 + gz + \frac{p}{\bar{\rho}}\right)_{in} \bar{\rho} V_{in} A_{in} \quad (4.21)$$

Based on the continuity equation, $\bar{\rho} V_{out} A_{out} = \bar{\rho} V_{in} A_{in}$. Neglecting the change of internal energy between the inlet and outlet section in Fig.4.3, we manipulate the equation above into the following formation,

$$\frac{p_{in} - p_{out}}{\bar{\rho}} = \frac{V_{out}^2 - V_{in}^2}{2} + g(z_{out} - z_{in}) \quad (4.22)$$

or

$$\frac{\Delta p}{H_m} = \bar{\rho} \frac{V_{out}^2 - V_{in}^2}{2H_m} + \bar{\rho} g \quad (4.23)$$

where $H_m = z_{out} - z_{in}$. From the formula above, we find that when the height of fluidized bed is large enough or the velocity difference between the inlet and outlet is small enough to neglect the first term on the right side of Eq.4.23, the pressure gradient is approximated as a constant, namely,

$$-\frac{\partial p}{\partial z} = \frac{\Delta p}{H_m} \cong \bar{\rho} g \quad (4.24)$$

Since we don't include the static pressure in the formula above, the expression is represented by,

$$-\frac{\partial p}{\partial z} \cong \alpha(\rho_s - \rho) g \quad (4.25)$$

However, it is incorrect to apply Eq.4.25 to the transition stage of fluidized bed prior to complete fluidization because of the approximate from Eq.4.23 to Eq.4.24,and hence, we need to find a way to approximate the first term on the right side of Eq.4.23 so that it can be applied to the transition stage as well.

Guo (2002) developed a very effective matching approach, the logarithmic matching, to approximate a complicated nonlinear problem. The basic statement is that for a nonlinear engineering problem, if two extreme cases as two asymptotic situations can be accurately expressed, then the logarithmic matching can combine the two cases into a single solution. Assuming the two asymptotes can be expressed as,

$$y = K_1 lnx + C_1 \quad x \ll x_0 \tag{4.26}$$

and

$$y = K_2 lnx + C_2 \quad x \gg x_0 \tag{4.27}$$

He proposed two logarithmic model s (select one of them to match two asymptotes) as the approximated solution for a nonlinear problem as follows,

$$y = K_1 lnx + \frac{K_2 - K_1}{\beta_1} ln\left[1 + \left(\frac{x}{x_0}\right)^{\beta_1}\right] + C_1 \quad \text{for model 1} \tag{4.28}$$

and

$$y = K_2 lnx - \frac{K_2 - K_1}{\beta_2} ln\left\{1 - exp\left[-\left(\frac{x}{x_0}\right)^{\beta_2}\right]\right\} + C_2 \quad \text{for model 2} \tag{4.29}$$

in which x_0 are determined with K_1, K_2, C_1 and C_2, namely, $x_0 = exp[(C_1 - C_2)/(K_2 - K_1)]$. β_1 or β_2, depending the selection of models, as a transitional shape parameter is verified by the collocation method, such as the observed value at x_0, or the least squares method.

Now we employ Guo (2002)'s approach to merge two asymptotes, the Ergun equation and the constant pressure drop gradient equation. We define $X = V_{in} = V$, so the Ergun equation is written as,

$$Y_1 = -gradp = -\frac{\partial p}{\partial z} = \frac{1.75\rho(1-\emptyset)}{\emptyset^3 D}X^2 + \frac{150\mu(1-\emptyset)^2}{\emptyset^3 D^2}X \tag{4.30}$$

Since we consider the extreme case for small Reynolds number, the Ergun equation above can be further simplified as the Kozeny-Carman equation by,

$$Y_1 = \frac{150\mu(1-\emptyset)^2}{\emptyset^3 D^2}X \tag{4.31}$$

The constant gradient of pressure drop equation is written as,

$$Y_2 = -\frac{\partial p}{\partial z} = \alpha(\rho_s - \rho)g \tag{4.32}$$

in which $C_1 = ln[150\mu(1-\emptyset)^2/(\emptyset^3 D^2)]$, $C_2 = ln(\alpha(\rho_s - \rho)g)$, $K_1 = 1$, $K_2 = 0$

Further, we adopt model 1 as the logarithmic match by the following expression,

$$y = lnX - \frac{1}{\beta_1} ln\left[1 + \left(\frac{X}{X_0}\right)^{\beta_1}\right] + ln\left[\frac{150\mu(1-\emptyset)^2}{\emptyset^3 D^2}\right] \tag{4.33}$$

Therefore, we obtain the single equation including the two asymptotes and the transition curve as follows,

$$Y = \frac{\left[\frac{150\mu(1-\emptyset)^2}{\emptyset^3 D^2}\right]X}{\left[1 + \left(\frac{X}{X_0}\right)^{\beta_1}\right]^{\frac{1}{\beta_1}}} \tag{4.34}$$

where

$$X_0 = exp\left(\frac{C_1 - C_2}{K_2 - K_1}\right) = exp\left\{-ln\left[\frac{150\mu(1-\emptyset)^2}{\alpha(\rho_s - \rho)g\emptyset^3 D^2}\right]\right\}$$

$$= \frac{\alpha(\rho_s - \rho)g\emptyset^3 D^2}{150\mu(1-\emptyset)^2} \qquad (4.35)$$

and $\alpha = 1 - \emptyset_{mf}$, in which $\emptyset_{mf}$ is the minimum fluidization porosity.

We can use the collocation method to determine the value of β_1. When the superficial velocity of flow is closed to the minimum fluidization velocity, the packed bed will be fluidized and the gradient of pressure drop can be approximately independent on the superficial velocity. The minimum fluidization velocity, determined by Wen and Yu (1966)'s formula, can be adapted to calculate the parameter β_1 that we need. Here, we assume the particle diameter is larger than 0.1 mm within the range of particle's diameter for Wen and Yu's expression as follows,

$$Re_{mf} = \frac{\rho V_{mf} d}{\mu} = 33.7\left[\sqrt{(33.7 + 3.592 \times 10^{-5} Ar)} - 1\right] \qquad (4.36)$$

where

$$Ar = \frac{\rho(\rho_s - \rho)gd^3}{\mu^2} \qquad (4.37)$$

Based on the equations above, we can conclude that the parameter β_1 is a function of the minimum fluidization velocity, and X_0 dependent on the minimum fluidization porosity.

To take a case with the air flow through the packed sediment bed with a particle's diameter of 0.287 mm for example, the parameter $Ar = 2311.1$, and thus, we can obtain the minimum fluidization velocity, $V_{mf} = 7.15\ cm/s$. According to the experimental data in Table 4.2, the minimum fluidization porosity is determined as $\emptyset_{mf} = 0.32$ by using Ergun equation, so $\alpha = 0.68$. We can obtain the parameters,

$$X_0 = 0.03 \text{ and } \beta_1 = 2$$

Table 4.2 Experiment data for air flow through a packed sediment bed (Citation from http://www.scribd.com/doc/36549923/Lab-1-Fluidized-Bed).

Superficial Velocity (cm/s)	Pressure Drop (mm)	Bed Height (mm)
0	0	150
1.20286	106	150
1.80429	152	150
2.40572	173	154
3.00716	184	155
3.60859	187	160

Fig.4.6 shows the comparison among experimental data from Table 4.2, Ergun equation and modified Ergun equation. The modified Ergun equation fits the experimental data very well while the Ergun equation gradually fails to match the experimental points when the bed begins to fluidize. The modified Ergun equation may overestimate the pressure drop when the superficial velocity is very high. The reason of this overestimate is that the modified Ergun equation doesn't consider the influence of turbulent flow on the potential energy of the system, however, as a fact, the effect from the turbulent flow become more and more obvious to the system's potential energy with the superficial velocity's increase.

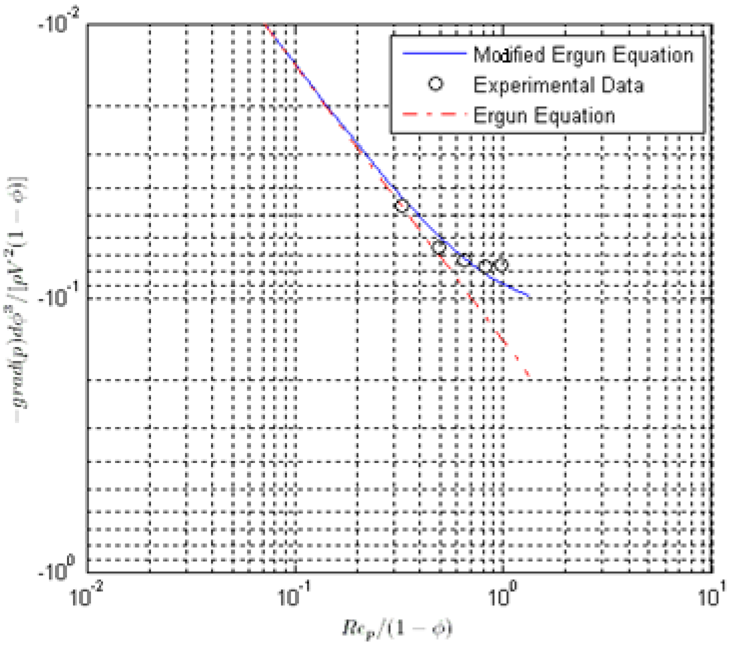

Figure 4.5 Comparison of dimensionless parameters among experimental data from Table 4.2, Ergun and modified Ergun equation.

To compare Gupte (1970), Kyan et al. (1976) and Dudgeon (1970)'s experimental data, we require to use the dimensionless formation for Eq.4.34 as follows,

$$Y_* = \frac{150}{\left[1+\left(\frac{X_*}{X_{*0}}\right)^{\beta_1}\right]^{\frac{1}{\beta_1}} X_*} \tag{4.38}$$

where

$$Y_* = \frac{-gradp \cdot d \cdot \emptyset^3}{\rho V^2(1-\emptyset)}$$

$$X_* = \frac{Re_p}{(1-\emptyset)}$$

$$X_{*0} = \frac{\left(1-\emptyset_{mf}\right)(s-1)\emptyset^3\rho^2 d^3 g}{(1-\emptyset)^3\mu^2}$$

Gupte (1970) conducted a series of experiment with the comprehensive data. Eight different porosities of bed with the same diameter of particle were tested. The results for different tests with the range of 0.365-0.64 bed porosity produced the different constant factors with the mean value of 133 and 1.29 compared to 150 and 1.75 in the Ergun equation. Fig.4.7 provides the comparison and shows that both of the Ergun equation and modified Ergun equation fit the experimental data very well for low particle Reynolds number. Gupte's experiment doesn't make the bed fluidized, and hence, both the Ergun equation and Gupte's data are not able to follow the modified Ergun equation at high particle Reynolds number.

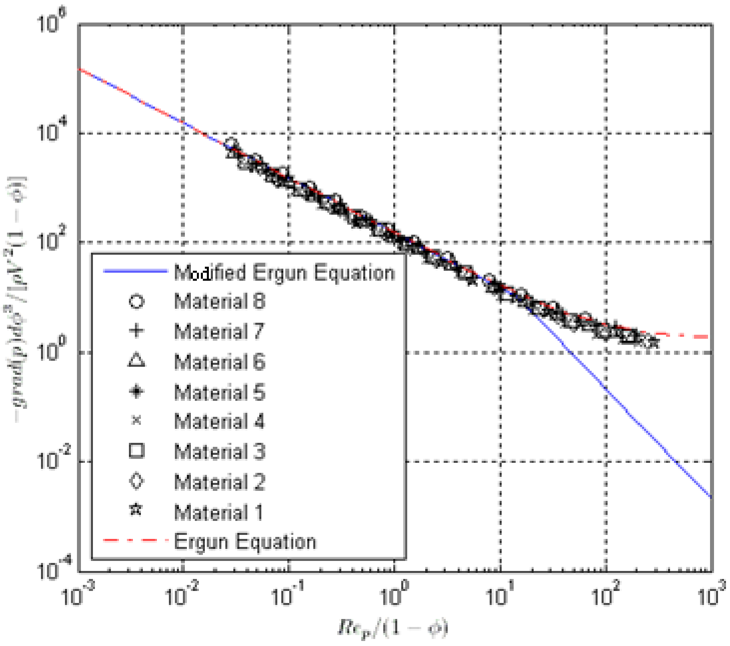

Figure 4.6 Comparison among Gupte's data, Ergun and modified Ergun equation.

Kyan (1976)'s data on high porosity fibrous beds is limited in the flow condition in which the viscous resistance predominates. The seven different tests based on three materials are examined, and different constant factors with the mean value of 194 and

8.22 are also obtained in contrast on 150 and 1.75 in the Ergun equation. The corresponding comparison is shown in Fig.4.8 which explains the agreement at low particle Reynolds number among them but deviation at high value because of the non-fluidization condition used by Kyan.

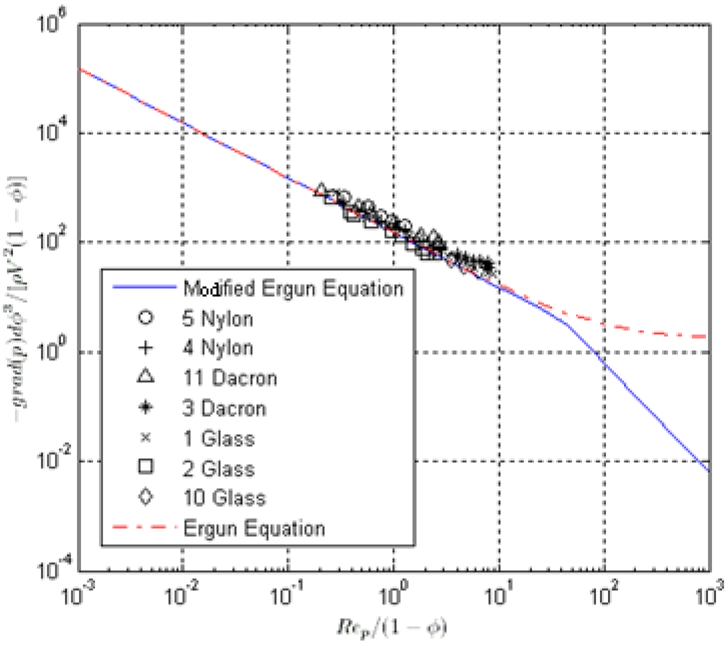

Figure 4.7 Comparison among Kyan's data, Ergun and modified Ergun equation.

Dudgeon(1970)'s data include three groups, (a) smooth, spherical marbles, (b) moderately rough gravel particles, (c) quite rough blue metal particles. We select five data sets in the group (a) and (b) to compare with the modified Ergun equation and the Ergun equation as plotted in Fig.4.9. Dudgeon determined the different constant factors with the mean value of 321 and 1.3 in the non-fluidized condition.

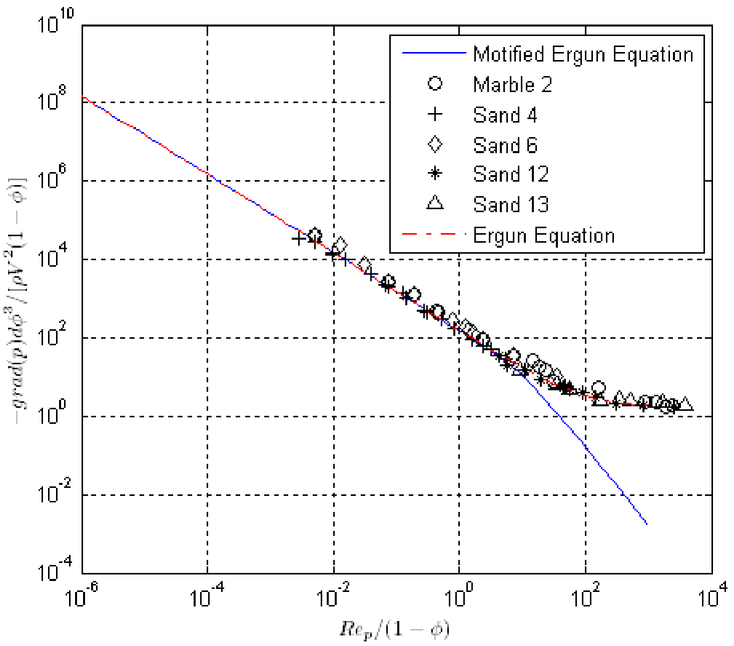

Figure 4.8 Comparison among Dudgeon’s data, Ergun and modified Ergun equation.

Table 4.3 tabulates the parameters in the modified Ergun equation which illustrates that both X_{*0} and β_1 are not constant but variables dependent on the experimental condition.

Table 4.3 X_{*0} and β_1

Data Name	X_{*0}	β_1
Gupte	14.49825	9.2612
Kyan	42.4112	10.0022
Dudgeon	10.5527	1.971

For the case of sediment transport, we cannot directly employ the modified Ergun equation to calculate the pressure drop gradient for the bed load layer by experiments because it is difficult to determine the parameters X_{*0} and β_1. The other reason is that the flow condition is steady and the fluidized particle velocity is assumed to be zero for the modified Ergun equation while the sediment particles in the bed load layer have vertical velocity in the unsteady flow. When the sediment particles in the bed load layer are fluidized by the pressure drop and the local bed shear stress, the pressure drop will include two components, one is from the calculation of Ergun equation when the bed surface just fluidizes, and the other is from the dynamic pressure drop that balances the net weight of particles after fluidization. Therefore, we consider that the particles can saltate with the minimum upward fluidization velocity as the initially trajectory velocity along the vertical direction. From Fig.4.4, the potential energy of all particles comes from the alternation of the superficial velocity transitioned from the status a to the status c as well as the potential energy of the fluidized particles is balanced by the dynamic pressure energy produced by the upward superficial velocity. Therefore, the total pressure drop in the bed load layer equals the addition of the pressure drop in the status a and the additional pressure drop balancing the potential height of the particles. Hence, the pressure drop equation for a fluidized bed neglecting the turbulent influence in the bed load layer can be approximately represented by,

$$-dp = \left[\frac{1.75\rho(1-\emptyset)}{\emptyset^3 D}V^2 + \frac{150\mu(1-\emptyset)^2}{\emptyset^3 D^2}V\right]L + \alpha(\rho_s - \rho)gL' \qquad (4.39)$$

Where dp is the pressure drop between the top and the bottom of the bed. ρ is the fluid density, $\emptyset$ is a packed bed porosity, D is a mean diameter of particles, μ is the coefficient of dynamic viscosity. V is the minimum fluidized velocity. L is the original thickness of bed. L' is the expanding thickness on the basis of L .

We can assume $L^{'} \cong L$ when it comes to the bed load layer because the bed load layer is just several times of sediment particle diameter. Therefore,

The expression above can be written as,

$$-\frac{dp}{L} = \frac{1.75\rho(1-\emptyset)}{\emptyset^3 D}V^2 + \frac{150\mu(1-\emptyset)^2}{\emptyset^3 D^2}V + \alpha(\rho_s - \rho)g \qquad (4.40)$$

4.4 Bed Load Thickness of Layer

We use Bagnold's definition for the bed load transport layer. The theoretical maximum saltation height in a give flow condition can be determined from the equations of motion for the individual bed load particle without the influence of turbulence flow. When the sediment particles with a jump height larger than the maximum saltation height these particles are classified as suspended load, otherwise, the particles are transported as a part of bed load. The particles in the bed load layer extract their momentum directly from the flow pressure and viscous stress. The trajectory consists of two stages, upward and downward. Both the normal component of drag and the gravitational force are pointed to downward on the rising stage; when the particles fall along their trajectories, the gravitational force opposes the normal component of drag. The lift acted on the particles, caused by the velocity gradient of flow and the spinning motion of the particle, is upward as long as their velocity is smaller than the flow velocity. Further, the impact of a particle on the bed surface may either be trapped into the packed surface or rebound off it and most of its momentum is dissipated by the other particles on the bed surface, which may initiate the rolling of particle.

The equation of motion of particle controlled by the complex force system, drag, lift and gravitational force, is semi-empirically and numerically solved by van Rijn dependent on the known parameters of drag, lift and initial velocity of particle determined by physical experiments. The average value of saltating length from van Rijin's numerical solution is about 16 times of particle diameter which is the same as the empirical result of Fernandez Luque and van Beek (1976).

However, in this study, several assumptions are used to attain the trajectory of particle instead of numerically solving derivative equation: (1) The trajectory of particle is approximately parabolic based on the solution of Leo and van; (2) the intercept of parabola or jumping length of saltation along the downstream direction equals the average value of Leo and van's solution; (3) for the case with bed slope, the jumping length of saltation along the horizontal direction is still closed to 16 times of particle diameter. This simplification avoids solving complex derivative equations by approximating the final track of particle controlled by drag, lift and gravity force to parabola.

The sediment concentration near the bed actually has influence on the bed load transport and bed shear stress. From view of momentum, when a particle leaves the bed, it extracts momentum from the fluid, locally reducing the shear stress of the fluid on the bed. At some position near the bed, the sediment obtains sufficient momentum from the adjacent fluid and thus reduces the bed shear stress from the flow up to the critical value at which the net erosion will not occur. Contrarily, the saltating particles can deposit in the bed surface where the volume concentration of grains decreases to allow the bed shear stress to recover above the critical value, some grains will be of incipient motion. Owen (1964) adopted this self-equilibrium condition to partition the total stress in the bed load layer into the stress the local fluid exerts on the adjacent other fluid elements and the stress the local fluid exerts on the sediment. Thus, the concentration of saltating grains and the amount of momentum transferred from the fluid to sediment, primarily achieved by the horizontal component of the drag force, determine the stress applied to sediment. Based on the self-equilibrium condition the sediment concentration near the bed has the following functional form,

$$\alpha = f(\tau_* - \tau_{*c}) \tag{4.41}$$

where α is the volume concentration of sediment particle. τ_* is the dimensionless bed shear stress and τ_{*c} is the critically dimensionless bed shear stress. The specific form used in this dissertation will be written in the section later.

4.5 Derivation of Governing Equation

4.5.1 Continuity Equation

The sediment transport mostly occurs in the bed load layer which just has the thickness of several averaged sediment diameters. The exchange of material between the bed load layer and packed sediment layer causes the formation of scour profile on the river bed. Consider a bed load layer with the volume concentration, α, and a packed sediment layer with porosity, β below the bed load layer, thus, the average density on these two layers are $\rho_b = \rho(1-\alpha) + \rho_s\alpha$ and $\rho_p = \rho\beta + \rho_s(1-\beta)$. We select the control volume crossing the bed load and packed bed layer at the interface of them to derive the mass conservation equation, as shown in Fig.4.10. The top-surface of bed load layer and the interface between these two layers are defined by the following equations,

$$\begin{cases} \varphi_1(x,y,t) - z = 0 & top\ surface\ of\ bed\ load\ layer \\ \varphi_2(x,y,t) - z = 0 & interface\ between\ two\ layers \end{cases} \tag{4.42}$$

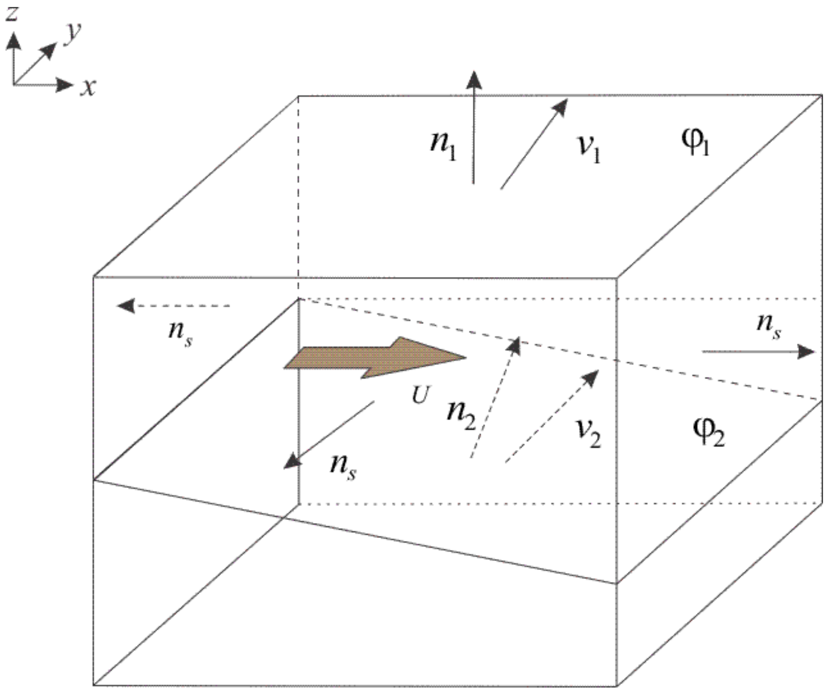

Figure 4.9 Definition sketch for two-layer model.

The unit normal for these two layers above can be calculated as,

$$\boldsymbol{n}_i = \frac{(\varphi_{ix}, \varphi_{iy}, -1)}{\sqrt{\varphi_{ix}{}^2 + \varphi_{iy}{}^2 + 1}}, i = 1,2 \tag{4.43}$$

where

$$\varphi_{ix} = \frac{\partial \varphi_i}{\partial x}, \varphi_{iy} = \frac{\partial \varphi_i}{\partial y}$$

The mass conservation equation in the bed load layer can be written as,

$$\frac{\partial}{\partial t}\iiint \rho_b dV + \iint \rho_b(\vec{U} - \vec{V}_2)\cdot \boldsymbol{n_2} dA_2 -$$

$$\iint \rho_b(\vec{U} - \vec{V}_1)\cdot \boldsymbol{n_1} dA_1 + \iint \rho_b \vec{U}\cdot \boldsymbol{n_s} dA_s = \boldsymbol{0} \tag{4.44}$$

where $\boldsymbol{n_s}$ is the outward unit normal of perimeter surface in the horizontal x-y plane in Fig.4.10.

Consider the total derivative of time for Eq.4.42, we have the following equations,

$$\frac{\partial\varphi_1}{\partial t}+\frac{\partial\varphi_1}{\partial x}\frac{\partial x}{\partial t}+\frac{\partial\varphi_1}{\partial y}\frac{\partial y}{\partial t}-\frac{\partial z}{\partial t}=0 \tag{4.45a}$$

$$\frac{\partial\varphi_2}{\partial t}+\frac{\partial\varphi_2}{\partial x}\frac{\partial x}{\partial t}+\frac{\partial\varphi_2}{\partial y}\frac{\partial y}{\partial t}-\frac{\partial z}{\partial t}=0 \tag{4.45b}$$

The local velocity of moving top surface and interface can be represented by

$$\vec{V}_1=\frac{\partial x}{\partial t}\boldsymbol{i}+\frac{\partial y}{\partial t}\boldsymbol{j}+\frac{\partial z}{\partial t}\boldsymbol{k}=u_1\boldsymbol{i}+v_1\boldsymbol{j}+w_1\boldsymbol{k} \tag{4.46a}$$

$$\vec{V}_2=\frac{\partial x}{\partial t}\boldsymbol{i}+\frac{\partial y}{\partial t}\boldsymbol{j}+\frac{\partial z}{\partial t}\boldsymbol{k}=u_2\boldsymbol{i}+v_2\boldsymbol{j}+w_2\boldsymbol{k} \tag{4.46b}$$

Also, the local velocity of flow in the control volume is written as,

$$\vec{U}=u\boldsymbol{i}+v\boldsymbol{j}+w\boldsymbol{k} \tag{4.47}$$

Thus, plugging the Eq.4.46 into Eq.4.45 can be manipulated as,

$$\left(\varphi_{1x},\varphi_{1y},-1\right)\cdot\left(u_1\boldsymbol{i}+v_1\boldsymbol{j}+w_1\boldsymbol{k}\right)=-\frac{\partial\varphi_1}{\partial t} \tag{4.48a}$$

$$\left(\varphi_{2x},\varphi_{2y},-1\right)\cdot\left(u_2\boldsymbol{i}+v_2\boldsymbol{j}+w_2\boldsymbol{k}\right)=-\frac{\partial\varphi_2}{\partial t} \tag{4.48b}$$

Combine the Eq.4.48 with Eq.4.43, we have the following equation,

$$\vec{V}_i\cdot\boldsymbol{n_i}=-\frac{\partial\varphi_i}{\partial t}\frac{1}{\sqrt{{\varphi_{ix}}^2+{\varphi_{iy}}^2+1}} \tag{4.49}$$

Thus, the transport parts in the mass conservation results in the following formula,

$$\iint \rho_b(\vec{U}-\vec{V}_i)\cdot\boldsymbol{n_i}dA_i = \iint \rho_b(\vec{U}\cdot\boldsymbol{n_i}-\vec{V}_i\cdot\boldsymbol{n_i})\,dA_i$$

$$= \iint \frac{\rho_b\left(u\varphi_{ix}+v\varphi_{iy}-w+\frac{\partial\varphi_i}{\partial t}\right)}{\sqrt{{\varphi_{ix}}^2+{\varphi_{iy}}^2+1}}dA_i$$

$$= \iint \frac{\rho_b\left(u\varphi_{ix}+v\varphi_{iy}-w+\frac{\partial\varphi_i}{\partial t}\right)}{\sqrt{{\varphi_{ix}}^2+{\varphi_{iy}}^2+1}}\sqrt{{\varphi_{ix}}^2+{\varphi_{iy}}^2+1dA_p} =$$

$$= \iint \rho_b\left(u\varphi_{ix}+v\varphi_{iy}-w+\frac{\partial\varphi_i}{\partial t}\right)dA_p$$

$$= \iint \rho_b\Pi_i\,dA_p \qquad (4.50)$$

where A_p = the projected area to *x*-*y* plane, $\Pi_i = u\varphi_{ix}+v\varphi_{iy}-w+\frac{\partial\varphi_i}{\partial t}$, which can be called the function of transport.

The first term on the left side of the equation of mass conservation can be written as (Leibniz rule),

$$\frac{\partial}{\partial t}\iiint \rho_b dV = \frac{\partial}{\partial t}\iint\int_{\varphi_2}^{\varphi_1}\rho_b dz\,dA_p$$

$$= \iint\left(\int_{\varphi_2}^{\varphi_1}\frac{\partial\rho_b}{\partial t}dz+\rho_b|_{\varphi_1}\frac{\partial\varphi_1}{\partial t}-\rho_b|_{\varphi_2}\frac{\partial\varphi_2}{\partial t}\right)dA_p \qquad (4.51)$$

Here, we assume the uniform distribution of density on the bed load layer and packed layer, respectively, which means $\rho_b|_{\varphi_1}=\rho_b|_{\varphi_2}=\rho_b$.

The last term for the continuity equation is manipulated as follows,

$$\iint \rho_b\vec{U}\cdot\boldsymbol{n_s}dA_s = \iint \rho_b\vec{U}\cdot\boldsymbol{n_s}dzdS = \int\int_{\varphi_2}^{\varphi_1}\rho_b\vec{U}dz\cdot\boldsymbol{n_s}\,dS$$

$$= \int F \cdot \boldsymbol{n}_s \, dS = \iint \nabla_h \cdot F dA_p \tag{4.52}$$

In which, dS denotes the arch length along the projected area to x-y plane, $\nabla_h = \left(\frac{\partial}{\partial \mathrm{x}}, \frac{\partial}{\partial \mathrm{y}}, 0\right)$, $F = \int_{\varphi_2}^{\varphi_1} \rho_b \vec{U} dz$. In fact, F denotes the addition of the mean mass bed load of sediment and water flow per unit width.

Based on the deduction above, the mass balance equation in the bed load layer is as follows,

$$\begin{aligned} &\iint \left(\int_{\varphi_2}^{\varphi_1} \frac{\partial \rho_b}{\partial t} dz + \rho_b|_{\varphi_1} \frac{\partial \varphi_1}{\partial t} - \rho_b|_{\varphi_2} \frac{\partial \varphi_2}{\partial t} \right) dA_p + \iint \rho_b \varPi_2|_{\varphi_2} \, dA_p \\ &\qquad - \iint \rho_b \varPi_1|_{\varphi_1} \, dA_p + \iint \nabla_h \cdot F dA_p = 0 \end{aligned} \tag{4.53}$$

Thereafter, the differential form of mass balance is obtained as,

$$\int_{\varphi_2}^{\varphi_1} \frac{\partial \rho_b}{\partial t} dz + \rho_b|_{\varphi_1} \frac{\partial \varphi_1}{\partial t} - \rho_b|_{\varphi_2} \frac{\partial \varphi_2}{\partial t} + \rho_b \varPi_2|_{\varphi_2} - \rho_b \varPi_1|_{\varphi_1} + \nabla_h \cdot F = 0 \tag{4.54}$$

We can also obtain the mass conservation equation in the packed sediment layer by the similar way,

$$\int_{\varphi_b}^{\varphi_2} \frac{\partial \rho_p}{\partial t} dz + \rho_p|_{\varphi_2} \frac{\partial \varphi_2}{\partial t} - \rho_p|_{\varphi_b} \frac{\partial \varphi_b}{\partial t} + \rho_p \varPi_b|_{\varphi_b} - \rho_p \varPi_2|_{\varphi_2} + \nabla_h \cdot F_p = 0 \tag{4.55}$$

where φ_b is the function of the bottom surface in the packed layer, $\varPi_b$ is the function of transport on the bottom surface, F_p is the transport load in the packed layer corresponding to the bed load layer. The continuity on the interface between these two layer must be satisfied, which results in $\rho_b \varPi_2|_{\varphi_2} = \rho_p \varPi_2|_{\varphi_2}$. The assumption of uniformity makes $\rho_p|_{\varphi_2} = \rho_p|_{\varphi_b} = \rho_p$.

We need to consider some assumptions for simplifying Eq.4.55. (a) the mean density in the packed layer, ρ_p, is independent on the time, $\int_{\varphi_b}^{\varphi_2} \frac{\partial \rho_p}{\partial t} dz = 0$, namely it is a time-averaged value; (b) the bottom surface on the sand bed is not changed with time, $\rho_p|_{\varphi_b} \frac{\partial \varphi_b}{\partial t} = 0$; (c) the transport load on the bottom surface of packed layer is ignored, $\rho_p \Pi_b \cong 0$.Therefore, we write Eq.4.55 as,

$$\rho_p \frac{\partial \varphi_2}{\partial t} - \rho_p \Pi_2|_{\varphi_2} + \nabla_h \cdot F_p = 0 \tag{4.56}$$

We can obtain the total mass balance equation by adding Eq.4.56 and Eq.4.54,

$$\int_{\varphi_2}^{\varphi_1} \frac{\partial \rho_b}{\partial t} dz + \rho_b \frac{\partial \varphi_1}{\partial t} + \left(\rho_p - \rho_b\right) \frac{\partial \varphi_2}{\partial t} - \rho_b \Pi_1 + \nabla_h \cdot \left(F + F_p\right) = 0 \tag{4.57}$$

If we consider no suspended sediment transport and flow penetration to the upward water region, namely, $\rho_b \Pi_1 = 0$, the equation above is written as,

$$\int_{\varphi_2}^{\varphi_1} \frac{\partial \rho_b}{\partial t} dz + \rho_b \frac{\partial \varphi_1}{\partial t} + \left(\rho_p - \rho_b\right) \frac{\partial \varphi_2}{\partial t} + \nabla_h \cdot \left(F + F_p\right) = 0 \tag{4.58}$$

Therefore, we have two equations represented by,

$$\begin{cases} \rho_b \Pi_1 = 0 \xrightarrow{yields} \dfrac{\partial \varphi_1}{\partial t} + u\varphi_{1x} + v\varphi_{1y} - w = 0 & (4.59a) \\ \displaystyle\int_{\varphi_2}^{\varphi_1} \frac{\partial \rho_b}{\partial t} dz + \rho_b \frac{\partial \varphi_1}{\partial t} + \left(\rho_p - \rho_b\right) \frac{\partial \varphi_2}{\partial t} + \nabla_h \cdot \left(F + F_p\right) = 0 & (4.59b) \end{cases}$$

Usually, the practical thickness of bed load layer is just several diameters of sediment particle, thus, we may have a reasonable assumption that the surface functions, φ_1 and φ_2, has the following relationship,

$$\varphi_2 = \varphi_1 - \delta(D, t) \tag{4.59c}$$

where $\delta(D,t)$ is the thickness of bed load layer as a function of diameter of sediment particle and time. In addition, the equilibrium status of sediment erosion is a dynamic process in which the entrainment rate of sediment equals to the deposition rate ultimately.

Plugging Eq.59a and Eq.59c into Eq.59b, the following relationship is obtained,

$$\int_{\varphi_2}^{\varphi_1} \frac{\partial \rho_b}{\partial t} dz + \rho_p \frac{\partial \varphi_1}{\partial t} - (\rho_p - \rho_b) \frac{\partial \delta}{\partial t} + \nabla_h \cdot (F + F_p) = 0 \qquad (4.60)$$

If the scour equilibrium condition occurs during this course, Eq.4.60 is reduced as,

$$\rho_b(u\varphi_{2x} - w) = \rho_p(u_p\varphi_{2x} - w_p)$$

We define the transport load in the bed load layer as following formation,

$$F = F_s + F_f \qquad (4.61a)$$

and

$$F_p = F_{ps} + F_{pf} \qquad (4.61b)$$

where F_s is the mass bed load of sediment per unit width, F_f is the mass transport rate of flow per unit width, the subscript of p denotes the corresponding parameters in the packed sediment layer where the mass of sediment transport through the perimeter area rate can be ignored because most of sediment particles are static in this layer, namely, $F_{ps} = 0$. The dimensionless bed load q_* is as follows,

$$q_* = \frac{q}{\sqrt{(s-1)gDD}} \qquad (4.61c)$$

which is employed in the next sections to simplify the equations.

4.5.2 Momentum Equation

Based on the Fig.4.10, the momentum conservation equation with integral formation can be written as,

$$\frac{\partial}{\partial t}\iiint \rho_b \vec{U} dV + \iint \rho_b \vec{U}\left(\vec{U} - \vec{V}_2\right) \cdot \boldsymbol{n_2} dA_2 - \iint \rho_b \vec{U}\left(\vec{U} - \vec{V}_1\right) \cdot \boldsymbol{n_1} dA_1$$
$$+ \iint \rho_b \vec{U}\left(\vec{U} \cdot \boldsymbol{n_s}\right) dA_s = \iiint \rho \boldsymbol{f}\, dV + \oiint \vec{T_n}\, dA \qquad (4.62)$$

where f is the body force per unit mass, $\vec{T_n}$ is the surface force acted on the boundary of control volume.

The first term of Eq.4.62 on the left side in the bed load layer can be manipulated as follows,

$$\frac{\partial}{\partial t}\iiint \rho_b \vec{U} dV = \frac{\partial}{\partial t}\iint \int_{\varphi_2}^{\varphi_1} \rho_b \vec{U} dz\, dA_p$$
$$= \iint \left(\int_{\varphi_2}^{\varphi_1} \frac{\partial\left(\rho_b \vec{U}\right)}{\partial t} dz + \rho_b \vec{U}|_{\varphi_1} \frac{\partial \varphi_1}{\partial t} - \rho_b \vec{U}|_{\varphi_2} \frac{\partial \varphi_2}{\partial t}\right) dA_p \qquad (4.63)$$

The transport parts of momentum in the momentum conservation results in the following formula similar to Eq.4.50,

$$\iint \rho_b \vec{U}\left(\vec{U} - \vec{V}_i\right) \cdot \boldsymbol{n_i} dA_i = \iint \rho_b \vec{U}\left(\vec{U} \cdot \boldsymbol{n_i} - \vec{V}_i \cdot \boldsymbol{n_i}\right) dA_i$$
$$= \iint \frac{\rho_b \vec{U}\left(u\varphi_{ix} + v\varphi_{iy} - w + \frac{\partial \varphi_i}{\partial t}\right)}{\sqrt{{\varphi_{ix}}^2 + {\varphi_{iy}}^2 + 1}} dA_i$$
$$= \iint \rho_b \vec{U}\left(u\varphi_{ix} + v\varphi_{iy} - w + \frac{\partial \varphi_i}{\partial t}\right) dA_p$$
$$= \iint \rho_b \vec{U} \Pi_i\, dA_p \qquad (4.64)$$

The last term is manipulated as follows,

$$\iint \rho_b\vec{U}\,(\vec{U}\cdot\boldsymbol{n_s})dA_s = \iint \rho_b\vec{U}\,(\vec{U}\cdot\boldsymbol{n_s})dzdS = \int\int \rho_b\vec{U}\vec{U}\cdot\boldsymbol{n_s}\,dS\,dz$$

$$= \int\iint \nabla_h\cdot\left(\rho_b\vec{U}\vec{U}\right)dA_p\,dz = \iint\int_{\varphi_2}^{\varphi_1}\nabla_h\cdot\left(\rho_b\vec{U}\vec{U}\right)dz\,dA_p \quad (4.65)$$

The addition of Eq.4.63, Eq.4.64 and Eq.4.65 results in the following form as the left side of Eq.4.62,

$$\iint\left(\int_{\varphi_2}^{\varphi_1}\frac{\partial\left(\rho_b\vec{U}\right)}{\partial t}dz + \rho_b\vec{U}|_{\varphi_1}\frac{\partial\varphi_1}{\partial t} - \rho_b\vec{U}|_{\varphi_2}\frac{\partial\varphi_2}{\partial t}\right)dA_p + \iint \rho_b\vec{U}\Pi_2\,dA_p$$

$$-\iint \rho_b\vec{U}\Pi_1\,dA_p + \iint\int_{\varphi_2}^{\varphi_1}\nabla_h\cdot\left(\rho_b\vec{U}\vec{U}\right)dz\,dA_p$$

$$= \iint\left(\int_{\varphi_2}^{\varphi_1}\left(\frac{\partial\left(\rho_b\vec{U}\right)}{\partial t} + \nabla_h\cdot\left(\rho_b\vec{U}\vec{U}\right)\right)dz + \rho_b\vec{U}|_{\varphi_1}\frac{\partial\varphi_1}{\partial t} - \rho_b\vec{U}|_{\varphi_2}\frac{\partial\varphi_2}{\partial t} + \rho_b\vec{U}\Pi_2\right.$$

$$\left. - \rho_b\vec{U}\Pi_1\right)dA_p \quad (4.66)$$

Here, we can extend the part in the first pair of brackets in Eq.4.66 above,

$$\frac{\partial\left(\rho_b\vec{U}\right)}{\partial t} + \nabla_h\cdot\left(\rho_b\vec{U}\vec{U}\right)$$

$$= \vec{U}\frac{\partial\rho_b}{\partial t} + \rho_b\frac{\partial\vec{U}}{\partial t} + \left[\vec{U}\nabla_h\cdot\left(\rho_b\vec{U}\right) + \rho_b\left(\vec{U}\cdot\nabla_h\right)\vec{U}\right]_{xy\,plane} \quad (4.67)$$

Thus, the left side for Eq.4.66 has the following form,

$$\iint \left\{ \int_{\varphi_2}^{\varphi_1} \left[\vec{U}\frac{\partial \rho_b}{\partial t} + \rho_b \frac{\partial \vec{U}}{\partial t} + \left[\vec{U}\nabla_h\cdot(\rho_b\vec{U}) + \rho_b(\vec{U}\cdot\nabla_h)\vec{U}\right]_{xy\ plane} \right] dz + \rho_b \vec{U}|_{\varphi_1}\frac{\partial\varphi_1}{\partial t} - \rho_b\vec{U}|_{\varphi_2}\frac{\partial \varphi_2}{\partial t} + \rho_b\vec{U}\Pi_2 - \rho_b\vec{U}\Pi_1 \right\} dA_p \qquad (4.68)$$

The left side of Eq.4.62 in the packed sediment layer has the following form,

$$\frac{\partial}{\partial t}\iiint \rho_p\vec{U}_p dV + \iint \rho_p\vec{U}_p(\vec{U}_p - \vec{V}_b)\cdot \boldsymbol{n_b} dA_b - \iint \rho_p\vec{U}_p(\vec{U}_p - \vec{V}_2)\cdot \boldsymbol{n_2} dA_2 + \iint \rho_p\vec{U}_p\,(\vec{U}_p\cdot \boldsymbol{n_{bs}})dA_{\boldsymbol{bs}} \qquad (4.69)$$

where the subscript p denotes the corresponding physical parameter in the packed sediment layer, $\boldsymbol{n_b}$, A_b, $\boldsymbol{n_{bs}}$ and $A_{\boldsymbol{bs}}$ represent the unit normal of the bottom surface, surface area, the laterally outward unit normal and surface area.

Based on the assumption we discussed before, we have one term equal zero in the packed sediment layer on the left side of Eq.4.69, namely,

$$\iint \rho_p\vec{U}_p(\vec{U}_p - \vec{V}_b)\cdot \boldsymbol{n_b} dA_b = 0$$

Therefore, the left side of Eq.4.69 for the packed layer is simplified as,

$$\frac{\partial}{\partial t}\iiint \rho_p\vec{U}_p dV - \iint \rho_p\vec{U}_p(\vec{U}_p - \vec{V}_b)\cdot \boldsymbol{n_2} dA_2 + \iint \rho_p\vec{U}_p\,(\vec{U}_p\cdot \boldsymbol{n_{bs}})dA_{\boldsymbol{bs}}$$

$$= \iint \left(\int_{\varphi_b}^{\varphi_2} \frac{\partial(\rho_b\vec{U}_p)}{\partial t} dz + \rho_p\vec{U}_p|_{\varphi_2}\frac{\partial\varphi_2}{\partial t} - \rho_p\vec{U}_p|_{\varphi_b}\frac{\partial\varphi_b}{\partial t} \right) dA_p - \iint \rho_p\vec{U}_p\Pi_2\, dA_p + \iint \int_{\varphi_b}^{\varphi_2} \nabla_h\cdot(\rho_b\vec{U}_p\vec{U}_p) dz\, dA_p$$

$$
\begin{aligned}
= \iint \Bigg\{ \int_{\varphi_b}^{\varphi_2} \Bigg[\vec{U}_p \frac{\partial \rho_p}{\partial t} + \rho_p \frac{\partial \vec{U}_p}{\partial t} + \left[\vec{U}_p \nabla_h \cdot (\rho_p \vec{U}_p) + \rho_p (\vec{U}_p \cdot \nabla_h)\vec{U}_p\right]_{xy\ plane} \Bigg] dz \\
+ \rho_p \vec{U}_p|_{\varphi_2} \frac{\partial \varphi_2}{\partial t} - \rho_p \vec{U}_p|_{\varphi_b} \frac{\partial \varphi_b}{\partial t} - \rho_p \vec{U}_p \Pi_2 \Bigg\} dA_p
\end{aligned}
$$

$$
\begin{aligned}
= \iint \Bigg\{ \int_{\varphi_b}^{\varphi_2} \Bigg[\vec{U}_p \frac{\partial \rho_p}{\partial t} + \rho_p \frac{\partial \vec{U}_p}{\partial t} + \left[\vec{U}_p \nabla_h \cdot (\rho_p \vec{U}_p) + \rho_p (\vec{U}_p \cdot \nabla_h)\vec{U}_p\right]_{xy\ plane} \Bigg] dz \\
+ \rho_p \vec{U}_p|_{\varphi_2} \frac{\partial \varphi_2}{\partial t} - \rho_p \vec{U}_p \Pi_2 \Bigg\} dA_p
\end{aligned}
\tag{4.70}
$$

Similarly, adding Eq.4.70 into Eq.4.68 results in the total expression of left side for momentum conservation equation written as,

$$
\begin{aligned}
\iint \Bigg\{ \int_{\varphi_2}^{\varphi_1} \Bigg[\vec{U} \frac{\partial \rho_b}{\partial t} + \rho_b \frac{\partial \vec{U}}{\partial t} + \left[\vec{U} \nabla_h \cdot (\rho_b \vec{U}) + \rho_b (\vec{U} \cdot \nabla_h)\vec{U}\right]_{xy\ plane} \Bigg] dz + \rho_b \vec{U}|_{\varphi_1} \frac{\partial \varphi_1}{\partial t} \\
- \rho_b \vec{U}|_{\varphi_2} \frac{\partial \varphi_2}{\partial t} - \rho_b \vec{U} \Pi_1 + \int_{\varphi_b}^{\varphi_2} \Bigg[\vec{U}_p \frac{\partial \rho_p}{\partial t} + \rho_p \frac{\partial \vec{U}_p}{\partial t} \Bigg] dz \\
+ \int_{\varphi_b}^{\varphi_2} \Big[\left[\vec{U}_p \nabla_h \cdot (\rho_p \vec{U}_p) + \rho_p (\vec{U}_p \cdot \nabla_h)\vec{U}_p\right]_{xy\ plane} \Big] dz \\
+ \rho_p \vec{U}_p|_{\varphi_2} \frac{\partial \varphi_2}{\partial t} \Bigg\} dA_p
\end{aligned}
$$

$$
\begin{aligned}
= \iint \Bigg\{ \int_{\varphi_2}^{\varphi_1} \Bigg[\rho_b \frac{\partial \vec{U}}{\partial t} + \left[\vec{U} \nabla_h \cdot (\rho_b \vec{U}) + \rho_b (\vec{U} \cdot \nabla_h)\vec{U}\right]_{xy\ plane} \Bigg] dz + \rho_b \vec{U}|_{\varphi_1} \frac{\partial \varphi_1}{\partial t} \\
+ \left(\rho_p \vec{U}_p|_{\varphi_2} - \rho_b \vec{U}|_{\varphi_2}\right) \frac{\partial \varphi_2}{\partial t} \\
+ \int_{\varphi_b}^{\varphi_2} \Bigg[\rho_p \frac{\partial \vec{U}_p}{\partial t} + \left[\vec{U}_p \nabla_h \cdot (\rho_p \vec{U}_p) + \rho_p (\vec{U}_p \cdot \nabla_h)\vec{U}_p\right]_{xy\ plane} \Bigg] dz \Bigg\} dA_p
\end{aligned}
$$

$$
\begin{aligned}
= \iint \Bigg\{ \int_{\varphi_2}^{\varphi_1} \left[\rho_b \frac{\partial \vec{U}}{\partial t} + \left[\vec{U}\nabla_h \cdot (\rho_b \vec{U}) + \rho_b (\vec{U}\cdot\nabla_h)\vec{U}\right]_{xy\,plane} \right] dz + \rho_b \vec{U}|_{\varphi_1} \frac{\partial \varphi_1}{\partial t} \\
+ \left(\rho_p \vec{U}|_{\varphi_2} - \rho_b \vec{U}|_{\varphi_2}\right) \frac{\partial \varphi_2}{\partial t} + \left(\rho_p \vec{U}_p|_{\varphi_2} - \rho_p \vec{U}|_{\varphi_2}\right) \frac{\partial \varphi_2}{\partial t} \\
+ \int_{\varphi_b}^{\varphi_2} \left[\rho_p \frac{\partial \vec{U}_p}{\partial t} + \left[\vec{U}_p \nabla_h \cdot (\rho_p \vec{U}_p) + \rho_p (\vec{U}_p \cdot \nabla_h)\vec{U}_p\right]_{xy\,plane} \right] dz \Bigg\} dA_p
\end{aligned}
$$

$$
\begin{aligned}
= \iint \Bigg\{ \int_{\varphi_2}^{\varphi_1} \left[\rho_b \frac{\partial \vec{U}}{\partial t} + \left[\vec{U}\nabla_h \cdot (\rho_b \vec{U}) + \rho_b (\vec{U}\cdot\nabla_h)\vec{U}\right]_{xy\,plane} \right] dz \\
+ \bar{U} \left[\rho_b \frac{\partial \varphi_1}{\partial t} + (\rho_p - \rho_b) \frac{\partial \varphi_2}{\partial t} \right] + \left(\rho_p \vec{U}_p|_{\varphi_2} - \rho_p \vec{U}|_{\varphi_2}\right) \frac{\partial \varphi_2}{\partial t} \\
+ \int_{\varphi_b}^{\varphi_2} \left[\rho_p \frac{\partial \vec{U}_p}{\partial t} + \left[\vec{U}_p \nabla_h \cdot (\rho_p \vec{U}_p) + \rho_p (\vec{U}_p \cdot \nabla_h)\vec{U}_p\right]_{xy\,plane} \right] dz \Bigg\} dA_p
\end{aligned}
$$

$$
\begin{aligned}
= \iint \Bigg\{ \int_{\varphi_2}^{\varphi_1} \left[\rho_b \frac{\partial \vec{U}}{\partial t} + \left[\vec{U}\nabla_h \cdot (\rho_b \vec{U}) + \rho_b (\vec{U}\cdot\nabla_h)\vec{U}\right]_{xy\,plane} \right] dz \\
+ \bar{U}\left(-\nabla_h \cdot (F + F_p)\right) + \rho_p \left(\vec{U}_p|_{\varphi_2} - \vec{U}|_{\varphi_2}\right) \frac{\partial \varphi_2}{\partial t} + \int_{\varphi_b}^{\varphi_2} \left[\rho_p \frac{\partial \vec{U}_p}{\partial t} \right] dz \\
+ \int_{\varphi_b}^{\varphi_2} \left[\left[\vec{U}_p \nabla_h \cdot (\rho_p \vec{U}_p) + \rho_p (\vec{U}_p \cdot \nabla_h)\vec{U}_p\right]_{xy\,plane} \right] dz \Bigg\} dA_p \qquad (4.71)
\end{aligned}
$$

where $\rho_b \vec{U} \Pi_1 = 0$ according to the assumption without suspended sediment transported, $\bar{U}$ is the average velocity over the bed load layer, which means $\vec{U}|_{\varphi_2} = \vec{U}|_{\varphi_1} = \bar{U}$.

The right side for momentum equation 4.62 consists of the resultant forces acted on the control volume including body force and distributed surface force.

For the body force acted on the control volume,

$$
\begin{aligned}
\iiint \rho f\, dV &= \iiint -\rho g_1 \boldsymbol{k}\, dV_b + \iiint (-\rho g_2 \boldsymbol{k})\, dV_p \\
&= \iint (-\rho g_1 \boldsymbol{k})\, \delta dA_p + \iint (-\rho g_2 \boldsymbol{k})(\varphi_2 - \varphi_b)\, dA_p \\
&= -\iint [\rho(g_1 - g_2)\delta + \rho g_2(\delta + Z_e)]\, \boldsymbol{k} dA_p \qquad (4.72)
\end{aligned}
$$

where δ is the thickness of the bed load, and define $\varphi_2 - \varphi_b = Z_e$. The mean acceleration terms in these two layers, $g_1 = 1 - \alpha + (s-1)\alpha$ and $g_2 = \beta + (s-1)(1-\beta)$, respectively.

The surface force can be represented by,

$$\vec{\emptyset} = \oiint \overrightarrow{T_n}\, dA \qquad (4.73)$$

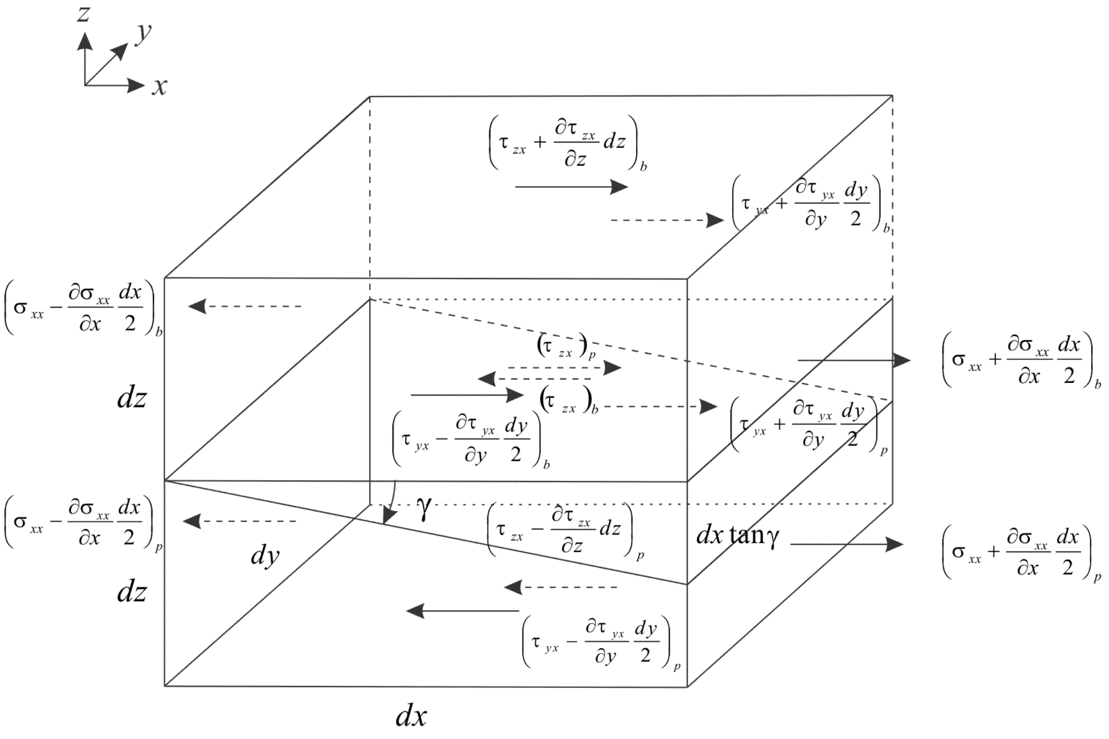

Figure 4.10 Force distribution sketch on a micro-element body.

Based on the analysis of force distributed on an element body at the interface between the bed load layer and packed layer in Fig.4.12 without the consideration of transverse slope, the x component for the surface force is deduced as,

$$\begin{aligned}\emptyset_x = {} & \left(\sigma_{xx} + \frac{\partial \sigma_{xx}}{\partial x}\frac{dx}{2}\right)\bigg|_b dy(dz + dxtan\gamma) - \left(\sigma_{xx} - \frac{\partial \sigma_{xx}}{\partial x}\frac{dx}{2}\right)\bigg|_b dydz \\ & + \left(\tau_{zx} + \frac{\partial \tau_{zx}}{\partial z}dz\right)\bigg|_b dxdy - (\tau_{zx})|_b dxdy \\ & + \left(\tau_{yx} + \frac{\partial \tau_{yx}}{\partial y}\frac{dy}{2}\right)\bigg|_b dxdz - \left(\tau_{yx} - \frac{\partial \tau_{yx}}{\partial y}\frac{dy}{2}\right)\bigg|_b dxdz \\ & + \left(\sigma_{xx} + \frac{\partial \sigma_{xx}}{\partial x}\frac{dx}{2}\right)\bigg|_p dy(dz - dxtan\gamma) - \left(\sigma_{xx} - \frac{\partial \sigma_{xx}}{\partial x}\frac{dx}{2}\right)\bigg|_p dydz \\ & - \left(\tau_{zx} - \frac{\partial \tau_{zx}}{\partial z}dz\right)\bigg|_p dxdy + (\tau_{zx})|_p dxdy \\ & + \left(\tau_{yx} + \frac{\partial \tau_{yx}}{\partial y}\frac{dy}{2}\right)\bigg|_p dxdz - \left(\tau_{yx} - \frac{\partial \tau_{yx}}{\partial y}\frac{dy}{2}\right)\bigg|_p dxdz\end{aligned}$$

$$\begin{aligned} = {} & \left[\left(\frac{\partial \sigma_{xx}}{\partial x}\right)\bigg|_b dxdydz + \left(\sigma_{xx} + \frac{\partial \sigma_{xx}}{\partial x}\frac{dx}{2}\right)\bigg|_b dxdytan\gamma\right] \\ & + \left[\left(\tau_{zx} + \frac{\partial \tau_{zx}}{\partial z}dz\right)\bigg|_b dxdy - (\tau_{zx})|_b dxdy\right] + \left(\frac{\partial \tau_{yx}}{\partial y}\right)\bigg|_b dxdydz \\ & + \left[\left(\frac{\partial \sigma_{xx}}{\partial x}\right)\bigg|_p dxdydz - \left(\sigma_{xx} + \frac{\partial \sigma_{xx}}{\partial x}\frac{dx}{2}\right)\bigg|_p dxdytan\gamma\right] \\ & + \left[-\left(\tau_{zx} - \frac{\partial \tau_{zx}}{\partial z}dz\right)\bigg|_p dxdy + (\tau_{zx})|_p dxdy\right] + \left(\frac{\partial \tau_{yx}}{\partial y}\right)\bigg|_p dxdydz\end{aligned}$$

$$= \left[\left(\frac{\partial \sigma_{xx}}{\partial x}\right)\bigg|_b dz + \left(\frac{\partial \tau_{yx}}{\partial y}\right)\bigg|_b dz + \left(\tau_{zx} + \frac{\partial \tau_{zx}}{\partial z}dz\right)\bigg|_b\right]dxdy$$

$$+\left[\left(\sigma_{xx}+\frac{\partial\sigma_{xx}}{\partial x}\frac{dx}{2}\right)\bigg|_b tan\gamma\right]dxdy+\left[\left(\frac{\partial\sigma_{xx}}{\partial x}\right)\bigg|_p dz+\left(\frac{\partial\tau_{yx}}{\partial y}\right)\bigg|_p dz\right]dxdy$$

$$+\left[-\left(\tau_{zx}-\frac{\partial\tau_{zx}}{\partial z}dz\right)\bigg|_p-\left(\sigma_{xx}+\frac{\partial\sigma_{xx}}{\partial x}\frac{dx}{2}\right)\bigg|_p tan\gamma\right]dxdy \tag{4.74}$$

Note since the internal force in the bed and packed layer cancel each other, $(\tau_{zx})|_p dxdy=(\tau_{zx})|_b dxdy$. The formula above is rewritten as,

$$\emptyset_x=\left[\left(\frac{\partial\sigma_{xx}}{\partial x}\right)\bigg|_b dz+\left(\frac{\partial\tau_{yx}}{\partial y}\right)\bigg|_b dz\right]dxdy$$

$$+\left[\left(\tau_{zx}+\frac{\partial\tau_{zx}}{\partial z}dz\right)\bigg|_b+\left(\sigma_{xx}+\frac{\partial\sigma_{xx}}{\partial x}\frac{dx}{2}\right)\bigg|_b tan\gamma\right]dxdy$$

$$+\left[\left(\frac{\partial\sigma_{xx}}{\partial x}\right)\bigg|_p dz+\left(\frac{\partial\tau_{yx}}{\partial y}\right)\bigg|_p dz-\left(\tau_{zx}-\frac{\partial\tau_{zx}}{\partial z}dz\right)\bigg|_p\right.$$

$$\left.-\left(\sigma_{xx}+\frac{\partial\sigma_{xx}}{\partial x}\frac{dx}{2}\right)\bigg|_p tan\gamma\right]dxdy \tag{4.75}$$

We can define

$$\tau_{ax}=\left[\left(\sigma_{xx}+\frac{\partial\sigma_{xx}}{\partial x}\frac{dx}{2}\right)\bigg|_b-\left(\sigma_{xx}+\frac{\partial\sigma_{xx}}{\partial x}\frac{dx}{2}\right)\bigg|_p\right] \tag{4.76}$$

in which, in fact, $\tau_{ax}tan\gamma$ is an additionally normal stress downstream caused by the alternative streamwise slope.

We separate the pressure from the normal stress and $\emptyset_x$ is expressed by the integral form as,

$$\emptyset_x = \iint \left[\int_{\varphi_2}^{\varphi_1} \left(-\frac{\partial p}{\partial x} + \frac{\partial \tau_{xx}}{\partial x} + \frac{\partial \tau_{zx}}{\partial z} + \frac{\partial \tau_{yx}}{\partial y}\right)\Bigg|_b dz\right] dxdy + \iint (\tau_{zx})|_b \, dxdy$$

$$+ \iint \left[\int_{\varphi_b}^{\varphi_2} \left(-\frac{\partial p}{\partial x} + \frac{\partial \tau_{xx}}{\partial x} + \frac{\partial \tau_{zx}}{\partial z} + \frac{\partial \tau_{yx}}{\partial y}\right)\Bigg|_p dz\right] dxdy$$

$$- \iint (\tau_{zx})|_p \, dxdy + \iint \tau_{ax} \, tan\gamma dxdy$$

$$= \iint \left[\int_{\varphi_2}^{\varphi_1} \left(-\frac{\partial p}{\partial x} + \frac{\partial \tau_{xx}}{\partial x} + \frac{\partial \tau_{zx}}{\partial z} + \frac{\partial \tau_{yx}}{\partial y}\right)\Bigg|_b dz\right] dxdy$$

$$+ \iint \left[\int_{\varphi_b}^{\varphi_2} \left(-\frac{\partial p}{\partial x} + \frac{\partial \tau_{xx}}{\partial x} + \frac{\partial \tau_{zx}}{\partial z} + \frac{\partial \tau_{yx}}{\partial y}\right)\Bigg|_p dz\right] dxdy + \iint \tau_{ax} tan\gamma \, dxdy \qquad (4.77)$$

Here, we define,

$$\xi_{bx} = \iint \left[\int_{\varphi_2}^{\varphi_1} \left(-\frac{\partial p}{\partial x} + \frac{\partial \tau_{xx}}{\partial x} + \frac{\partial \tau_{zx}}{\partial z} + \frac{\partial \tau_{yx}}{\partial y}\right)\Bigg|_b dz\right] dxdy \qquad (4.78a)$$

$$\xi_{px} = \iint \left[\int_{\varphi_b}^{\varphi_2} \left(-\frac{\partial p}{\partial x} + \frac{\partial \tau_{xx}}{\partial x} + \frac{\partial \tau_{zx}}{\partial z} + \frac{\partial \tau_{yx}}{\partial y}\right)\Bigg|_p dz\right] dxdy \qquad (4.78b)$$

In the bed load and packed sediment layer, respectively, we simplify the formula above as,

$$\xi_{bx} = \iint \left[\int_{\varphi_2}^{\varphi_1} \left(-\frac{\partial p}{\partial x} + \frac{\partial \tau_{xx}}{\partial x} + \frac{\partial \tau_{zx}}{\partial z} + \frac{\partial \tau_{yx}}{\partial y}\right)\Bigg|_b dz\right] dxdy$$

$$= \iint \left[\int_{\varphi_2}^{\varphi_1} \left(-\frac{\partial p}{\partial x} + \frac{\partial \tau_{xx}}{\partial x} + \frac{\partial \tau_{yx}}{\partial y}\right)\Bigg|_b dz + \left(\tau_{zx}|_{\varphi_1} - \tau_{zx}|_{\varphi_2}\right)\right] dA_p \qquad (4.79a)$$

$$\xi_{px} = \iint \left[\int_{\varphi_b}^{\varphi_2} \left(-\frac{\partial p}{\partial x} + \frac{\partial \tau_{xx}}{\partial x} + \frac{\partial \tau_{zx}}{\partial z} + \frac{\partial \tau_{yx}}{\partial y}\right)\Bigg|_p dz\right] dxdy$$

$$= \iint \left[\int_{\varphi_b}^{\varphi_2} \left(-\frac{\partial p}{\partial x} + \frac{\partial \tau_{xx}}{\partial x} + \frac{\partial \tau_{yx}}{\partial y} \right) \Big|_p dz + \left(\tau_{zx}|_{\varphi_2} - \tau_{zx}|_{\varphi_b} \right) \right] dA_p \qquad (4.79b)$$

Therefore,

$$\xi_{bx} + \xi_{px} = \iint \left[\int_{\varphi_2}^{\varphi_1} \left(-\frac{\partial p}{\partial x} + \frac{\partial \tau_{xx}}{\partial x} + \frac{\partial \tau_{yx}}{\partial y} \right) \Big|_b dz \right.$$
$$\left. + \int_{\varphi_b}^{\varphi_2} \left(-\frac{\partial p}{\partial x} + \frac{\partial \tau_{xx}}{\partial x} + \frac{\partial \tau_{yx}}{\partial y} \right) \Big|_p dz + \left(\tau_{zx}|_{\varphi_1} - \tau_{zx}|_{\varphi_b} \right) \right] dA_p \quad (4.80)$$

Assume the surface forces except for pressure can be ignored in the packed sediment layer because of its static feature without the shear deformation, we obtain the following form,

$$\emptyset_x = \iint \left[\int_{\varphi_2}^{\varphi_1} \left(-\frac{\partial p}{\partial x} + \frac{\partial \tau_{xx}}{\partial x} + \frac{\partial \tau_{yx}}{\partial y} \right) \Big|_b dz + \int_{\varphi_b}^{\varphi_2} \left(-\frac{\partial p}{\partial x} \right) \Big|_p dz + \tau_{zx}|_{\varphi_1} \right] dA_p$$
$$+ \iint \tau_{ax} tan\gamma \, dxdy \qquad (4.81a)$$

Similarly, we have the other two components of force along y and z axis as follows,

$$\emptyset_y = \iint \left[\int_{\varphi_2}^{\varphi_1} \left(-\frac{\partial p}{\partial y} + \frac{\partial \tau_{yy}}{\partial y} + \frac{\partial \tau_{xy}}{\partial x} \right) \Big|_b dz + \int_{\varphi_b}^{\varphi_2} \left(-\frac{\partial p}{\partial y} \right) \Big|_p dz \right.$$
$$\left. + \tau_{zy} \big|_{\varphi_1} \right] dA_p \qquad (4.81b)$$

$$\emptyset_z = \iint \left[\int_{\varphi_2}^{\varphi_1} \left(-\frac{\partial p}{\partial z} + \frac{\partial \tau_{zz}}{\partial z} + \frac{\partial \tau_{xz}}{\partial x} + \frac{\partial \tau_{yz}}{\partial y} \right) \Big|_b dz + \int_{\varphi_b}^{\varphi_2} \left(-\frac{\partial p}{\partial z} \right) \Big|_p dz \right] dA_p$$
$$- \iint [\rho(g_1 - g_2)\delta + \rho g_2(\delta + Z_e)] \, dA_p \qquad (4.81c)$$

Here, we drop the items, τ_{ay} and τ_{az}, closed to the infinitesimal amounts of the second order wherein the change of horizontal slope have little effect on the normal stress along y and z axis.

Also, we assume there is no additional normal stress from the deformation in the bed load layer, namely, $\tau_{xx} = \tau_{yy} = \tau_{zz} = 0$ resulting in,

$$\emptyset_x = \iint \left[\int_{\varphi_2}^{\varphi_1} \left(-\frac{\partial p}{\partial x} + \frac{\partial \tau_{yx}}{\partial y} \right) \bigg|_b dz + \int_{\varphi_b}^{\varphi_2} \left(-\frac{\partial p}{\partial x} \right) \bigg|_p dz + \tau_{zx}|_{\varphi_1} \right] dA_p$$

$$+ \iint \tau_{ax} tan\gamma \; dxdy \qquad (4.82a)$$

$$\emptyset_y = \iint \left[\int_{\varphi_2}^{\varphi_1} \left(-\frac{\partial p}{\partial y} + \frac{\partial \tau_{xy}}{\partial x} \right) \bigg|_b dz + \int_{\varphi_b}^{\varphi_2} \left(-\frac{\partial p}{\partial y} \right) \bigg|_p dz + \tau_{zy}\Big|_{\varphi_1} \right] dA_p \qquad (4.82b)$$

$$\emptyset_z = \iint \left[\int_{\varphi_2}^{\varphi_1} \left(-\frac{\partial p}{\partial z} + \frac{\partial \tau_{xz}}{\partial x} + \frac{\partial \tau_{yz}}{\partial y} \right) \bigg|_b dz + \int_{\varphi_b}^{\varphi_2} \left(-\frac{\partial p}{\partial z} \right) \bigg|_p dz \right] dA_p$$

$$- \iint [\rho(g_1 - g_2)\delta + \rho g_2(\delta + Z_e)] \, dA_p \qquad (4.82c)$$

The right side of momentum equation totally yields,

$$\iint \left[\int_{\varphi_2}^{\varphi_1} (\rho \boldsymbol{f} - \nabla p + \nabla \cdot \bar{\bar{\tau}})|_b dz + \int_{\varphi_b}^{\varphi_2} (\rho \boldsymbol{f} - \nabla p + \nabla \cdot \bar{\bar{\tau}})|_p dz \right] dA_p \qquad (4.83)$$

where $\bar{\bar{\tau}}$ is the stress tensor, the first term of integral above is the result force in the bed load layer, the other in the packed sediment layer. Here, $= -g\boldsymbol{k}$, $\nabla = \left(\frac{\partial}{\partial x}, \frac{\partial}{\partial y}, \frac{\partial}{\partial z} \right)$ and $(\nabla \cdot \bar{\bar{\tau}})_p \cong 0$ since no elastic deformation occurs in the packed sediment layer, and only through the interaction between the flow and sediment surface does the erosion occur.

The complete integral formation for the momentum equation 4.62 is expressed as,

$$\iint \left\{ \int_{\varphi_2}^{\varphi_1} \left[\rho_b \frac{\partial \vec{U}}{\partial t} + \left[\vec{U} \nabla_h \cdot \left(\rho_b \vec{U} \right) + \rho_b \left(\vec{U} \cdot \nabla_h \right) \vec{U} \right]_{xy\ plane} \right] dz \right.$$
$$\left. + \bar{U} \left(-\nabla_h \cdot \left(F + F_p \right) \right) \right\} dA_p$$

$$+ \iint \left\{ \rho_p \left(\vec{U}_p |_{\varphi_2} - \vec{U} |_{\varphi_2} \right) \frac{\partial \varphi_2}{\partial t} \right.$$
$$\left. + \int_{\varphi_b}^{\varphi_2} \left[\rho_p \frac{\partial \vec{U}_p}{\partial t} + \left[\vec{U}_p \nabla_h \cdot \left(\rho_p \vec{U}_p \right) + \rho_p \left(\vec{U}_p \cdot \nabla_h \right) \vec{U}_p \right]_{xy\ plane} \right] dz \right\} dA_p$$

$$= \iint \left[\int_{\varphi_2}^{\varphi_1} \left(\rho \boldsymbol{f} - \nabla p + \nabla \cdot \bar{\bar{\tau}} \right)|_b dz + \int_{\varphi_b}^{\varphi_2} \left(\rho \boldsymbol{f} - \nabla p + \nabla \cdot \bar{\bar{\tau}} \right)|_p dz \right] dA_p \qquad (4.84)$$

Since the projected area is arbitrary the momentum equation is rewritten as,

$$\int_{\varphi_2}^{\varphi_1} \left[\rho_b \frac{\partial \vec{U}}{\partial t} + \left[\vec{U} \nabla_h \cdot \left(\rho_b \vec{U} \right) + \rho_b \left(\vec{U} \cdot \nabla_h \right) \vec{U} \right]_{xy\ plane} \right] dz + \bar{U} \left(-\nabla_h \cdot \left(F + F_p \right) \right)$$
$$+ \rho_p \left(\vec{U}_p |_{\varphi_2} - \vec{U} |_{\varphi_2} \right) \frac{\partial \varphi_2}{\partial t}$$
$$+ \int_{\varphi_b}^{\varphi_2} \left[\rho_p \frac{\partial \vec{U}_p}{\partial t} + \left[\vec{U}_p \nabla_h \cdot \left(\rho_p \vec{U}_p \right) + \rho_p \left(\vec{U}_p \cdot \nabla_h \right) \vec{U}_p \right]_{xy\ plane} \right] dz$$

$$= \int_{\varphi_2}^{\varphi_1} \left(\rho \boldsymbol{f} - \nabla p + \nabla \cdot \bar{\bar{\tau}} \right)|_b dz + \int_{\varphi_b}^{\varphi_2} \left(\rho \boldsymbol{f} - \nabla p + \nabla \cdot \bar{\bar{\tau}} \right)|_p dz \qquad (4.85)$$

We can presume the incompressibility of flow field in both of two layers, namely, $\vec{U} \nabla_h \cdot \left(\rho_b \vec{U} \right) = \rho_b \vec{U} \nabla_h \cdot \vec{U} = 0$, and $\vec{U}_p \nabla_h \cdot \left(\rho_p \vec{U}_p \right) = \rho_p \vec{U}_p \nabla_h \cdot \vec{U}_p = 0$. Define $q_t = F + F_p$.The component equations of the momentum conservation result in,

$$\int_{\varphi_2}^{\varphi_1}\left[\rho_b\left(\frac{\partial u}{\partial t}+u\frac{\partial u}{\partial x}+v\frac{\partial u}{\partial y}\right)\right]dz-u\left(\frac{\partial q_{tx}}{\partial x}+\frac{\partial q_{ty}}{\partial y}\right)+\rho_p\left(u_p|_{\varphi_2}-u|_{\varphi_2}\right)\frac{\partial\varphi_2}{\partial t}$$

$$+\int_{\varphi_b}^{\varphi_2}\left[\rho_p\left(\frac{\partial u_p}{\partial t}+u_p\frac{\partial u_p}{\partial x}+v_p\frac{\partial u_p}{\partial y}\right)\right]dz$$

$$=\int_{\varphi_2}^{\varphi_1}\left(-\frac{\partial p}{\partial x}+\frac{\partial\tau_{yx}}{\partial y}\right)\bigg|_b dz+\int_{\varphi_b}^{\varphi_2}\left(-\frac{\partial p}{\partial x}\right)\bigg|_p dz+\tau_{zx}|_{\varphi_1}+\tau_{ax}tan\gamma \qquad (4.86a)$$

$$\int_{\varphi_2}^{\varphi_1}\left[\rho_b\left(\frac{\partial v}{\partial t}+u\frac{\partial v}{\partial x}+v\frac{\partial v}{\partial y}\right)\right]dz-v\left(\frac{\partial q_{tx}}{\partial x}+\frac{\partial q_{ty}}{\partial y}\right)+\rho_p\left(v_p|_{\varphi_2}-v|_{\varphi_2}\right)\frac{\partial\varphi_2}{\partial t}$$

$$+\int_{\varphi_b}^{\varphi_2}\left[\rho_p\left(\frac{\partial v_p}{\partial t}+u_p\frac{\partial v_p}{\partial x}+v_p\frac{\partial v_p}{\partial y}\right)\right]dz$$

$$=\int_{\varphi_2}^{\varphi_1}\left(-\frac{\partial p}{\partial y}+\frac{\partial\tau_{xy}}{\partial x}\right)\bigg|_b dz+\int_{\varphi_b}^{\varphi_2}\left(-\frac{\partial p}{\partial y}\right)\bigg|_p dz+\tau_{zy}\big|_{\varphi_1} \qquad (4.86b)$$

$$\int_{\varphi_2}^{\varphi_1}\left[\rho_b\left(\frac{\partial w}{\partial t}\right)\right]dz+\rho_p\left(w_p|_{\varphi_2}-w\right)\frac{\partial\varphi_2}{\partial t}+\int_{\varphi_b}^{\varphi_2}\left[\rho_p\left(\frac{\partial w_p}{\partial t}\right)\right]dz$$

$$=\int_{\varphi_2}^{\varphi_1}\left(-\frac{\partial p}{\partial z}+\frac{\partial\tau_{xz}}{\partial x}+\frac{\partial\tau_{yz}}{\partial y}\right)\bigg|_b dz+\int_{\varphi_b}^{\varphi_2}\left(-\frac{\partial p}{\partial z}\right)\bigg|_p dz$$

$$-\left[\rho(g_1-g_2)\delta+\rho g_2(\delta+Z_e)\right] \qquad (4.86c)$$

If we only consider the case with 2D sediment transport, they are reduced to,

$$\int_{\varphi_2}^{\varphi_1}\left[\rho_b\left(\frac{\partial u}{\partial t}+u\frac{\partial u}{\partial x}\right)\right]dz-u\frac{\partial q_{tx}}{\partial x}+\rho_p\left(u_p|_{\varphi_2}-u|_{\varphi_2}\right)\frac{\partial\varphi_2}{\partial t}$$

$$+\int_{\varphi_b}^{\varphi_2}\left[\rho_p\left(\frac{\partial u_p}{\partial t}+u_p\frac{\partial u_p}{\partial x}\right)\right]dz$$

$$=\int_{\varphi_2}^{\varphi_1}\left(-\frac{\partial p}{\partial x}\right)\bigg|_b dz+\int_{\varphi_b}^{\varphi_2}\left(-\frac{\partial p}{\partial x}\right)\bigg|_p dz+\tau_{zx}|_{\varphi_1}+\tau_{ax}tan\gamma \qquad (4.87)$$

$$\int_{\varphi_2}^{\varphi_1}\left[\rho_b\left(\frac{\partial w}{\partial t}\right)\right]dz+\rho_p\left(w_p|_{\varphi_2}-w\right)\frac{\partial\varphi_2}{\partial t}+\int_{\varphi_b}^{\varphi_2}\left[\rho_p\left(\frac{\partial w_p}{\partial t}\right)\right]dz$$

$$=\int_{\varphi_2}^{\varphi_1}\left(-\frac{\partial p}{\partial z}+\frac{\partial\tau_{xz}}{\partial x}\right)\bigg|_b dz+\int_{\varphi_b}^{\varphi_2}\left(-\frac{\partial p}{\partial z}\right)\bigg|_p dz$$

$$-\left[\rho(g_1-g_2)\delta+\rho g_2(\delta+Z_e)\right] \qquad (4.88)$$

CHAPTER 5 Numerical Solution of Governing Equation

5.0 Discretization of Governing Equation

At first, we require to transfer the conservation equations into the dimensionless formation represented as follows.

Define the characterized dimensionless parameters,

$$x^* = \frac{x}{D}, t^* = \frac{t}{t_a}, \varphi_1^* = \frac{\varphi_1}{D}$$

$$\delta^* = \frac{\delta}{D}, M^* = \frac{M}{\rho(s-1)g}, H^* = \frac{H}{D}$$

$$\tau_{ax}^* = \frac{\tau_{ax}}{\rho(s-1)gD}, q_* = \frac{q}{\sqrt{(s-1)gD}D}$$

where t_a is the equilibrium time of scour. The other dimensionless parameters are the same as the definitions employed in the next section 5.2.

The continuity equation:

$$A\frac{\partial}{\partial t^*}\left[\delta^*[(1-\alpha)+s\alpha]+(\varphi_1^*-\delta^*)[\beta+s(1-\beta)]\right] + \frac{\partial\left(sq_*cos\gamma+\bar{u}_*\delta^*(1-\alpha)+\bar{u}_{p*}(\varphi_1^*-\delta^*)\beta\right)}{\partial x^*} = 0 \quad (5.1)$$

$$A\frac{\partial\varphi_1^*}{\partial t^*} + \bar{u}_*\frac{\partial\varphi_1^*}{\partial x^*} - \bar{w}_* = 0 \quad (5.2)$$

The momentum equation for X component:

$$
\begin{aligned}
A\frac{\partial(\bar{u}_*\delta^*[(1-\alpha)+s\alpha])}{\partial t^*} &+ A[\beta+s(1-\beta)](\varphi_1^*-\delta^*)\frac{\partial\left(\bar{u}_{p*}\right)}{\partial t^*} \\
&- A\frac{[\delta^*M^*+(\varphi_1^*-\delta^*)N^*]}{\bar{u}_*}\frac{\partial\varphi_1^*}{\partial t^*} + \bar{u}_*\delta^*[(1-\alpha)+s\alpha]\frac{\partial\bar{u}_*}{\partial x^*} \\
&+ (\varphi_1^*-\delta^*)[\beta+s(1-\beta)]\bar{u}_{p*}\frac{\partial\bar{u}_{p*}}{\partial x^*} - [\delta^*M^*+(\varphi_1^*-\delta^*)N^*]\frac{\partial\varphi_1^*}{\partial x^*} \\
= \frac{H^*}{s-1}\frac{tan\gamma}{[1+(tan\gamma)^2]} &+ \left\{-e[(1-\alpha)+s\alpha](cos\gamma)^2\bar{u}_*^2 + l[\beta+s(1-\beta)]\bar{u}_{p*}^2\right\}tan\gamma
\end{aligned}
\tag{5.3}
$$

The momentum equation for Z component:

$$
\begin{aligned}
A\delta^*[(1-\alpha)+s\alpha]\left(\frac{\partial\bar{w}_*}{\partial t^*}\right) &+ A(\varphi_1^*-\delta^*)[\beta+s(1-\beta)]\left(\frac{\partial\bar{w}_{p*}}{\partial t^*}\right) \\
&- A\frac{tan\gamma}{[1+(tan\gamma)^2]}\delta^*M^*\frac{1}{\bar{u}_*}\frac{\partial\varphi_1^*}{\partial t^*} - \delta^*M^*\frac{tan\gamma}{[1+(tan\gamma)^2]}\frac{\partial\varphi_1^*}{\partial x^*} \\
&= \delta^*M^* + (\varphi_1^*-\delta^*)N^* - \left[\frac{n^*}{a^*}\delta^* + \frac{1}{a^*}\varphi_1^*\right]
\end{aligned}
\tag{5.4}
$$

where

$$A = \sqrt{\frac{D}{(s-1)gt_a^2}}$$

$$N^* = \frac{1.75(1-\beta)}{\beta^3}\bar{w}_{p*}^2 + \frac{150(1-\beta)^2}{\beta^3}\frac{1}{RE_{w_p}}\bar{w}_{p*}^2$$

$$M^* = c^*\delta_*' + \alpha$$

We employ the first-order forward difference method to discretize conservation equations as follows, Continuity Equation:

$$\delta^*{}_i^{n+1}[(1-\alpha_i^{n+1})+s\alpha_i^{n+1}]+\left[(\varphi_1^*)_i^{n+1}-\delta^*{}_i^{n+1}\right][\beta+s(1-\beta)]$$

$$=-\frac{\Delta t^*}{A\Delta x^*}\Big\{sq_*{}_{i+1}^{n}(cos\gamma)_{i+1}^{n}+(\bar{u}_*)_{i+1}^{n}\delta^*{}_{i+1}^{n}(1-\alpha_{i+1}^{n})$$

$$+\left(\bar{u}_{p*}\right)_{i+1}^{n}[(\varphi_1^*)_{i+1}^{n}-\delta^*{}_{i+1}^{n}]\beta\Big\}$$

$$+\frac{\Delta t^*}{A\Delta x^*}\Big\{sq_*{}_i^{n}(cos\gamma)_i^{n}+(\bar{u}_*)_i^{n}\delta^*{}_i^{n}(1-\alpha_i^{n})$$

$$+\left(\bar{u}_{p*}\right)_i^{n}[(\varphi_1^*)_i^{n}-\delta^*{}_i^{n}]\beta\Big\}+\delta^*{}_i^{n}[(1-\alpha_i^{n})+s\alpha_i^{n}]$$

$$+[(\varphi_1^*)_i^{n}-\delta^*{}_i^{n}][\beta+s(1-\beta)] \qquad (5.5)$$

$$(\varphi_1^*)_i^{n+1}=(\varphi_1^*)_i^{n}-\frac{\Delta t^*}{A\Delta x^*}(\bar{u}_*)_i^{n}[(\varphi_1^*)_{i+1}^{n}-(\varphi_1^*)_i^{n}]+\frac{\Delta t^*}{A}(\overline{w}_*)_i^{n} \qquad (5.6)$$

Momentum Equation for X component:

$$(\bar{u}_*)_i^{n+1}\delta^*{}_i^{n+1}[(1-\alpha_i^{n+1})+s\alpha_i^{n+1}]+[\beta+s(1-\beta)][(\varphi_1^*)_i^{n}-\delta^*{}_i^{n}]\left(\bar{u}_{p*}\right)_i^{n+1}$$

$$-\frac{[\delta^*{}_i^{n}M^*{}_i^{n}+[(\varphi_1^*)_i^{n}-\delta^*{}_i^{n}]N^*{}_i^{n}]}{(\bar{u}_*)_i^{n}}(\varphi_1^*)_i^{n+1}$$

$$=-\frac{\Delta t^*}{A\Delta x^*}(\bar{u}_*)_i^{n}\delta^*{}_i^{n}[(1-\alpha_i^{n})+s\alpha_i^{n}][(\bar{u}_*)_{i+1}^{n}-(\bar{u}_*)_i^{n}]$$

$$-\frac{\Delta t^*}{A\Delta x^*}[(\varphi_1^*)_i^{n}-\delta^*{}_i^{n}][\beta+s(1-\beta)]\left(\bar{u}_{p*}\right)_i^{n}\left[\left(\bar{u}_{p*}\right)_{i+1}^{n}-\left(\bar{u}_{p*}\right)_i^{n}\right]$$

$$+\frac{\Delta t^*}{A\Delta x^*}[\delta^*M^*+(\varphi_1^*-\delta^*)N^*][(\varphi_1^*)_{i+1}^{n}-(\varphi_1^*)_i^{n}]$$

$$+(\bar{u}_*)_i^{n}\delta^*{}_i^{n}[(1-\alpha_i^{n})+s\alpha_i^{n}]+[\beta+s(1-\beta)][(\varphi_1^*)_i^{n}-\delta^*{}_i^{n}]\left(\bar{u}_{p*}\right)_i^{n}$$

$$-\frac{[\delta^*{}_i^{n}M^*{}_i^{n}+[(\varphi_1^*)_i^{n}-\delta^*{}_i^{n}]N^*{}_i^{n}]}{(\bar{u}_*)_i^{n}}(\varphi_1^*)_i^{n}+\frac{\Delta t^*}{A}\frac{H^*}{s-1}\left\{\frac{tan\gamma}{[1+(tan\gamma)^2]}\right\}_i^{n}$$

$$+\frac{\Delta t^*}{A}\left\{-e[(1-\alpha_i^n)+s\alpha_i^n]\left\{\frac{1}{[1+(tan\gamma)^2]}\right\}_i^n(\bar{u}_*^2)_i^n\right.$$

$$\left.+\,l[\beta+s(1-\beta)]\left(\bar{u}_{p*}^2\right)_i^n\right\}(tan\gamma)_i^n \tag{5.7}$$

Momentum Equation for Z component:

We can obtain the approximate relationship according to the continuity in the packed layer,

$$\bar{w}_{p*}=\frac{\bar{w}_*}{1-\beta} \tag{5.8}$$

Accordingly, the Z component of momentum equation is discretized as,

$$\left\{A\delta^{*n}_{\ i}[(1-\alpha_i^n)+s\alpha_i^n]+A[(\varphi_1^*)_i^n-\delta^{*n}_{\ i}]\frac{[\beta+s(1-\beta)]}{1-\beta}\right\}(\bar{w}_*)_i^{n+1}$$

$$-A\left\{\frac{tan\gamma}{[1+(tan\gamma)^2]}\right\}_i^n\delta^{*n}_{\ i}M^{*n}_{\ i}\frac{(\varphi_1^*)_i^{n+1}}{(\bar{u}_*)_i^n}$$

$$=\left\{A\delta^{*n}_{\ i}[(1-\alpha_i^n)+s\alpha_i^n]+A[(\varphi_1^*)_i^n-\delta^{*n}_{\ i}]\frac{[\beta+s(1-\beta)]}{1-\beta}\right\}(\bar{w}_*)_i^n$$

$$-A\left\{\frac{tan\gamma}{[1+(tan\gamma)^2]}\right\}_i^n\delta^{*n}_{\ i}M^{*n}_{\ i}\frac{(\varphi_1^*)_i^n}{(\bar{u}_*)_i^n}+\Delta t^*\delta^{*n}_{\ i}M^{*n}_{\ i}$$

$$+\frac{\Delta t^*}{\Delta x^*}\delta^{*n}_{\ i}M^{*n}_{\ i}\left\{\frac{tan\gamma}{[1+(tan\gamma)^2]}\right\}_i^n[(\varphi_1^*)_{i+1}^n-(\varphi_1^*)_i^n]+\Delta t^*[(\varphi_1^*)_i^n-\delta^{*n}_{\ i}]N^{*n}_{\ i}$$

$$-\Delta t^*\left[\frac{n^{*n}_{\ i}}{a^*}\delta^{*n}_{\ i}+\frac{1}{a^*}(\varphi_1^*)_i^n\right] \tag{5.9}$$

5.1 Two Dimensional Solution

Now we simplify the mass balance and momentum equation for calculating the maximum scour depth. When the scour process approaches the equilibrium status the variables in the flow field will be independent on the change of time, therefore, the mass conservation equation can be rewritten as,

$$\begin{cases} & u\varphi_{1x} - w = 0 \\ \nabla_h \cdot (F + F_p) = 0 & \xrightarrow{yields} F_{sx} + F_{fx} + F_{pfx} = m \qquad m\ is\ a\ constant \end{cases}$$

or

$$\begin{cases} \bar{u}\varphi_{1x} - \bar{w} = 0 \\ \rho_s q_s cos\gamma + \rho\bar{u}A(1-\alpha) + \rho\overline{u_p}A_p\beta = m \end{cases} \tag{5.10}$$

In which q_s is the volume sediment transport rate unit width in the bed load layer, and $\overline{u_p}$, A_p the horizontally averaged velocity and cross section, respectively, over the packed layer. Also, $\bar{u}$ and $\bar{w}$ are respectively the local averaged x- and z-components over the packed layer.

For momentum equations, all the time change rate of variables equals to zero, and since $\nabla_h \cdot (F + F_p) = 0$, $u\frac{\partial q_{tx}}{\partial x} = 0$. If we define the bottom of control volume as $\varphi_b = Z_{max}$, the parameter of Z_e limited to zero at the location of maximum scour depth with the coming of equilibrium status. Hence, the momentum equations can be simplified as,

$$\begin{cases} \int_{\varphi_2}^{\varphi_1} \rho_b u \frac{\partial u}{\partial x} dz + \int_{\varphi_b}^{\varphi_2} \rho_p u_p \frac{\partial u_p}{\partial x} dz = \int_{\varphi_2}^{\varphi_1} \left(-\frac{\partial p}{\partial x}\right)\Big|_b dz \\ \qquad + \int_{\varphi_b}^{\varphi_2} \left(-\frac{\partial p}{\partial x}\right)\Big|_p dz + \tau_{zx}|_{\varphi_1} + \tau_{ax} tan\gamma \\ 0 = \int_{\varphi_2}^{\varphi_1} \left(-\frac{\partial p}{\partial z} + \frac{\partial \tau_{xz}}{\partial x}\right)\Big|_b dz + \int_{\varphi_b}^{\varphi_2} \left(-\frac{\partial p}{\partial z}\right)\Big|_p dz \\ \qquad -[\rho(g_1 - g_2)\delta + \rho g_2(\delta + Z_e)] \end{cases} \tag{5.11}$$

The x component of acceleration in the steady flow field equals to zero, which means

$$\int_{\varphi_2}^{\varphi_1} \rho_b u \frac{\partial u}{\partial x} dz + \int_{\varphi_b}^{\varphi_2} \rho_p u_p \frac{\partial u_p}{\partial x} dz = 0 \tag{5.12}$$

Since

$$\varphi_{1x} = \frac{\overline{w}}{\overline{u}} = \frac{dz}{dx} = -tan\gamma \tag{5.13}$$

and assume it is a single valued function of x variable. Also, as we know, $\tau_{xz} = \tau_{zx}$ which results in the following deduction on a bed with slope.

$$\int_{\varphi_2}^{\varphi_1} \left(\frac{\partial \tau_{xz}}{\partial x}\right)\Big|_b dz = \int_{\varphi_2}^{\varphi_1} \left(\frac{\partial \tau_{zx}}{\partial z}\right)\Big|_b \frac{dz}{dx} dz = \left(\tau_{zx}|_{\varphi_1} - \tau_{zx}|_{\varphi_2}\right)(-tan\gamma)$$

$$= -\delta[a\overline{w}^2 + b\overline{w} + \alpha(\rho_s - \rho)g] sin\gamma cos\gamma tan\gamma$$

$$= -\delta[a\overline{w}^2 + b\overline{w} + \alpha(\rho_s - \rho)g](sin\gamma)^2 \tag{5.14}$$

$$\int_{\varphi_2}^{\varphi_1} \left(-\frac{\partial p}{\partial x}\right)\Big|_b dz = \int_{\varphi_2}^{\varphi_1} \left(-\frac{\partial p}{\partial z}\right)\Big|_b \frac{dz}{dx} dz$$

$$= \delta[a\overline{w}^2 + b\overline{w} + \alpha(\rho_s - \rho)g](-tan\gamma) \tag{5.15}$$

$$\int_{\varphi_b}^{\varphi_2} \left(-\frac{\partial p}{\partial x}\right)\Big|_p dz = Z_e[(a\overline{w}^2 + b\overline{w})]|_p(-tan\gamma) \tag{5.16}$$

We also can attain the horizontal shear stress on the surface of bed load layer,

$$\tau_{zx}|_{\varphi_1} = \rho g H sin\gamma cos\gamma \tag{5.17}$$

where H is the averaged water depth.

If we assume the additional shear stress which has the following form,

$$\tau_{ax} = -e\rho_b\bar{u}^2 + l\rho_p\bar{u}_p^2 \tag{5.18}$$

Here, e, l are different constant, respectively.

We obtain the following form of simplification for momentum equations.

$$\begin{cases} 0 = -\delta[a\bar{w}^2 + b\bar{w} + \alpha(\rho_s - \rho)g]tan\gamma - Z_e[(a\bar{w}^2 + b\bar{w})]|_p tan\gamma + \\ \qquad \rho g H sin\gamma cos\gamma + \left(-e\rho_b\bar{u}^2 + l\rho_p\bar{u}_p^2\right)tan\gamma \\ 0 = \delta[a\bar{w}^2 + b\bar{w} + \alpha(\rho_s - \rho)g] - \delta[a\bar{w}^2 + b\bar{w} + \alpha(\rho_s - \rho)g](sin\gamma)^2 \\ \qquad +Z_e[(a\bar{w}^2 + b\bar{w})]|_p - [\rho(g_1 - g_2)\delta + \rho g_2(\delta + Z_e)] \end{cases} \tag{5.19}$$

Define

$$M = a\bar{w}^2 + b\bar{w} + \alpha(\rho_s - \rho)g$$

$$N = [(a\bar{w}^2 + b\bar{w})]|_p$$

Combining the two equations in Eq.5.19 results in,

$$-\delta M(sin\gamma)^2 tan\gamma + \rho g H(cos\gamma)^2 tan\gamma + \tau_{ax} tan\gamma$$
$$- [\rho(g_1 - g_2)\delta + \rho g_2(\delta + Z_e)]tan\gamma = 0$$

or

$$\varphi_1 = \frac{-\delta M\varphi_{1x}^2 + [\rho g H + \tau_{ax}(1 + \varphi_{1x}^2)] - \rho(g_1 - g_2)\delta(1 + \varphi_{1x}^2)}{\rho(1 + \varphi_{1x}^2)g_2} \tag{5.20}$$

which has the dimensionless formation as follows,

$$\varphi_1^* = \frac{\varphi_1}{D} = \frac{-\frac{\delta}{D}M\varphi_{1x}^2 + \left[\rho g\frac{H}{D} + \frac{\tau_{ax}}{D}(1+\varphi_{1x}^2)\right] - \rho(g_1-g_2)\frac{\delta}{D}(1+\varphi_{1x}^2)}{\rho(1+\varphi_{1x}^2)g_2}$$

$$= \frac{-\frac{\delta}{D}M\varphi_{1x}^2 + \left[\rho g\frac{H}{D} + \frac{\tau_{ax}}{D}(1+\varphi_{1x}^2)\right] - \rho[1-\alpha-\beta+(s-1)(\alpha+\beta-1)]g\frac{\delta}{D}(1+\varphi_{1x}^2)}{\rho[(1-\beta)(s-1)+\beta](1+\varphi_{1x}^2)g}$$

$$= -\frac{\delta}{D}\frac{M}{\rho[(1-\beta)(s-1)+\beta]g}\frac{\varphi_{1x}^2}{(1+\varphi_{1x}^2)} + \frac{\left[\rho g\frac{H}{D} + \frac{\tau_{ax}}{D}(1+\varphi_{1x}^2)\right]}{\rho[(1-\beta)(s-1)+\beta]g(1+\varphi_{1x}^2)}$$

$$- \frac{[1-\alpha-\beta+(s-1)(\alpha+\beta-1)]\frac{\delta}{D}(1+\varphi_{1x}^2)}{[(1-\beta)(s-1)+\beta](1+\varphi_{1x}^2)}$$

$$= -\delta^*\frac{M^*(s-1)}{[(1-\beta)(s-1)+\beta]}\frac{\varphi_{1x}^2}{(1+\varphi_{1x}^2)}$$

$$+ \left\{\frac{H^*}{[(1-\beta)(s-1)+\beta](1+\varphi_{1x}^2)} + \frac{\tau_{ax}^*(s-1)}{[(1-\beta)(s-1)+\beta]}\right\}$$

$$- \frac{[1-\alpha-\beta+(s-1)(\alpha+\beta-1)]\delta^*}{[(1-\beta)(s-1)+\beta]} \tag{5.21}$$

Define the coefficients for simplifying the formula above,

$$a^* = \frac{(s-1)}{[(1-\beta)(s-1)+\beta]}$$

$$b^* = \frac{a^*}{s-1}$$

$$n^* = \frac{1-\alpha+(s-1)\alpha}{b^*} - 1$$

Thus, we obtain the scour profile model in the steady state represented by,

$$\varphi_1^* = -a^*\delta^*M^*\left(\frac{\varphi_{1x}^2}{1+\varphi_{1x}^2}\right) + \left(\frac{b^*H^*}{1+\varphi_{1x}^2} + a^*\tau_{ax}^*\right) - n^*\delta^* \tag{5.22}$$

where

$$\delta^* = \frac{\delta}{D}$$

$$M^* = \frac{M}{\rho(s-1)g}$$

$$H^* = \frac{H}{D}$$

$$\tau_{ax}^* = \frac{\tau_{ax}}{\rho(s-1)gD}$$

Estimate of Parameter M

To confirm the value of M must depend on the calculation of the mean upward velocity of flow, $\overline{w}$,in the bed load layer. We assume that the trajectory of particles has a similarly parabolic track. In this analysis, the transport rate of sediment q_s is defined as the product of the particle's velocity V_p , the thickness of bed load layer δ or saltation height and the volume concentration of particles α, namely, $q_s = V_p\delta\alpha$.

Referring to the experiments' results of Fernandez Luque and van Beek (FLvB), Parker (2002) manipulated the expression for the sediment particle's velocity for convenience, and hence, the dimensionless mean streamwise velocity of particles V_{*p} , sediment bed load q_s^* and saltation length L_{*s} are expressed as, respectively,

$$q_s^* = 5.7(\tau_* - \tau_{*c})^{3/2} \tag{5.23}$$

$$V_{*p} = 8.625(\tau_* - \tau_{*c})^{1/2} \tag{5.24}$$

$$L_{*s} = \frac{L_s}{D} \tag{5.25}$$

where τ_* is the Shields number at no bed load layer.τ_{*c} is the critical Shields number for an arbitrary streamwise slope. The dimensionless mean saltation length L_{*s} equals 16 determined by FLvB's experiments. The dimensionless parameters, q_s^*, V_{*p}, τ_* and τ_{*c} are defined as follows,

$$q_s^* = \frac{q_s}{\sqrt{(s-1)gD}D}$$

$$V_{*p} = \frac{V_p}{\sqrt{(s-1)gD}}$$

$$\tau_* = \frac{\tau}{\rho(s-1)gD}$$

$$\tau_{*c} = \frac{\tau_c}{\rho(s-1)gD}$$

and the critical Shields number can be calculated by the following formula,

$$\tau_{*c} = \tau_{*co} cos\gamma \left(1 - \frac{tan\gamma}{\mu_s}\right) \tag{5.26}$$

where τ_{*co} denotes the critical Shields number in the horizontal bed, μ_s the static coefficient of friction. Also, Fernandez and van developed formula for calculating q_{*s}, V_{*p} with a arbitrary slope, however, which is inconvenient to apply specific case because of complexity. Hence, Simona and Luca fitted these bed load transport equations developed by Fernandez and van beek to apply them conveniently, which are expressed as,

$$q_s^* = A_q(\gamma,\theta)\left(\frac{\tau_*}{\tau_{*co}}\right)^2 + B_q(\gamma,\theta)\left(\frac{\tau_*}{\tau_{*co}}\right) + C_q(\gamma,\theta) \tag{5.27}$$

$$V_{*p} = A_p(\gamma,\theta)\left(\frac{\tau_*}{\tau_{*co}}\right)^2 + B_p(\gamma,\theta)\left(\frac{\tau_*}{\tau_{*co}}\right) + C_p(\gamma,\theta) \tag{5.28}$$

$$A_q(\gamma,\theta) = \frac{a_q + b_q ln\gamma + c_q\theta}{1 + d_q ln\gamma + e_q\theta + f_q\theta^2} \tag{5.29}$$

$$B_q(\gamma,\theta) = g_q + h_q\gamma + i_q\theta^2 \tag{5.30}$$

$$C_q(\gamma,\theta) = j_q + k_q\gamma + l_q\gamma^2 + m_q\theta^2 + n_q\gamma\theta \tag{5.31}$$

$$A_{V_p}(\gamma,\theta) = a_{V_p} + b_{V_p}\theta^2 + c_{V_p}\gamma\theta \tag{5.32}$$

$$B_{V_p}(\gamma,\theta) = d_{V_p} + e_{V_p}\theta^2 + f_{V_p}\gamma\theta \tag{5.33}$$

$$C_{V_p}(\gamma,\theta) = g_{V_p} + h_{V_p}\gamma + i_{V_p}\theta + j_{V_p}\gamma\theta \tag{5.34}$$

Table 5.1 Coefficients ($\times 10^{-6}$) of A_q, B_q, C_q, A_{V_p}, B_{V_p} and C_{V_p}.

a_p	b_p	c_p	d_p	e_p	f_p	g_p
8677.849	-2521.125	-6.420916	-289785.4	228.1153	-79.52039	9543.719
h_p	i_p	j_p	k_p	l_p	m_p	n_p
1068.214	7.940476	-21673.80	827.6981	21.32117	3.180555	8.884528
a_{vp}	b_{vp}	c_{vp}	d_{vp}	e_{vp}	f_{vp}	g_{vp}
-46136.64	4.736102	-5.314831	856798.2	-53.598537	60.04791	187614.77
h_{vp}	i_{vp}	j_{vp}				
44260.106	27469.067	721.99853				

For our case without the transverse slope, these coefficents are rewritten as,

$$A_q(\gamma) = \frac{a_q + b_q ln\gamma}{1 + d_q ln\gamma} \tag{5.35}$$

$$B_q(\gamma) = g_q + h_q\gamma \tag{5.36}$$

$$C_q(\gamma) = j_q + k_q\gamma + l_q\gamma^2 \tag{5.37}$$

$$A_{V_p}(\gamma) = a_{V_p} \tag{5.38}$$

$$B_{V_p}(\gamma) = d_{V_p} \tag{5.39}$$

$$C_{V_p}(\gamma) = g_{V_p} + h_{V_p}\gamma \tag{5.40}$$

Simona and Luca's fitting curves for q_s^* and V_{*p} without the traverse slope are shown in Fig.5.1 and Fig.5.2 where the bed load of sediment and velocity of particle increase with the increment of bed shear stress and slope, respectively. The identical comparison of Simona and Luca's fitting curves with FLvB's empirical formula, as shows in Fig.5.3 and Fig.5.4, denotes that we can use this fitting expression for our convenient computation.

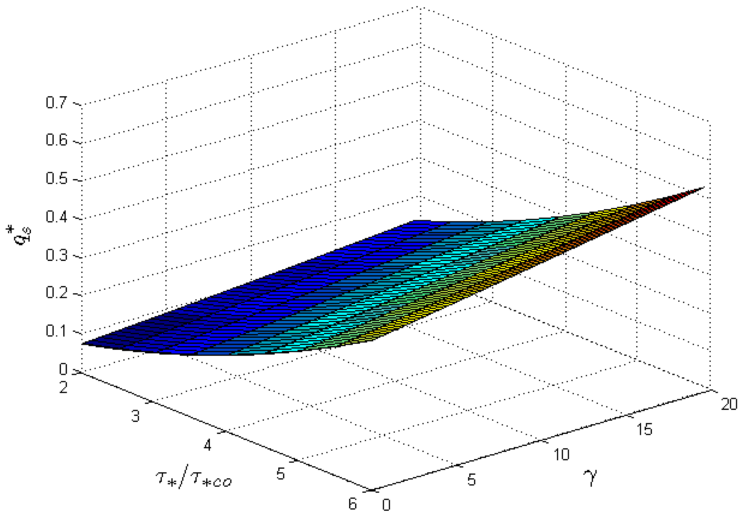

Figure 5.1 Simona and Luca's fitting formula for q_s^* without the traverse slope.

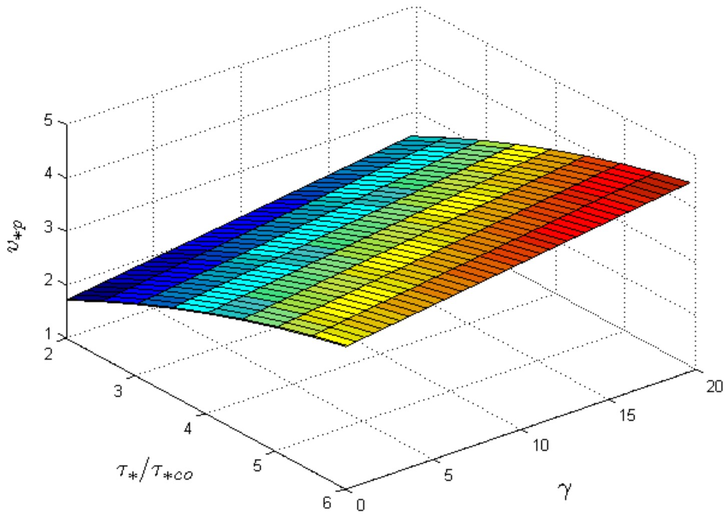

Figure 5.2 Simona and Luca’s fitting formula for V_{*p} without the traverse slope.

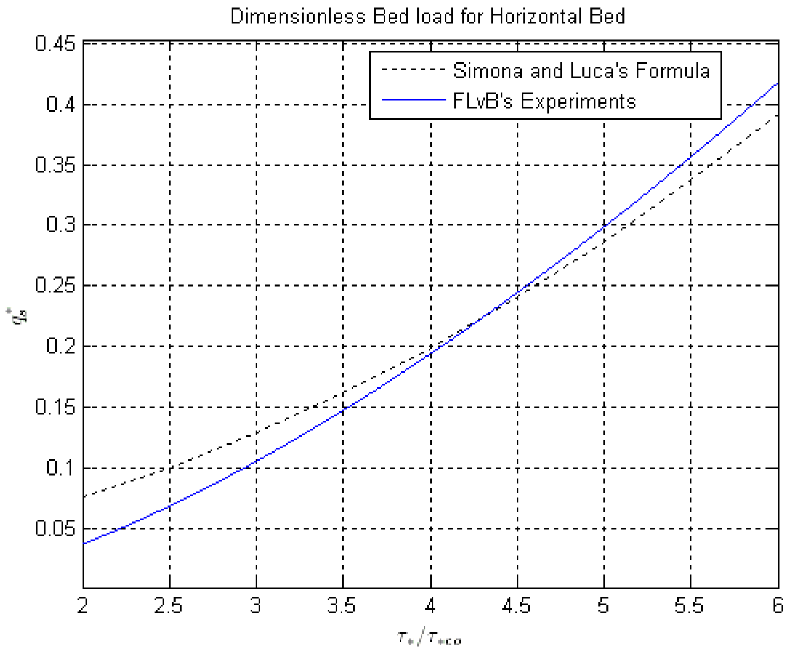

Figure 5.3 Simona’s fitting curve verse FLvB’s empirical formula for horizontal bed.

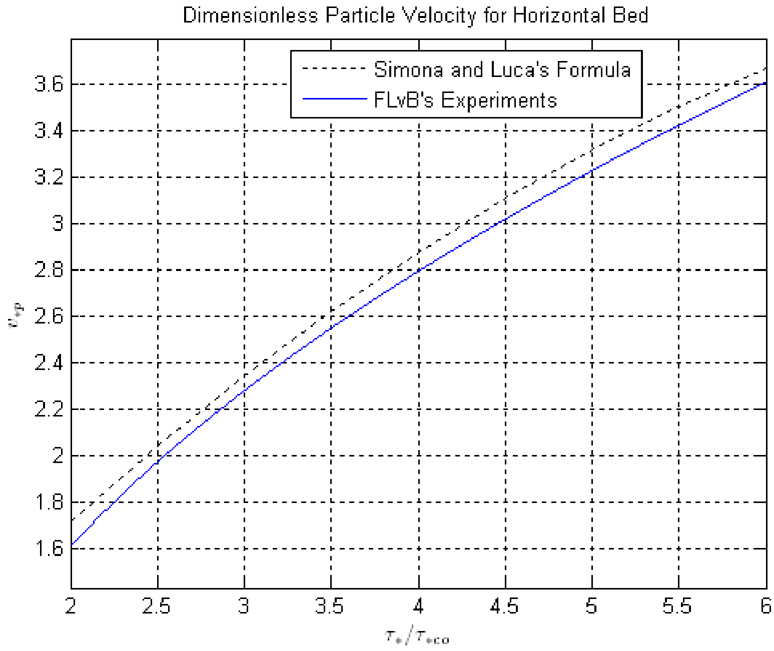

Figure 5.4 Simona's fitting curves verse FLvB's empirical formula for horizontal bed.

The forces acting on a saltating particle, including its submerged weight, lift force and drag force, control the motion of particle and verify the equation of motion. Fernandez Luque performed a series of experiments with four different bed materials: sand, gravel, magnetite and walnut grains to measure the particles' trajectories. The average dimensionless distance of saltation along a horizontal bed is measured as $L_{*s} = 16$. In this dissertation, we assume that the particle along the bed has a parabolic trajectory along which the average saltation distance in the horizontal direction equals to the value measured by Fernandez Luque.

We assume the particle has its trajectory traces, as shown in Fig.5.5 , on an angular bed with the expression as,

$$z = -\frac{4\delta'}{l^2}\left[x - \left(\frac{l}{2} + x_p\right)\right]^2 + \delta' + z_p \qquad (5.41)$$

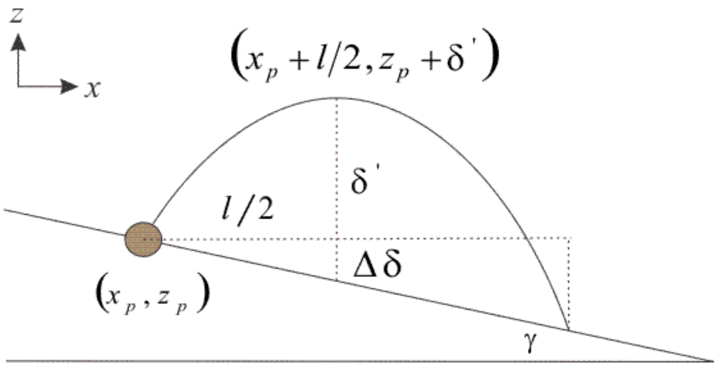

Figure 5.5 Trajectory traces of particle within the bed load layer.

The derivative expression is written as,

$$\frac{dz}{dx} = -\frac{8\delta'}{l^2}\left(x - \frac{l}{2} - x_p\right) = -tan\gamma \tag{5.42}$$

where (x_p, z_p) refers to the particle's coordinate in the global system. The coordinate (x_t, z_t) of the tangent point can be calculated

$$x_t = \frac{L_s^2}{8\delta'} tan\gamma + \frac{L_s}{2} + x_p \tag{5.43}$$

$$z_t = -\frac{L_s^2}{16\delta'} (tan\gamma)^2 + \delta' + z_p \tag{5.44}$$

Based on the geometrical relationship as shown in Fig.5.5, we obtain the expression of $\Delta\delta$

$$\Delta\delta = \frac{L_s^2}{8\delta'} tan\gamma|tan\gamma| + \frac{L_s}{2}|tan\gamma| \tag{5.45}$$

Since the accuracy of computation reduces with the increase of bed slope, we limit the range of slope with the same as Simona and Luca's. Thus, the thickness of bed load is represented by

$$\begin{cases} \delta = z_t - z_p + \Delta\delta = \dfrac{L_s^2}{16\delta'}(tan\gamma)^2 + \dfrac{L_s}{2}tan\gamma + \delta' & 0 < \gamma < 22^o \\ \delta = z_t - z_p - \Delta\delta = \dfrac{L_s^2}{16\delta'}(tan\gamma)^2 + \dfrac{L_s}{2}tan\gamma + \delta' & 158^o < \gamma < 180^o \end{cases} \tag{5.46}$$

which has a dimensionless formation written as,

$$\delta^* = \frac{\delta}{D} = \frac{L_{*s}^2}{16\delta_*'}tan\gamma|tan\gamma| + \frac{L_{*s}}{2}|tan\gamma| + \delta_*' \tag{5.47}$$

For $0 < \gamma < 22^o$ or $158^o < \gamma < 180^o$

$$\delta^* = \frac{L_{*s}^2}{16\delta_*'}(tan\gamma)^2 + \frac{L_{*s}}{2}tan\gamma + \delta_*' \tag{5.48}$$

$$\delta_*' = \frac{\delta'}{D} = \frac{L_s^2}{8sV_{*p}^2} \tag{5.49}$$

Note the situation for $158^o < \gamma < 180^o$ cannot be included due to the limitation of Simona and Luca's formula.

We limit the possible range of γ to obtain a reasonable accuracy based on the deduction of δ^*. Actually, it is seldom for river erosion to form the scour profile larger than 35^o in the normal scouring from shear stress.

The upward mean velocity and the displacement at the top-most position can be respectively denoted by,

$$\bar{w} = \sqrt{2(1 - 1/s)g\delta'} \tag{5.51}$$

$$\delta' = (1 - 1/s)g\frac{l^2}{8V_p^2} \tag{5.52}$$

The graphic Fig.5.6 shows the dependent correlation of thickness of bed load layer with the slope and the dimensionless ratio $\frac{\tau_*}{\tau_{*co}}$ for a small slope. It illustrates that when $1.5 < \frac{\tau_*}{\tau_{*co}} < 2.3$, the dimensionless thickness of bed load layer δ_* decreases as the slope of bed increase for a given $\frac{\tau_*}{\tau_{*co}}$, however, when $\frac{\tau_*}{\tau_{*co}} \geq 2.3$, it decreases with the slope's increase. For a given slope, δ_* decrease as the dimensionless ratio of shear stress $\frac{\tau_*}{\tau_{*co}}$ increases. In addition, there is a little alteration of bed load thickness for a

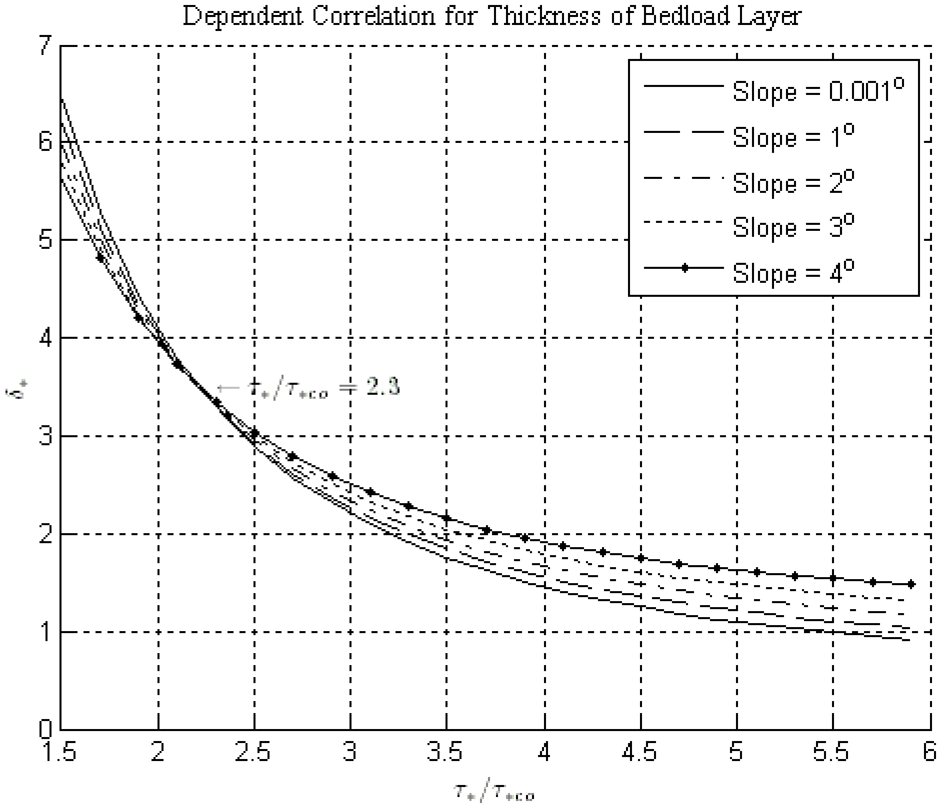

Figure 5.6 Thickness of bed load layer verse the bed slope.

given dimensionless ratio of shear stress with the range $2 < \frac{\tau_*}{\tau_{*co}} < 3$. Including the low and high slope of bed, the 3D graphic is shown in Fig.5.7. Fig.5.7 provides a specific correlation map among bed load thickness, shear stress ratio and bed slope; given two of them can verify the third variable. It shows that the bed load thickness increases as the bed slope's increment for a given ratio of shear stress. We can explain this trend in this way that the larger slope causes particles less stable and more vertically trajectory displacement if the bed shear stress keeps consistent. Likewise, given a bed slope, the bed load thickness decreases as the shear stress increases because more bed shear stress cause the increment of particles' velocity resulting in the deduction of the vertically trajectory displacement or bed load thickness.

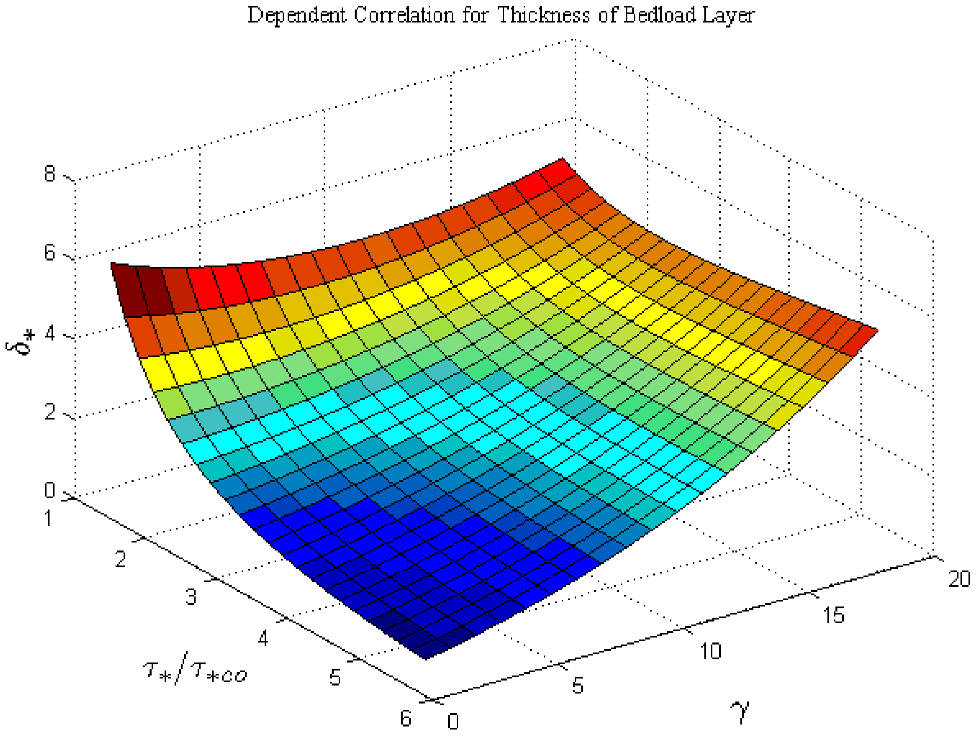

Figure 5.7 Thickness of bed load layer verse the bed slope and shear stress ratio.

Furthermore, we represent the parameter of M as,

$$M = a\overline{w}^2 + b\overline{w} + \alpha(\rho_s - \rho)g$$

$$= 2a(1 - 1/s)g\delta' + b\sqrt{2(1 - 1/s)g\delta'} + \alpha(\rho_s - \rho)g \quad (5.53)$$

Substituting the coefficients *a* and *b* into the formula above, its dimensionless formation can be expressed as,

$$M^* = \frac{M}{\rho(s-1)g}$$

$$= \frac{3.5(1-\beta)}{\beta^3 s}\delta_*' + \frac{150\sqrt{2}(1-\beta)^2}{\beta^3\sqrt{s}}\frac{\mu}{\rho D^{3/2}\sqrt{(s-1)g}}\sqrt{\delta_*'} + \alpha$$

$$= \frac{3.5(1-\beta)}{\beta^3 s}\delta_*' + \frac{300(1-\beta)^2}{\beta^3 s}\frac{1}{RE_w}\delta_*' + \alpha$$

$$= \left(\frac{3.5(1-\beta)}{\beta^3 s} + \frac{300(1-\beta)^2}{\beta^3 s}\frac{1}{RE_w}\right)\delta_*' + \alpha$$

$$= c^*\delta_*' + \alpha \quad (5.54)$$

where

$$RE_w = \frac{\rho D\overline{\mathrm{w}}}{\mu}, Paticle\ Renolds\ Number\ Based\ on\ \overline{\mathrm{w}}$$

$$c^* = \frac{3.5(1-\beta)}{\beta^3 s} + \frac{300(1-\beta)^2}{\beta^3 s}\frac{1}{RE_w}$$

M^* is numerically solved and plotted in Fig.5.8. It demonstrates that the vertically dimensionless pressure gradient reduces as the bed slope's increment for a given low ratio of shear stress since the larger slope causes the increase of particles' mean velocity V_p that reduces the vertically trajectory distance δ' and the vertical velocity component of particle $\overline{w}$. If given a bed slope, it decreases as the shear stress increases because the more bed shear stress cause the increment of particles' velocity resulting in the deduction of $\overline{w}$.

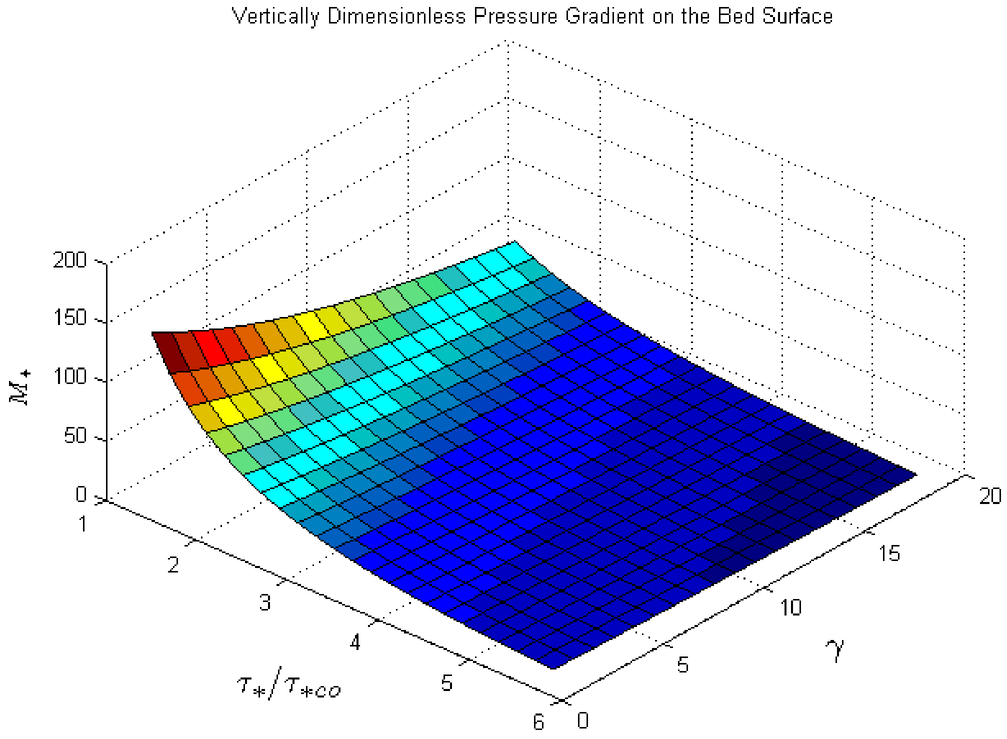

Figure 5.8 Vertically dimensionless pressure gradient in the bed load layer.

Estimate of the addition shear stress τ_{ax}

The conservation equation results in the acquisition of mean streamwise flow velocity in the packed layer,

$$\overline{u_p} = \frac{m - \rho_s q_s cos\gamma - \rho\bar{u}A(1-\alpha)}{\rho A_p \beta} \quad (5.55)$$

where m is determined by the inlet boundary condition on which we neglect any loading in the bed load and packed layer, in our case, namely,

$$m = \rho\overline{u_{p0}}A_p\beta + \rho_s q_{s0} cos\gamma + \rho\bar{u}_0 A(1-\alpha) = 0 \qquad (5.56)$$

In which q_{s0} is the sediment bed load and $\bar{u}_0$ the mean streamwise velocity in the bed load layer at the flow boundary, confirmed by the logarithmic law of wall,

$$\frac{\bar{u}_a}{u_\tau} = \frac{1}{k} ln\left(R\frac{\xi}{k_s}\right) \qquad (5.57)$$

where $\bar{u}_a$ is the locally mean velocity at the location of ξ ,the normal distance from bed surface in the bed load layer; $k = 0.4$, is von karman constant; when the particle Reynolds number $RE_p = \frac{u_\tau k_s}{v} > 100$ for a rough turbulent wall flow, $R = 30$; u_τ the shear velocity, $u_\tau = \sqrt{\tau/\rho}$; and k_s the bed roughness, $k_s = D$. We choose $\xi = 0.4\delta$ as the position of average velocity over the bed load layer.

Therefore,

$$\tau_{ax} = -e\rho_b\bar{u}^2 + l\rho_p\bar{u}_p^2$$

$$= -e\rho_b(\bar{u}_a cos\gamma)^2 + l\rho_p\left[\frac{\rho_s(-q_s)cos\gamma + \rho A(1-\alpha)(-\bar{u}_a)cos\gamma}{\rho A_p\beta}\right]^2 \qquad (5.58)$$

The dimensionless form above is denoted by,

$$\tau_{ax}^* = \frac{\tau_{ax}}{\rho(s-1)gD}$$

$$= -e[1+(s-1)\alpha](\bar{u}_a^* cos\gamma)^2$$

$$+ l[\beta + (1-\beta)s]\left[\frac{s(-q_s^*)cos\gamma}{Z_e^*\beta} + \frac{\delta^*(1-\alpha)}{Z_e^*\beta}(-\bar{u}_a^*)cos\gamma\right]^2$$

$$= -e[1 + (s-1)\alpha](cos\gamma)^2(\bar{u}_a^*)^2$$

$$+\frac{l[\beta + (1-\beta)s](cos\gamma)^2}{\beta^2}\left[\frac{s(-q_s^*)}{Z_e^*} + \frac{\delta^*(1-\alpha)}{Z_e^*}(-\bar{u}_a^*)\right]^2 \qquad (5.59)$$

We define the coefficients depending on cosγ as,

$$e^* = e[1 + (s-1)\alpha](cos\gamma)^2 = e[1 + (s-1)\alpha]\frac{1}{1+\varphi_{1x}^2} \qquad (5.60)$$

$$l^* = \frac{l[\beta + (1-\beta)s](cos\gamma)^2}{\beta^2} = \frac{l[\beta + (1-\beta)s]}{\beta^2}\frac{1}{1+\varphi_{1x}^2} \qquad (5.61)$$

Thus, the normal stress is expressed as,

$$\tau_{ax}^* = -e^*(\bar{u}_a^*)^2 + l^*\left[\frac{s(-q_s^*)}{Z_e^*} + \frac{\delta^*(1-\alpha)}{Z_e^*}(-\bar{u}_a^*)\right]^2 \qquad (5.62)$$

The additional stress or pressure due to the longitudinal slope is expressed as,

$$\tau_{add} = \tau_{ax}^* tan\gamma \qquad (5.63)$$

which is plotted in Fig.5.9 as follows,

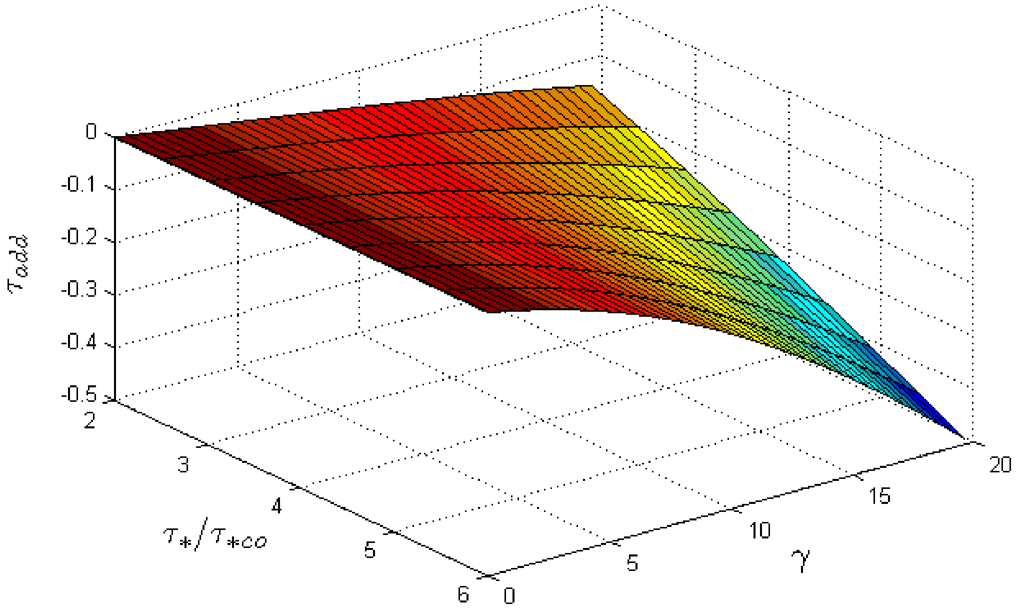

Figure 5.9 Additional stress verse shear stress ratio and bed slope.

The negative value for τ_{add} demonstrate that the longitudinal slope causes an additional pressure pointed to upstream which results in a back flow obviously coming up with a large slope, a small ratio of normal stress reduces the degree of a back flow in the meanwhile.

We have to depend on the numerical method to acquire the solution of Eq.5.22 because of the complex couple between φ_1^* and φ_{1x}. Eq.5.22 can be iteratively solved if only a^*, δ^*, M^*, b^*, H^* , τ_{ax}^* and $c^*$are specified.

The constant coefficients a^*, b^* are relatively easy to be calculate because we know the specific ratio of water and sediment $s = 2.65$, for our case, the porosity of packed bed layer, $\beta = 0.33$.

$$a^* = \frac{(s-1)}{[(1-\beta)(s-1)+\beta]} = 1.1494 \qquad (5.64)$$

$$b^* = \frac{a^*}{s-1} = 0.6966 \tag{5.65}$$

The factor n^* is calculated by,

$$n^* = \frac{1 - \alpha + (s-1)\alpha}{b^*} - 1 = 0.4355 + 0.9331\alpha \tag{5.66}$$

The mean volume concentration of bed load layer α can be obtained as follows,

$$\alpha = \frac{q_s^*}{V_{*p}\delta^*} \tag{5.67}$$

The experiment's results of Luque and Beek also show the average dimensionless saltation length L_{*s} equals 16.

$$c^* = 24.6238 + 1414.11\frac{1}{RE_w} \tag{5.68}$$

Combining Eq.5.49, Eq.5.67 and Eq.5.68 obtains the value of M^*. Since τ_{ax}^* is a function of scour depth φ_1^*, it must be solved iteratively.

The situation for an arbitrary slope described in Eq.5.22 is shown in Fig.5.10, which illustrates the scour depth decreases as the bed shear stress become high for a large bed slope and increases with the bed slope's increment.

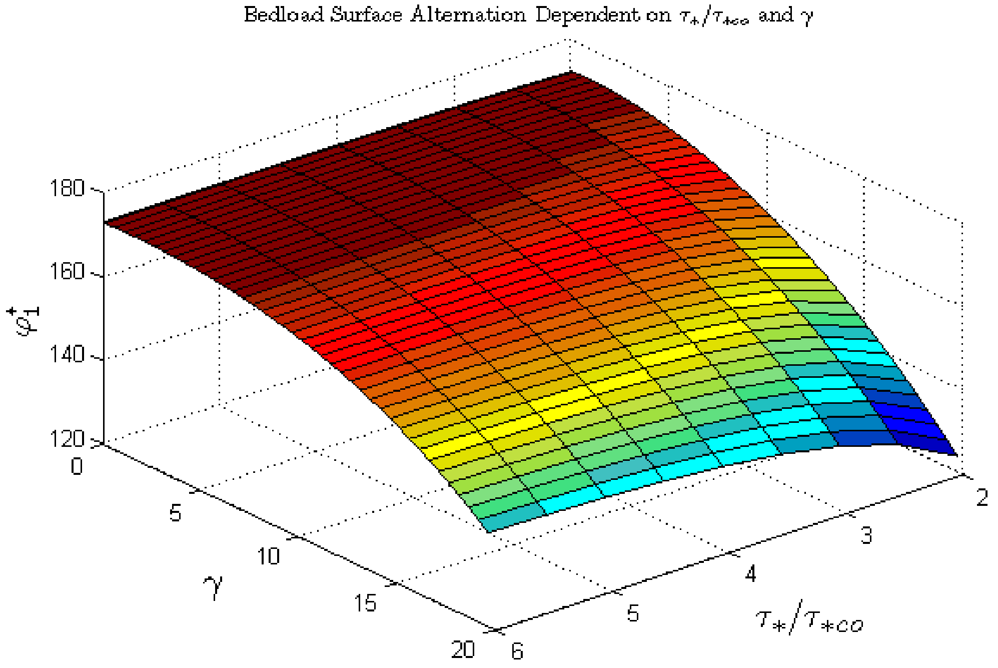

Figure 5.10 Bed load surface profile

CHAPTER 6 Conclusions and Future Work

6.0 Summary of Findings

The research topics on sediment transport have been developed in the last decades. The accurate models, however, no matter what they were conducted by Eistein, Balgnold, Yalin, etc, are not found yet due to the complex flow condition and sediment properties with different parameters. The other path followed by researchers is to use numerical approaches to model the process of erosion, however, it is impossible to apply the same numerical model to all cases we are interested in. Successful prediction to the localized pressure scour requires not only the traditionally laboratory experiments but also the supercomputing technology performing the numerical simulations beyond the reach of the physical modeling. Numerical models in contrast with physical models have more flexibility and avoid the limitation from physical scale. One successful numerical model can provide economic benefits and be applied to the physical cases with the environmental conditions that cannot be carried out in the laboratory conditions.

In this dissertation, two aspects are discussed and developed from numerical simulation and theoretical derivation. The four conclusions are summarized as follows,

First of all, in the numerical simulation, we found that the sediment transport model in FLOW3D is sensitive to the vertical cell size on the sediment interface. The cell size should is larger than the sediment diameter, 2 mm, in numerical calculation, however, the situation based on our analysis is that the vertical cell size should not exceed the dimension of sediment diameter of 2 mm in our case. Within the vertical cell size of

1.4 mm the sediment scour is not obviously dependent on the cell size. When the vertical cell size on the sediment interface is too large, for example, if it is 3 mm, the sediment transport underneath the bridge deck will not reflect the influence of pressure flow condition and no scour hole forms there. The qualitative analysis to the vortex distribution, x-velocity profile and the contour of scour profile the scour model of sediment is reasonable. The important limitation of FLOW3D is time-cost in simulation. The results of 12 min simulation cost the computational time of 40 days, which results in that we cannot get the equilibrium status to compare with physical experiments within reasonable periods.

Secondly, the morphing approach in STARCCM+ is successfully and indirectly applied to the scouring profile. This approach is a kind of indirect application because no any sediment transport model is employed in STARCCM+ to compute the governing equation. The morphing principal is based on two empirical formulas developed by Guo using experimental data from TFHWA. Through the numerical simulation is the relationship between the recession rate of bed and maximum bed shear stress developed as the morphing function or pick-up function. The approach is limited by two factors although numerically relates the sediment load rate to the maximum bed shear stress. One of them comes from the empirical formulas that are not capable of reflecting the deposition of sediment which results in the inaccurate bed shear stress distribution. The other one is produced by the roughness function in STARCCM+ which overestimates the magnitude of bed shear stress. The function of recession rate can be improved in future work by reducing the negative influence from these two factors.

Thirdly, the pressure drop when fluid flows over the bed load layer consists of an important component of force to drive sediment particles. The modified pressure drop equation is derived by adopting the energy equation to apply for fluidized bed surface. It compares well with several groups of experimental data from Gupte, Kyan and Dudgeon. Furthermore, a standard parabolic form is assumed as the quadratic trajectory of particle to calculate the thickness of the bed load layer. This assumption avoids solving complicated equations of motion for particles but it is an effective approximation for the track of particles.

Finally, the derivation of equations for two-layer model is developed by coupling the bed load layer and packed sediment layer to predict the erosion process. We found that the entrainment rate of sediment particles is also dependent on the changing rate of bed load layer thickness and mixture density from the continuity equation compared to Exner equation. Also, from the two dimensional computation, the dimensionless thickness of bed load layer δ_* decreases as the slope of bed increase for a given small $\frac{\tau_*}{\tau_{*co}}$, and the trend is reverse for a given large one. For a given slope, δ_* decrease as the dimensionless ratio of shear stress $\frac{\tau_*}{\tau_{*co}}$ increases. The additional stress or pressure due to the longitudinal slope is contributed to the momentum equation and it is a negative value for a large slope. This influence for a small slope, however, is not significant.

6.1 Future Work

In General, several different causes may result in the discrepancies between sediment transport model predictions and physical measurements, such as the oversimplification of the problem (1D versus 2D or 2D versus 3D), the incorrect input data, lack of appropriate data for calibration, the limitations of the sediment transport equations, and computational errors from the numerical schemes. For example, the recession rate of sediment transport is difficult to accurately be measured in the process of scour because the recession rate is the division of sediment mass flowing out of bed by scour time in our measurement and the collection for sediment mass cannot be accurately measured. Further, in our experiments, the recession rate can only be measured on the flat bed due to the limitation of flume, which results in some error when applying it to the bed with slope. Therefore, the sufficiently accurate data will be required to improve in future work so that they are effectively adopted in the calibration of numerical model.

On the other hand, morphing approach in STARCCM+ is based on Guo's empirical formula of scour profile without the consideration of deposition of particles. Therefore, the downstream profile under a bridge cannot explain the deposition or pile-up of sediment particles compared to experiments measurements. The corresponding morphing bed downstream under a bridge deck in the simulation in STARCCM+ is not able to fit the experimental data very well, which may results in the inaccurate distribution of bed shear stress.

Hence, the future work to improve the numerical simulation for scouring will focus on the following aspects,

a) Experimental measurement for the shear stress distribution on the bed in the process of scour

The shear stress distribution on the bed in different stages of scour is significant to research on the bed morphing. However, the current facilities of experimentation limits the measurements for the bed shear stress, and hence, we cannot compare the numerical results without them. The measurement for the shear stress distribution on the entire bed is a challenging topic in hydraulics.

b) Deposition of sediment particles on the upfront under a bridge deck

The scour profile on the river bed has a significant influence on the distribution of shear stress. If the deposition of sediment particles are not considered when developing a function of scour profile, the distribution of shear stress may not satisfy the equilibrium condition of scour. The derivation of scour profile based on the recession rate is necessary to be improved.

c) Entrainment rate of sediment particles transport and pick-up function

The entrainment rate for a flat sediment bed without any hydraulic structure can be approximated to be a constant in a given flow condition. Most of experiments for measuring the entrainment rate of particles are for the flat bed in open channel flow, and the rate is a time-averaged value. However, the entrainment rate of particles in a pressure flow is a time-dependent variable because the recession rate of bed becomes lower with a coming equilibrium status. Unfortunately, the time-dependent entrainment rate for a pressure flow condition is not measured by precious researchers. What we adopt in our research is based on an average value of entrainment rate. Similarly, the traditional pick-up functions of sediment particles in hydraulics are time-averaged values which are functions of difference between a local bed shear stress and a critical shear stress. Thus, it is not accurate to apply them to every status of scour. The time-dependent entrainment rate and pick-up function in a pressure flow condition may be experimentally researched in the future work.

d) Application of the two layer theoretical model to the scouring process

In this dissertation, the two layer model in the bed load and packed layer consists of continuity equation and momentum equation. The continuity equation can be manipulated and incorporated into STARCCM+ to improve the simulation in the future research.

To sum up, future research should focus on the cross-cutting issues resulting from the limitations of sediment transport models. The models should be capable of handling the simulation for different spatial and temporal scales, bed evolution and sediment exchange between the bed and fluid by developing an effective approach of reconciliation. The morphing mesh approach can be improved by incorporating updated model of sediment transport to obtain better shear stress distribution, and the two layer model needs to be further developed and improved.

LIST OF SYMBOLS

q_b = the gravel bed load

S = the specific weight of sediment

g = the gravitational acceleration

d_s = the sediment diameter on the bed surface

τ_* = the dimensionless wall shear stress or Shields parameter

e_s = the suspension efficiency

e_b = the bed load transport efficiency

U_s = the mean transport velocity of suspended grains

W = the fall velocity of suspended grains

ω = the total flow power per unit boundary area

θ = the dynamic friction angle

K_b = variable depending on the excess shear stress

d_{50} = the median sediment diameter on the bed surface.

q_s^* = the rate of bed load transport

V_{*p} = the average particle velocity

E = the entrainment rate

L_{*s} = the average length of individual steps of saltating bed load particles

R = the hydraulic radius

τ_{*c} = the critical Shields number.

τ_{*co} = the critical Shields stress on a horizontal slope

α = the bed slope angle

β_{μ} = a static coefficient of friction between particles and bed surface.

φ = the transverse slope angle

y_s = the equilibrium depth of scour

y_1 = the upstream water depth

H_b = the bridge opening between the bridge low chord and the bed prior to scour

V_a = the flow mean velocity through the bridge opening.

V_{uc} = the critical velocity of incipient sediment

s = the specific gravity of sediment

h_u = the water depth before scour

y_s = the maximum scour depth

h_b = the bridge opening prior to scour

V_u = the approaching velocity upstream

w = overtopping depth of bridge deck

$\bar{\rho}$ = the average density on the packed sediment bed

ρ_l = the local density of liquid

ρ_s = the sediment particles

τ = the shear stress due to the fluid viscosity

K = the drag coefficient among particles

f_s = the solid fraction of the sediment

$f_{s,co}$ = the cohesive solid fraction over which the interaction among particles occurs

$f_{s,cr}$ = the critical solid fraction over which the fluid flow ceases

u_{drift} = the drifting velocity of particles

u_{lift} = the lifting velocity of particles

d = the mean sediment diameter

μ = the liquid viscosity

μ_l = the molecular viscosity of the liquid

f_l = the liquid fraction

α = a factor of probability of a particle’s lifting from the packed sediment surface

n_s = the normal vector to the bed surface

τ_{crit} = the critical shear stress

θ_{crit} = the critical Shields Number

τ_{crit} = the critical shear stress on the packed sediment bed with a slope

τ^{0}_{crit} = the critical shear stress with a horizontal bed

φ = the actual angle between the normal vector of the bed interface and the gravity vector

ω = the angle of repose

u = the local velocity of advection

C_s = the local concentration of the suspended sediment

D = the diffusion coefficient

d_h = the hydraulic diameter

k_s = the effective roughness for 2 mm sediment diameter

Re = the Reynolds number

k_s/d_h = the relative effective roughness

f = the friction factor

h = the bed elevation relative to a given datum

t = the evolving time

C = a constant coefficient

U = the average flow velocity

x = the downward distance along the sedimentary bed

$\varphi_1(x, y, t)$ = the surface function for the top surface of bed load layer

$\varphi_2(x, y, t)$ = the surface function for the bottom interface of bed load layer

D_* = the particle parameter related to diameter

d_{50} = the median particle diameter of the bed material

s = the specific gravity

ν = the kinematic viscosity coefficient

θ_s = the particle mobility parameter

τ_b = the overall time-averaged bed shear stress

u_* = the overall bed shear velocity equal to $\sqrt{\tau_b/\rho}$.

$\mathrm{E_b}$ = the excess bed shear stress parameter

$\tau_{b,cr}$ = the critical time averaged bed shear stress

S_z = the suspension parameter,

w_s = the particle fall velocity in clear water

C_z = the ratio of sediment and fluid mixing coefficient

κ = von Karman constant.

q_* = the sediment transport rate

q_t = the volumetric total sediment transport rate

q_s = the volumetric sediment transport rate in the bed load layer

χ = the fraction of susceptible particles to move exposed to flow per unit area

n_p = the number of particles at rest on the bed surface per unit area

α_1 = the shape constant of particles

P_s = the number of pick-ups for each particle per unit time.

E = the pick-up rate of particles in mass per unit area and time

P_e = the probability of the lift force acting on the particle with exceeding the immersed weight of particle

α_e = a coefficient verified by experiments

α_f = a coefficient determined as 0.0199

θ_s = the particle mobility parameter or Shields number

$\theta_{s,cr}$ = the critical value of particle mobility parameter or Shields parameter.

α_y = a constant coefficient

P_y = the pick-up probability

ρ = the fluid density

$\emptyset$ = the porosity

V_f = the superficial velocity from fluid flow

H_b = the bed height altering with flow velocity

e = the total stored energy per unit mass fluid

I_e = the internal energy per unit mass

Q'_{net} = the addition of the net time rate of energy by heat transfer into system

W'_{net} = the net time rate of energy by work transfer into the system

K_1, K_2, C_1 and C_2 = the constants in the logrithmic formulas

V_{mf} = the minimum fluidization velocity,

$\emptyset_{mf}$ = the minimum fluidization porosity

dp = the pressure drop between the top and the bottom of the bed

ρ = the fluid density

$\emptyset$ = a packed bed porosity

D = a mean diameter of particles

μ = the coefficient of dynamic viscosity

V = the minimum fluidized velocity

L = the original thickness of bed

L' = the expanding thickness on the basis of L

Y_*, X_* and X_{*0} = the dimensionless parameters in Eq.4.38

ρ_b = the average density in the bed load layer

ρ_p = the average density in the packed layer

n_s = the outward unit normal of perimeter surface

A_p = the projected area to x-y plane

Π_i = the function of transport.

$\varphi_1(x, y, t)$ = the surface equation on the top surface of bed load layer

$\varphi_2(x, y, t)$ = the surface equation on the bottom of bed load layer

n_i = the unit normal on the surface of $\varphi_1(x, y, t), \varphi_2(x, y, t), i = 1,2$

$\varphi_{1x}, \varphi_{1y}$ = the partial derivative of φ_1 along x and y

$\varphi_{2x}, \varphi_{2y}$ = the partial derivative of φ_2 along x and y

$\vec{V}_1, \vec{V}_2$ = the local velocity of moving top surface and interface, respectively

$\vec{U}$ = the local velocity of flow in the control volume

u_1, v_1, w_1 = the components of the local velocity of flow in the bed load and packed layer

u_1, v_1, w_1 = the components of the local velocity of flow in the bed load and packed layer

dS = the arch length along the projected area to x-y plane

F = the total mean mass load

φ_b = the function of the bottom surface in the packed layer

Π_b = the function of transport on the bottom surface

F_p = the transport load in the packed layer corresponding to the bed load layer

F_s = the mass bed load of sediment per unit width

F_f = the mass transport rate of flow per unit width

f = the body force per unit mass

$\overrightarrow{T_n}$ = the surface force acted on the boundary of control volume

n_b = the unit normal of the bottom surface

A_b = the projected area of control volume on x-y plane in the bed load layer

n_{bs} = the laterally outward unit normal

A_{bs} = the surface area for the control volume in the bed load layer

δ = the thickness of the bed load

g_1, g_2 = the mean gravitational acceleration in the bed load layer and packed layer

$\tau_{ax} tan\gamma$ = the additionally normal stress downstream caused by the alternative streamwise slope

$x^*, t^*, \varphi_1^*, \delta^*, M^*, H^*, \tau_{ax}^*, q_*$ = the dimensionless parameter for those responding physical value

t_a = the equilibrium time of scour

$\bar{\bar{\tau}}$ = the stress tensor

∇ = $\left(\frac{\partial}{\partial x}, \frac{\partial}{\partial y}, \frac{\partial}{\partial z}\right)$

∇_h = $\left(\frac{\partial}{\partial x}, \frac{\partial}{\partial y}\right)$

$\overline{u_p}$ = the horizontally averaged velocity over the packed layer

A_p = the cross section over the packed layer

$\bar{u}$ = the local averaged x component over the packed layer

$\bar{w}$ = the local averaged z components over the packed layer

V_p = the particle's velocity

δ = the thickness of bed load layer or saltation height

α = the volume concentration of particles

V_{*p} = the dimensionless mean streamwise velocity of particles

q_s^* = the dimensionless sediment bed load

L_{*s} = the dimensionless saltation length

τ_{*co} = the critical Shields number in the horizontal bed

μ_s = the static coefficient of friction

$\bar{u}_a$ = the locally mean velocity at certain location away from bed

RE_p = the particle Reynolds number for a rough turbulent wall flow

u_τ = the shear velocity, $u_\tau = \sqrt{\tau/\rho}$

k_s = the bed roughness, $k_s = D$

τ_{add} = the additional stress or pressure due to the longitudinal slope

$\varphi_1^*, a^*, \delta^*, M^*, b^*, H^*, \tau_{ax}^*, c^*$ = the dimensionless parameters corresponding to the ones without star signs

REFERENCES

Abed, L.M. (1991). “Local Scour around Bridge Piers in Pressure Flow.” Ph.D Dissertation, Colorado State University.

Arneson, L A and Abt, S R. “Vertical contraction scour at bridges with water flowing under pressure conditions.” Stream stability and scour at highway bridge, 1998, 1647: 10-17.

Asano. T. (1992). “Observations of Granular-Fluid Mixture under an Oscillatory Flow.” Proc., 23rd Coast. Eng. Conf., Venice, Italy, 1896-1909.

Ashida, K., and Michiue,M. (1972). “Study on Hydraulic Resistance and Bed load Transport Rate in Alluvial Streams.” Proc., Japan Soc. Civ. Engrg., 206, 59-69.

Bagnold, R.A.(1956). “The Flow of Cohesionless Grains in Fluids.” Proc. Royal Soc., London, England, 249, 1956.

Bagnold, R.A.(1966). “An Approach to the Sediment Transport Problem from General Physics.” Geological Survey Prof., 422-I, Wash.

Bagnold,R.A.(1973). “The Nature of Saltation and of Bed-Load Transport in Water.” Proc. Royal Soc., London, England, A 332, 473-504.

Bakhtiary, A.Y. (1997). “Velocity Profile of Sediment-Laden Flow in Transition from Saltation to Sheet-Flow.” Proc., 27th John F. Kennedy Student Paper Competition and Specialty Seminar Summaries, 27th Congress of IAHR, 1-6.

Ballio, F., Teruzzi, A., and Radice, A.(2009). “Constriction Effects in Clear-Water Scour at Abutments.” *J. Hydraul. Eng*., 135(2), 140-145.

Bey, A.B., Faruque, M.A.A., and Balachandar, R.(2007). “Two-Dimensional Scour Hole Problem: Role of Fluid Structures.” J. Hydraul. Eng., 133(4), 414-430.

Brethour J. “Modeling Sediment Scour.” Technical Document No. FSI-03-TN62, 1-6.

Chan, H.C., Leu, J.M., Lai, C.J., and Jia, Y.(2007).”Turbulent Flow over a Channel with Fluid-Saturated Porous Bed.” J. Hydraul. Eng., 133(6), 610-617.

Chang, H. H. (1998). Generalized computer program: Users’ manual for FLUVIAL-12: Mathematical model for erodible channels, San Diego.

Chang, W., Lai, J., and Yen, C.(2004). “Evolution of Scour Depth at Circular Bridge Piers.” J., Hydraul., Eng., 130(9), 905-913.

Cheng N.(2002). “Exponential Formula for Bed load Transport.” J., Hydraul., Eng., 128(10), 942-946.

Cheng, N.(2003). “A Diffusive Model for Evaluating Thickness of Bed load Layer.” Advances in Water Resources, 26, 875-882.

Chreties, C., Simarro, G., and Teixeira, L.(2008). “New Experimental Method to Find Equilibrium Scour at Bridge Piers.” *J. Hydraul. Eng.*, 134(10), 1491-1495.

de Vries, M. (1973). “Application of Physical and Mathematical Models for River Problems.” Pub. No. 12, Delft Hydraulics Laboratory.

Delft Hydraulics. (1999). Delft3D users’ manual, Delft Hydraulics, The Netherlands.

Denson, K.H. (1982). "Steady-State Drag, Lift, and Rolling-moment Coefficients for Inundated Inland Bridges." Rep. No. MSHD-RD-82-077, National Technical Information Service, Springfield, Virg., 1-23.

Dey, S. and Singh, N.P.(2008). "Clear-Water Scour below Underwater Pipelines under Steady Flow." *J. Hydraul. Eng.*, 134(5), 588-600.

Dey, S., Raikar, R.V., and Roy, A.(2008). "Scour at Submerged Cylindrical Obstacles under Steady Flow." J., Hydraul., Eng., 134(1), 105-109.

Einstein, H.A.(1942). "Formulas for the transportation of bed load." Trans. ASCE, 107, 561-73.

Einstein, H.A.(1950). "The Bed-Load Function for Sediment Transportation in Open Channel Flow." Technical Bulletin No. 1026, United States Department of Agriculture, Washingtong, D.C.

Fernandez Luque, R. (1974). "Erosion and Transport of Bed-Load Sediment." Dissertation, Krips Repro B.B., Meppel, The Netherlands.

Fernandez Luque, R., and van Beek, R.(1976). "Erosion and Transport of Bed-Load Sediment." J. Hydraul, Res., 14(2), 127-144.

FLOW3D User Manual Version 9.3, Flow Science Inc., Santa Fe, NM.

Francalanci, S., and Solari, L.(2008). "Bed-Load Transport Equation on Arbitrarily Sloping Beds." *J., Hydraul., Eng.*, 134(1), 110-115.

Gao, P. (2008). " Transition Between Two Bed-Load Transport Regimes: Saltation and Sheet Flow." J. Hydraul. Eng., 134(3), 340-349.

Gilbert, G.K.(1914). “The Transportation of Debris by Running Water.” Prof. Paper 86, U.S. Geological Survey, Reston, Va.

Goutiere, L., Soares-Frazao,S., Savary, C., Laraichi, T., and Zech, Y.(2008). “One-Dimensional Model for Transient Flows Involving Bed-Load Sediment Transport and Changes in Flow Regimes.” *J. Hydraul. Eng.*, 134(6), 726-735.

Greimann, B., Lai, Y., and Huang, J.(2008). “Two-Dimensional Total Sediment Load Model Equations.” *J. Hydraul. Eng.*, 134(8), 1142-1146.

Guo, J. “Bridge pressure flow scour at clear water threshold condition.” Transactions of Tianjin University. 2009, 15(2):79-94.

Guo, J., and Julien, P.Y. (2005). “Shear Stress in Smooth Rectangular Open-Channel Flows.” J. Hydraul. Eng., 131(1), 30-37.

Guo,J. (2002). “Logarithmic Matching and Its Applications in Computational Hydraulics and Sediment Transport.” J. Hydraul. Res., 40(5), 555-565.

Habel, F., Mendoza, C., Bagtzoglou, A.C.(2002). “Solute transport in open channel flows and porous streambeds.” Advances in Water Resources, 25, 455-469.

Haltigin, T.W., Biron, P.M., and Lapointe, M.F.(2007). “Predicting Equilibrium Scour-Hole Geometry near Angled Stream Deflectors Using a Three-Dimensional Numerical Flow Model.” J. Hydraul. Eng., 133(8), 983-988.

Haltigin, T.W., Biron, P.M., and Lapointe, M.F.(2007). “Predicting Equilibrium Scour-Hole Geometry near Angled Stream Deflectors Using a Three-Dimensional Numerical Flow Model.” J. Hydraul. Eng., 133(8), 983-988.

Hanes, D.M., and Bowen, A.J. (1985). “A granular-Fluid model for Steady Intense Bed-Load Transport.” J. Geophys. Res., 90(C5), 9149-9158.

Holly, F. M., and Rahuel, J. L. (1990). “New numerical/physical framework for mobile-bed modeling. Part 1: Numerical and physical principles.” J. Hydraul. Res., 28(4), 401–416.

Jena, H.M., Roy, G.K., and Biswal, K.C. (2008). “Studies on Pressure Drop and Minimum Fluidization Velocity of Gas-Solid Fluidization of Homogeneous Well-Mixed Ternary Mixtures in Un-promoted and Promoted Square Bed.” Chem. Eng. Jour., 145, 16-24.

Jia, Y., and Wang, S. S. (1999). “Numerical model for channel flow and morphological change studies.” J. Hydraul. Eng., 125_9_, 924–933.

Kalinske,A.A. (1947). “Movement of Sediment as Bed in Rivers.” Trans. Am. Geophys. Union, 28, 615.

Karim, M. F., and Kennedy, J. F. (1982). “IALLUVIAL: A commuter based flow and sediment routing for alluvial streams and its application to the Missouri River.” Rep. No. 250, Iowa Institute of Hydraulic Research, Univ. of Iowa, Iowa City, Iowa.

Kawanisi, K. and Shiozaki, R.(2008). “Turbulent Effects on the Setting Velocity of Suspended Sediment.” *J. Hydraul. Eng.*, 134(2), 261-266.

Kerenyi, K., Sofu, T. and Guo, J.(2009). “Hydrodynamic Forces on Inundated Bridge Decks.” Rep. No. FHWA-HRT-09-028, Federal Highway Administration, Turner-Fairbank Highway Research Center, Mclean, Virginia, 1-38.

Khosronejad, A., Rennie, C.D., Neyshabouri, S.S.A.A., and Townsend, R.D.(2007). "3D Numerical Modeling of Flow and Sediment Transport in Laboratory Channel Bends." J. Hydraul. Eng., 133(10), 1123-1134.

Kothyari, U.C., Hager, W.H., and Oliveto, G.(2007). "Generalized Approach for Clear-Water Scour at Bridge Foundation Elements." J. Hydraul. Eng., 133(11), 1229-1240.

Krishnappan, B. G. (1981). User's manual: Unsteady, non-uniform, mobile boundary flow model—MOBED. Hydraulic Division, National Water Research Institute, CCIW, Burlington, Ontario.

Kubatko, E.J., and Westerink, J.J.(2007). "Exact Discontinuous Solutions of Exner's Bed Evolution Model: Simple Theory for Sediment Bores." J. Hydraul. Eng., 133(3), 305-311.

Landsberg, A., Chtchelkanova, A., Lind, C., Boris, J., and Young, T.(1998). Fast3D user and programmer reference manual.

Leeder, M.R. (1979). "Bed load Dynamics: Grain Impacts, Momentum Transfer and Derivation of a Grain Frounde Number." Earth Surface Processes, 4, 291-295.

Li, S.S., and Millar, R.G.(2007). "Simulating Bed-Load Transport in a Complex Gravel-Bed River." J. Hydraul. Eng., 133(3), 323-328.

Linares, M.D., and Belleudy, P.(2007). "Critical Shear Stress of Bimodal Sediment in Sand-Gravel Rivers." J. Hydraul. Eng., 133(5), 555-559.

Lyn, D A. "Pressure-flow scour: A re-examination of the HEC-18 equation." J. Hydraul. Eng., 2008, 134(7):1015-1020.

Lyn, D.A.(2008). “Pressure-Flow Scour: A Reexamination of the HEC-18 Equation.” *J. Hydraul. Eng.*, 134(7), 1015-1020.

Macdonald, I.F., EI-Sayad, M.S., Mow, K., and Dullen, F.A.L.(1979). “Flow through Porous Media- the Ergun Equation Revistied.” Ind. Eng. Chem. Fundam., 18(3), 199-208.

Meyer-Peter, E., and Muller, R.(1948). “Formula for Bed load Transport.” In 2nd Congress of the International Association of Hydraulic Research, 39-64.

Minh Duc, B., Wenka, T., and Rodi, W. (1998). “Depth-average numerical modeling of flow and sediment transport in the Elbe River.” Proc., 3rd Int. Conf. on Hydroscience and Eng., Berlin.

Nifio, Y., and Garcfa, M.(1994). “Gravel Saltation” Water Resources Research, 30(6), 1907-1914.

Owen, P.R.(1964). “Saltation of Uniform Grains in Air.” J. Fluid Mech., 20(2),225-242.

Pagliara, S., Hager, W.H., and Unger, J.(2008).”Temporal Evaluation of Plunge Pool Scour.” *J. Hydraul.Eng.*, 134(11), 1630-1638.

Paola, C., and Voller, V.R.(2005). “A Generalized Exner Equation for Sediment Mass Balance.” J. Geophys. Res., 110, 274-281.

Papanicolaou, A., Bdour, A., and Wicklein, E. (2004). “A numerical model for the study of sediment transport in steep mountain streams.” J. Hydraul. Res., 42(4), 357–366.

Papanicolaou, A.N., Elhakeem, M., Krallis, G., Prakash, S., and Edinger,J.(2008). “Sediment Transport Modeling Review-Current and Future Developments.” J. Hydraul. Eng., 134(1),1-14.

Parker, G.,Seminara, G., and Solari, L.(2003). “Bed Load at Low Shields Stress on Arbitrarily Sloping Bed: Alternative Entrainment Formulation.” Water Resources Research, 39(7), 1183-1193.

Radice, A., Malavasi, S., and Ballo, F.(2008). “Sediment Kinematics in Abutment Scour.” *J., Hydraul., Eng*., 134(1), 146-156.

Rijn, L. C. van (1993). Principles of sediment transport in rivers estuaries and coastal seas, Aqua Publications, The Netherlands.

Rijn, L. C. van, and Tan, G. L. (1985). “Sutrench model: Two dimensional vertical mathematical model for sedimentation in dredged channels and trenches by currents and waves.” Water Resources communications, No. 41.

Rijn, L.C. van (1982). “Equivalent Roughness of Alluvial Bed.” J. Hydraul. Div., ASCE, No. HY10.

Rijn, L.C. van (1986). “Application of Sediment Pick-up Function.” J. Hydraul. Eng., 112(9), 867-874.

Rijn,L.C.van (1984). “Sediment Transport, Part 1: Bed Load Transport.” J. Hydraul. Eng., 110(10), 1431-1456.

Sau, D.C., Mohanty, S., Biswal, K.C. (2007). “Minimum Fluidization Velocities and Maximum Bed Pressure Drops for Gas-Solid Tapered Fluidized Beds.” Chem. Eng. Jour., 132, 151-157.

Schmeeckle, M.W., and Nelson, J.M. (1999). "A Dynamic Boundary Condition for Bed Load Sediment Transport in Non-Uniform, Hydraulically Rough Turbulent Boundary Layers." Annu. *J. Hydraul. Eng*. Jpn. Soc. Civ. Eng., 43, 653-659.

Schmeeckle, M.W., and Nelson, J.M. (2003). "Direct Numerical Simulation of bed load Transport Using a Local, Dynamic Boundary Condtion." *Sedimentology*, 50, 279-301.

Seminara, G., Solari, L., and Parker, G. (2002). "Bed Load at Low Shields Stress on Arbitrarily Sloping Beds: Failure of the Bagnold Hypothesis." Water Resources Research, 38(11), 1249-1264.

Simons, D.B., and Richardson, E.V. (1963). "Forms of Bed Roughness in Alluvial Channels." Trans. Am. Soc. Civ. Eng., 128(1), 284-302.

Singh, K.M., Sandham, N.D., and Williams, J.J.R.(2007). "Numerical Simulation of Flow over a Rough Bed." J. Hydraul. Eng., 133(4), 389-398.

Smith, H.D. and Foster, D.L. "Modeling flow and scour around a pipeline." Coast Engineering 2002, 1722-1732.

Spasojevic, M., and Holly, F. M. (1990a). "MOBED2: Numerical simulation of two-dimensional mobile-bed processes." Technical Report No. 344, Iowa Institute of Hydraulic Research, Univ. of Iowa, Iowa City, Iowa.

Spasojevic, M., and Holly, F. M. (1994). "Three-dimensional numerical simulation of mobile-bed hydrodynamics." Contract Rep. HL-94-2, U.S. Army Engineer Waterways Experiment Station, Vicksburg, Miss.

STAR-CD Version 4.12 Methodology, CD-ADAPCO Inc,2009

STAR-CD Version 4.12 User Guide, CD-ADAPCO Inc, 2009

Stoesser, T., Braun, C., Garcia-Villalba, M., and Rodi, W.(2008). “Turbulence Structures in Flow over Two-Dimensional Dunes.” J., Hydraul., Eng., 134(1), 42-55.

Sun, Z., and Donahue, J. (2000). “Statistically Derived Bed load Formula for Any Fraction of Nonuniform Sediment.” J. Hydraul. Eng., 126(2), 105-111.

Thomas, W. A., and Prashum, A. I. (1977). “Mathematical model of scour and deposition.” J. Hydr. Div., 110(11), 1613–1641.

Umbrell, E.R., Young, K., Stein, S.M., and Jones, J.S.(1998). “Clear-Water Contraction Scour under Bridges in Pressure Flow.” *J. Hydraul. Eng*.,124(2), 235-240.

Umbrell, Edward R., Young, G.Kenneth et al (1998). “Clear-Water Contraction Scour under Bridges in Pressure Flow.” J. Hydraul. Eng., 124(2), 236-240.

Vardy, A.E., and Brown, J.M.B.(2007). “Approximation of Turbulent Wall Shear Stresses in Highly Transient Pipe Flows.” *J. Hydraul. Eng*., 133(11), 1219-1228.

Walstra, D. J. (1997). “UNIBEST TC-2.0 model: Overview of formulations.” Rep. H2305-42, Delft Hydraulics, The Netherlands.

Wang, G., Fu, X., Huang, Y., and Huang, G.(2008). “Analysis of Supspended Sediment Transport in Open-Channel Flows: Kinetic-Model-Based Simulation.” J., Hydraul., Eng., 134(3), 328-339.

Wang, X., Zheng, J., Li, D., and Qu, Z.(2008). “Modification of the Einstein Bed-Load Formula.” *J. Hydraul. Eng*., 134(9), 1363-1369.

Wiberg, P.L., and Smith, J.D.(1989). “Model for Calculating Bed Load Transport of Sediment.” J. Hydraul. Eng., 115(1), 101-123.

Wilson, K.C. (1966). “Bed Load Transport at High Shear Stress.” J. Hydr. Div., ASCE, 92(6), 49-59.

Xu, C.C., and Zhu, J. (2009). “Prediction of the Minimum Fluidization Velocity for Fine Particles of Various Degrees of Cohesiveness.” Chem. Eng. Comm., 196, 499-517.

Xu, P., and Yu, B.(2008). “Developing a New Form of Permeability and Kozeny-Carman Constant for Homogeneous Porous Media by Means of Fractal Geometry. ” Advances in Water Resources, 31, 74-81.

Yalin, M. S. (1972). Mechanics of sediment transport, Pergamon Press,U.K.

Yalin, M.S.(1963). “An Expression for Bed Load Transportation.” J. Hydr. Div., ASCE, 89(3),221-250.

Yalin, M.S.(1972). “Mechanics of Sediment Transport.” Pergamon Press, New York, N.Y., 54-61.

Yang, C.(1986). “On Bagnold’s Sediment Transport Equation in Tidal Marine Environments and the Practical Definition of Bed load.” Sedimentology, 33, 465-486.

Yanmaz, A.M.(2006). “Temporal Variation of Clear Water Scour at Cylindrical Bridge Piers.” Can. J., Civ., Eng., 33, 1098-1102.

Zarrati, A.R., Jin, Y.C., and Karimpour, S.(2008). “Semi-analytical Model for Shear Stress Distribution in Simple and Compound Open Channels.” *J., Hydraul., Eng.*, 134(2), 205-215.

Zessen, E.van, Tramper,J, Rinzema, A., Beeftink, H.H. (2005). “Fluidized-Bed and Packed-Bed Characteristices of Gel Beads.” Chem. Eng. Jour., 115, 103-111.

Zhao,M., and Cheng,L.(2008). “Numerical Modeling of Local Scour Below a Piggyback Pipeline in Currents.” *J. Hydraul. Eng*., 134(10), 1452-1463.

APPENDIX A

```
% Comparison of dimensionless parameters among experimental data from table 4.2,
% Ergun and modified Ergun equation

% Constant Parameters Definiation

Phi_mf = 0.32; Rou_p = 2600; Rou_f = 1.2; s = Rou_p./Rou_f;

D = 0.000287; g = 9.81; Phi = 0.303; x0 = 0.03; mu = 1.82e-5;

 data_import = importdata('pE.txt'); % pE.txt is the data file

% Extract Data

x_or = data_import(:,1); y_or = data_import(:,2);

x1 = x_or(1:6,1);y1 = y_or(1:6);

 A = 150.*mu.*(1 - Phi).^2./Phi.^3./D.^2;

B = 1.75.*Rou_f.*(1-Phi)./Phi.^3./D;

x = linspace(0,0.05,20);

B1 = 2; % B1 is β1

y_star = A.*x./(1 + (x./x0).^B1).^(1./B1);

Ergun = B.*x.^2 + A.*x;


yy = - y_star.*D.*Phi.^3./(Rou_f.^3.*(1-Phi)); xx = Rou_f.*D.*x./mu./(1-Phi);
```

```
yy1 = - y1.*D.*Phi.^3./(Rou_f.^3.*(1-Phi)); xx1 = Rou_f.*D.*x1./mu./(1-Phi);

Ergun1 = - Ergun.*D.*Phi.^3./(Rou_f.^3.*(1-Phi));

loglog(xx,yy);grid on;

xlabel('\it$$Re_{p} /(1-\phi)$$','interpreter','latex','FontName','cambria math')

ylabel('\it$$-grad(p)d\phi^{3}/[\rhoV^{2}(1-\phi)]$$','interpreter','latex','FontName','cambria math')

hold on; loglog(xx1,yy1,'ok');

hold on; loglog(xx,Ergun1,'-.r');

legend('Motified Ergun Equation','Experimental Data','Ergun Equation');

% Comparison among Dudgeon’s data, Ergun and modified Ergun equation

% Constant Parameters Definiation

Phi_mf = 0.5;Rou_p = 2600; Rou_f = 1.2;s = Rou_p./Rou_f;

D = 0.53e-3; g = 9.81;Phi = 0.38; mu = 1.82e-5; y_observed = 10;

data_import = importdata('dudgeon.txt'); % dudgeon.txt is the data file

% Extract Data

x_or = data_import(:,1);y_or = data_import(:,2);

x1 = x_or(1:16,1);x2 = x_or(17:35,1);x3 = x_or(36:48,1);x4 = x_or(49:60,1);

x5 = x_or(61:68,1);
```

```
y1 = y_or(1:16);y2 = y_or(17:35);y3 = y_or(36:48);y4 = y_or(49:60);

y5 = y_or(61:68);

 A = (1 - Phi_mf).*(s - 1).*Phi.^3.*Rou_f.^2.*D.^3.*g./(1 - Phi).^3./mu.^2;

x0 = (1 - Phi_mf).*(s - 1).*Phi.^3.*Rou_f.^2.*D.^3.*g./(1 - Phi).^3./mu.^2./150;

x = logspace(-6,3); B1 = log(2)./log(150./x0./y_observed);

y_star = 150./(x.*(1 + (x./x0).^B1).^(1./B1));

Ergun = 150./x + 1.75;

loglog(x,y_star); grid on; grid minor;

xlabel('\it$$Re_{p} /(1-\phi)$$','interpreter','latex','FontName','cambria math')

ylabel('\it$$-grad(p)d\phi^{3}/[\rhoV^{2}(1-
\phi)]$$','interpreter','latex','FontName','cambria math')

hold on;

loglog(x1,y1,'ok',x2,y2,'+k',x3,y3,'dk',x4,y4,'*k',x5,y5,'^k');

hold on; loglog(x,Ergun,'-.r');

legend('Motified Ergun Equation','Marble 2','Sand 4',...

'Sand 6','Sand 12','Sand 13','Ergun Equation');


% Comparison among Gupte’s data, Ergun and modified Ergun equation
```

```
% Constant Parameters Definiation
Phi_mf = 0.55;Rou_p = 2300; Rou_f = 1.2;s = Rou_p./Rou_f;
D = 0.77e-3; g = 9.81;Phi = 0.336; mu = 1.82e-5;y_observed = 9.6;
data_import = importdata('data.dat'); % data.dat is the data file
% Extract Data
x_or = data_import(:,1);y_or = data_import(:,2);
x1 = x_or(1:13,1);x2 = x_or(14:27,1);x3 = x_or(28:41,1);x4 = x_or(42:55,1);
x5 = x_or(56:70,1);x6 = x_or(71:84,1);x7 = x_or(85:103,1);x8 = x_or(104:122,1);
y1 = y_or(1:13);y2 = y_or(14:27);y3 = y_or(28:41);y4 = y_or(42:55);
y5 = y_or(56:70);y6 = y_or(71:84);y7 = y_or(85:103);y8 = y_or(104:122);
 A = (1 - Phi_mf).*(s - 1).*Phi.^3.*Rou_f.^2.*D.^3.*g./(1 - Phi).^3./mu.^2;
x0 = (1 - Phi_mf).*(s - 1).*Phi.^3.*Rou_f.^2.*D.^3.*g./(1 - Phi).^3./mu.^2./150;
x = logspace(-3,3);
B1 = log(2)./log(150./x0./y_observed);
y_star = 150./(x.*(1 + (x./x0).^B1).^(1./B1));
Ergun = 150./x + 1.75; loglog(x,y_star);
grid on; grid minor;
xlabel('\it$$Re_{p} /(1-\phi)$$','interpreter','latex','FontName','cambria math')
```

```
ylabel('\it$$-grad(p)d\phi^{3}/[\rhoV^{2}(1-\phi)]$$','interpreter','latex','FontName','cambria math')
hold on;
loglog(x1,y1,'ok',x2,y2,'+k',x3,y3,'^k',x4,y4,'*k',x5,y5,'Xk',x6,y6,'sk',x7,y7,'dk',x8,y8,'pk');
hold on; loglog(x,Ergun,'-.r');
legend('Matified Ergun Equation','Material 8','Material 7','Material 6',...
'Material 5','Material 4','Material 3','Material 2','Material 1','Ergun Equation');
% Comparison among Kyan’s data, Ergun and modified Ergun equation
% Constant Parameters Definiation
Phi_mf = 0.9;Rou_p = 2300; Rou_f = 1.2;s = Rou_p./Rou_f;
D = 0.23e-3; g = 9.81;Phi = 0.8; mu = 1.82e-5; y_observed = 3.3;
data_import = importdata('kayan.txt'); % kayan.txt is the data file
% Extract Data
x_or = data_import(:,1);y_or = data_import(:,2);
x1 = x_or(1:5,1);x2 = x_or(6:10,1);x3 = x_or(11:18,1);x4 = x_or(19:26,1);
x5 = x_or(27:36,1);x6 = x_or(37:46,1);x7 = x_or(47:51,1);
y1 = y_or(1:5);y2 = y_or(6:10);y3 = y_or(11:18);y4 = y_or(19:26);
y5 = y_or(27:36);y6 = y_or(37:46);y7 = y_or(47:51);
```

```
A = (1 - Phi_mf).*(s - 1).*Phi.^3.*Rou_f.^2.*D.^3.*g./(1 - Phi).^3./mu.^2;

x0 = (1 - Phi_mf).*(s - 1).*Phi.^3.*Rou_f.^2.*D.^3.*g./(1 - Phi).^3./mu.^2./150;

x = logspace(-3,3); B1 = log(2)./log(150./x0./y_observed);

y_star = 150./(x.*(1 + (x./x0).^B1).^(1./B1));

Ergun = 150./x + 1.75;

loglog(x,y_star); hold on;

grid on; grid minor;

xlabel('\it$$Re_{p} /(1-\phi)$$','interpreter','latex','FontName','cambria math')

ylabel('\it$$-grad(p)d\phi^{3}/[\rhoV^{2}(1-\phi)]$$','interpreter','latex','FontName','cambria math')

hold on;

loglog(x1,y1,'ok',x2,y2,'+k',x3,y3,'^k',x4,y4,'*k',x5,y5,'Xk',x6,y6,'sk',x7,y7,'dk');

hold on; loglog(x,Ergun,'-.r');

legend('Matified Ergun Equation','5 Nylon','4 Nylon','11 Dacron',...

'3 Dacron','1 Glass','2 Glass','10 Glass','Ergun Equation');
```

APPENDIX B

```
% Arbitrary Angle's Slope for process of Scouring
  %{
  Variables Description:
  L, the domain length; h is the height at the right edge of block;
  Delta_star, the mean dimensionless thickness of bed load layer;
  Ls_star, the saltation length every step;
  Alfa, the mean volume concentration of bed load layer;
  Beta, the procity of packed layer;
  qs_star, the dimensionless bed load;
  Vp_star, the mean streamwise velocity of sediment on the bed;
    %}

% Configure the initial domain and boundary value
h = 0.2; L = 6; D = 0.001; H = 0.25; g=9.81; Rou = 998.1; Mu =1.005e-3;
s=2.65; Beta = 0.33; Repose_angle = 35.*pi./180;
x0_star = 0; z0_star = h/D; Kapa=0.4; e=1; l=1;
iteration = 100;
```

```
Tau_star = 2:0.5:6; R=30; Tau_star_co = 0.034;
u_tau = sqrt(Tau_star.*Tau_star_co./Rou);
 Gamma_degree = [0.001 0.1:0.5:20];
Gamma = Gamma_degree.*pi./180;
[s_x,s_y] = size(Tau_star);
[ss_x,ss_y] = size(Gamma);
Phi_star = cell(1,size(Gamma,2));
 H_star = H./D;
Ls_star = 16;
 % Constants related to qs_star and vp_star
    a_q=8677.849e-6;b_q=-2521.125e-6;d_q=-289785.4e-6;g_q=9543.719e-6;
    h_q=1068.214e-6;j_q=21673.804e-6;k_q=827.69811e-6;
    l_q=21.321179e-6;a_vp=-46136.64e-6;d_vp=856798.23e-6;g_vp=187614.77e-6;
    h_vp=44260.106e-6;
% Initialize storage space
Storage_l = ones(ss_y,s_y); Storage_h = ones(ss_y,s_y);
Storage_delta = ones(ss_y,s_y); Storage_qs_star = ones(ss_y,s_y);
Storage_vp_star = ones(ss_y,s_y); Storage_Tau_ax_star = ones(ss_y,s_y);
```

```
 % Define cell storage space

St_cell_l = cell(1,iteration+1); St_cell_h = cell(1,iteration+1);

St_cell_m=cell(1,iteration+1);

Delta_star = cell(1,ss_y);

  for j = 1:ss_y

  x_l = 1.*ones(ss_y,s_y); x_h = 700.*ones(ss_y,s_y);

  St_cell_l(1,1) = {x_l(j,:)};

  St_cell_h(1,1) = {x_h(j,:)};

 qs_star = ((a_q + b_q.*log(Gamma_degree(j))) / (1 +

d_q.*log(Gamma_degree(j)))).*(Tau_star).^2 ...      + (g_q +

h_q.*Gamma_degree(j)).*(Tau_star) + j_q + k_q.*Gamma_degree(j) +

l_q.*Gamma_degree(j).^2;

Storage_qs_star(j,:) = qs_star;

vp_star = a_vp.*(Tau_star).^2 + d_vp.*(Tau_star) + g_vp + h_vp.*Gamma_degree(j);

Storage_vp_star(j,:) = vp_star;

x = Ls_star.^2./8./s./(vp_star.^2) % x is delta prime

Delta_star{1,j} = x + Ls_star.^2.*tan(Gamma(j)).^2./(16.*x) +

Ls_star.*tan(Gamma(j))./2;
```

```
u_bar_a = u_tau.*log(R.*0.4.*(x + Ls_star.^2.*tan(Gamma(j)).^2./(16.*x) +

Ls_star.*tan(Gamma(j))./2))./Kapa;

u_star_a = u_bar_a./sqrt((s-1).*g.*D);

e_star = e.*(1 + (s - 1).*qs_star./vp_star./(x + Ls_star.^2.*tan(Gamma(j)).^2./(16.*x)

+

Ls_star.*tan(Gamma(j))./2))./(1 + tan(Gamma(j)).^2);

l_star = l.*(Beta + (1 - Beta).*s)./(1 + tan(Gamma(j)).^2)./(Beta.^2);

Tau_ax_star = @(y) - e_star.*u_star_a.^2 + l_star.*(-s.*qs_star./(y -...

    (x + Ls_star.^2.*tan(Gamma(j)).^2./(16.*x) + Ls_star.*tan(Gamma(j))./2)) + ...

    (x + Ls_star.^2.*tan(Gamma(j)).^2./(16.*x) + Ls_star.*tan(Gamma(j))./2).*...

    (1 - qs_star./vp_star./(x + Ls_star.^2.*tan(Gamma(j)).^2./(16.*x) + ...

 Ls_star.*tan(Gamma(j))./2)).*(- u_bar_a)./(y - (x +

Ls_star.^2.*tan(Gamma(j)).^2./(16.*x) +

Ls_star.*tan(Gamma(j))./2))).^2;

 a_star = a_star_f(s,Beta); b_star = a_star/(s-1);

 a_add = a_star.*(tan(Gamma(j)).^2./(1 + tan(Gamma(j)).^2));

f_Phi = @(y)y - (- a_add.*3.5.*(1 - Beta).*(Ls_star.^2.*tan(Gamma(j)).^2./16 +

Ls_star.*tan(Gamma(j)).*x./2 + x.^2)./(Beta.^3.*s) -...  (1./b_star - 1).*(x +
```

```
Ls_star.^2.*tan(Gamma(j)).^2./(16.*x) + Ls_star.*tan(Gamma(j))./2) + ...  (- a_add -
(s –
2)./b_star).*qs_star./vp_star + (... - a_add.*300.*(1 –
Beta).^2.*(Ls_star.^2.*tan(Gamma(j)).^2./(16.*sqrt(x)) + ...
 Ls_star.*tan(Gamma(j)).*sqrt(x)./2 + x.^1.5).*Mu./(Beta.^3.*s.*Rou.*D.*sqrt(2.*(1 -
1....
 /s).*g))) + (b_star.*H_star./(1 + tan(Gamma(j)).^2) + a_star.*Tau_ax_star(y)));
for i=1:iteration

  St_cell_m{1,i} = (St_cell_l{1,i} + St_cell_h{1,i})./2;
  f_temp_l = f_Phi(St_cell_m{1,i});
  Storage_l(j,:) = f_temp_l;
  f_temp_h = f_Phi(St_cell_h{1,i});
  Storage_h(j,:) = f_temp_h;
  [row_l col_l] = find(Storage_l(j,:).*Storage_h(j,:) < 0);
  [row_h col_h] = find(Storage_l(j,:).*Storage_h(j,:) >= 0);
    if isempty(row_l)
     s_row_col_h = size(row_h,2);
     for k = 1:s_row_col_h
```

```
    x_h(j,col_h(k)) = St_cell_m{1,i}(1,col_h(k));

    end

elseif isempty(row_h)

     s_row_col_l = size(row_l,2);

    for k = 1:s_row_col_l

    x_l(j,col_l(k)) = St_cell_m{1,i}(1,col_l(k));

    end


else
     s_row_col_h = size(row_h,2);

    for k = 1:s_row_col_h

    x_h(j,col_h(k)) = St_cell_m{1,i}(1,col_h(k));

    end

     s_row_col_l = size(row_l,2);

    for k = 1:s_row_col_l

    x_l(j,col_l(k)) = St_cell_m{1,i}(1,col_l(k));

    end

  end

St_cell_l(1,i + 1) = {x_l(j,:)};
```

```
   St_cell_h(1,i + 1) = {x_h(j,:)};

   [row col] = find((abs((St_cell_l{1,i + 1}-St_cell_h{1,i + 1})./(St_cell_l{1,1} -
St_cell_h{1,1}))

- 0.00001) > 0);

    if isempty(row)

  count = i;

x_m_real = (Ls_star.^2.*tan(Gamma(j)).^2./(16.*St_cell_m{1,i}) +
Ls_star.*tan(Gamma(j)) +

St_cell_m{1,i});

  x_h_real = (Ls_star.^2.*tan(Gamma(j)).^2./(16.*x_h(j,:)) + Ls_star.*tan(Gamma(j))
+ x_h(j,:));

 Storage_delta(j,:) = (x_m_real+x_h_real)./2;% storage_delta store the matrix of Phi

 Storage_Tau_ax_star(j,:) = Tau_ax_star(Storage_delta(j,:)).*tan(Gamma(j));

          break;

   elseif i>=iteration

       count=I;

       sprintf('solution is not convergence')

         end

   end
```

```
end
[X_Tau_star,Y_Gamma] = meshgrid(Tau_star,Gamma_degree);
 Delta_test8 = test8();
figure(20);
Phi_2 = Storage_delta - Delta_test8;
surf(X_Tau_star,Y_Gamma,Phi_2);
title('Scour Profile Dependent on $$\tau_{*}/\tau_{*co}$$ and $$\gamma$$','interpreter','latex'); grid on;
xlabel('\it$$\tau_{*} /\tau_{*co}$$','interpreter','latex');
ylabel('\it$$\gamma$$','interpreter','latex');
zlabel('\it$$\varphi_{2}^{*}$$','interpreter','latex')
figure(19);
surf(X_Tau_star,Y_Gamma,Storage_delta);hold on;
view(50,36);
title('Bedload Surface Alternation Dependent on $$\tau_{*}/\tau_{*co}$$ and $$\gamma$$','interpreter','latex'); grid on;
xlabel('\it$$\tau_{*} /\tau_{*co}$$','interpreter','latex');
ylabel('\it$$\gamma$$','interpreter','latex');
zlabel('\it$$\varphi_{1}^{*}$$','interpreter','latex')
```

```
figure(4);
surf(X_Tau_star,Y_Gamma,Storage_qs_star);
xlabel('\it$$\tau_{*} /\tau_{*co}$$','interpreter','latex');
ylabel('\it$$\gamma$$','interpreter','latex');
zlabel('\it$$q_{s}^{*}$$','interpreter','latex')
figure(7)
plot(Tau_star,Storage_qs_star(1,:),':k');grid on;hold on;
ezplot(@(x)5.7.*(0.035).^1.5.*(x-1).^1.5,Tau_star);
title('Dimensionless Bed load for Horizontal Bed');legend('Simona and Luca''s Formula','FLvB''s Experiments');
xlabel('\it$$\tau_{*} /\tau_{*co}$$','interpreter','latex');
ylabel('\it$$q_{s}^{*}$$','interpreter','latex')
 figure(5);
surf(X_Tau_star,Y_Gamma,Storage_vp_star);
xlabel('\it$$\tau_{*} /\tau_{*co}$$','interpreter','latex');
ylabel('\it$$\gamma$$','interpreter','latex');zlabel('\it$$v_{*p}$$','interpreter','latex')
figure(8)
plot(Tau_star,Storage_vp_star(1,:),':k');grid on;hold on;
ezplot(@(x)8.625.*(0.035).^0.5.*(x-1).^0.5,Tau_star);
```

```
title('Dimensionless Particle Velocity for Horizontal Bed');legend('Simona and Luca''s Formula','FLvB''s Experiments');
xlabel('\it$$\tau_{*} /\tau_{*co}$$','interpreter','latex');
ylabel('\it$$v_{*p}$$','interpreter','latex')
 figure(6);
surf(X_Tau_star,Y_Gamma,Storage_Tau_ax_star);
xlabel('\it$$\tau_{*} /\tau_{*co}$$','interpreter','latex');
ylabel('\it$$\gamma$$','interpreter','latex');
zlabel('\it$$\tau_{add}$$','interpreter','latex')
% Computing delta_star based on the Fernandez and Van's expression
function Storage = test8()
 format long
h=0.2; D=0.001;
Repose_angle = 35.*pi./180;
 Tau_star = 2:0.5:6;
Gamma_degree = [0.001 0.1:0.5:20];
Gamma = Gamma_degree.*pi./180;
 [s_x,s_y] = size(Tau_star);
[ss_x,ss_y] = size(Gamma);
```

```
s = 2.65; Beta = 0.33; g = 9.81;
Rou = 998.1;Mu = 1.005e-3;L_s = 16;
 a_q = 8677.849e-6; b_q = -2521.125e-6; d_q = -289785.4e-6; g_q = 9543.719e-6;
h_q = 1068.214e-6; j_q = 21673.804e-6; k_q = 827.69811e-6; l_q = 21.321179e-6;
a_vp = -46136.64e-6; d_vp = 856798.23e-6; g_vp = 187614.77e-6;
h_vp=44260.106e-6;
Storage = ones(ss_y,s_y); Diff = ones(ss_y,s_y); Storage_m_star = ones(ss_y,s_y);
 for j = 1:ss_y
 Tau_star_o = Tau_star./(cos(Gamma(j)).*(1-tan(Gamma(j))./tan(Repose_angle)));
 Tau_star_ratio = meshgrid(Tau_star,1:ss_y);
 qs_star = ((a_q + b_q.*log(Gamma_degree(j)))/(1 +
d_q.*log(Gamma_degree(j)))).*(Tau_star_ratio).^2 ...
+ (g_q + h_q.*Gamma_degree(j)).*(Tau_star_ratio) + j_q +
k_q.*Gamma_degree(j)+l_q.*Gamma_degree(j).^2;
vp_star = a_vp.*(Tau_star_ratio).^2 + d_vp.*(Tau_star_ratio) + g_vp +
h_vp.*Gamma_degree(j);
 Delta_star = L_s.^2./(8.*s.*vp_star.^2);
Delta_star_real = L_s.^2.*tan(Gamma(j)).^2./(16.*Delta_star) +
L_s.*tan(Gamma(j))./2 + Delta_star;
```

```
Delta_star_real(j,:);
 w_bar = sqrt(2.*(1-1./s).*g.*Delta_star);
RE_w = Rou.*D.*w_bar./Mu;
c_star = 3.5.*(1 - Beta)./(Beta.^3.*s) + 300.*(1 - Beta).^2./(Beta.^3.*s.*RE_w);
M_star = c_star.*Delta_star + qs_star./vp_star./Delta_star_real;
 Storage_m_star(j,:) = M_star(j,:);Delta_star(j,:);
Storage(j,:) = Delta_star_real(j,:);
 Diff(j,:) = abs((Storage(j,:) - Storage(1,:))./Storage(1,:));
 end
 figure(1); hold on; grid on;
title('Dependent Correlation for Thickness of Bedload Layer','FontName','times new roman');
xlabel('\it$$\tau_{*}/\tau_{*co}$$','interpreter','latex');
ylabel('\it$$\delta_{*}$$','interpreter','latex');
plot(Tau_star,Storage(1,:),'-k'); hold on;
plot(Tau_star,Storage(2,:),'--k'); hold on;
plot(Tau_star,Storage(3,:),'-.k'); hold on;
plot(Tau_star,Storage(4,:),':k'); hold on;
```

```
plot(Tau_star,Storage(5,:),'-k.');
legend('Slope = 0.001^{o}','Slope = 1^o','Slope = 2^o','Slope = 3^o','Slope = 4^o','FontName','times new roman')
text(2.3,3.5,'$$\leftarrow \tau_{*} /\tau_{*co} = 2.3$$','interpreter','latex'); hold off;
 figure(3)
[X,Y] = meshgrid(Tau_star,Gamma_degree);
surf(X,Y,Storage);
title('Dependent Correlation for Thickness of Bedload Layer','FontName','times new roman');
xlabel('\it$$\tau_{*}/\tau_{*co}$$','interpreter','latex');
ylabel('\it$$\gamma$$','interpreter','latex');
zlabel('\it$$\delta_{*}$$','interpreter','latex');
 figure(4)
surf(X,Y,Storage_m_star);
title('Vertically Dimensionless Pressure Gradient on the Bed Surface')
xlabel('\it$$\tau_{*}/\tau_{*co}$$','interpreter','latex');
ylabel('\it$$\gamma$$','interpreter','latex');
zlabel('\it$$M_{*}$$','interpreter','latex');
```